SOLAR ENERGY FOR DESALINATION AND WATER PURIFICATION USING CARBON MATERIALS

Report to the
Water Research Commission

by

H. Badenhorst

University of Pretoria

WRC Report No. 2467/1/17
ISBN 978-1-4312-0957-6

March 2018

Obtainable from

Water Research Commission
Private Bag X03
Gezina 0031

orders@wrc.org.za or download from www.wrc.org.za

DISCLAIMER

This report has been reviewed by the Water Research Commission (WRC) and approved for publication. Approval does not signify that the contents necessarily reflect the views and policies of the WRC, nor does mention of trade names or commercial products constitute endorsement or recommendation for use.

Printed in the Republic of South Africa

EXECUTIVE SUMMARY

Globally water shortages are an issue of increasing concern both due to population growth and global warming. South Africa is in a rather precarious position where a water crisis is compounded by an energy crisis. The country has already utilized most of its fresh water supplies and many households do not yet have suitable water access. In addition, these same homes still do not have access to the electricity grid. The national energy supplier is undergoing an electricity shortage with rolling blackouts in many regions. It makes sense to attempt to solve these two problems simultaneously. This can be achieved through small scale (<0.1 m^3 / day) desalination units which utilize solar energy directly.

Traditional solar stills, or more accurately evaporators, lack the efficiency and high purities achieved with industrial thermal desalination. However, to replicate these conditions, high operating temperatures are required which in turn need highly concentrated solar energy to achieve. To accomplish this it was proposed to use a newly developed solar concentration platform. The system uses cheap, available components to achieve high levels of concentration. In addition, a suitable solar collector had to be developed to harness the energy and transfer it to the water. Laboratory scale testing under simulated conditions indicated that carbon materials in the form of graphite foams and carbon black nanofluids could be used as surface or volumetric collectors respectively.

The aim of this investigation was to extend the assessment of the two absorber materials to small-scale field testing, using real solar radiation. The foams were produced in-house using low cost, locally available raw materials. Coal tar pitch from Arcelor-Mittal was mixed with expandable graphite from Qingdao Graphite (China) to produce the foam. This is then graphitized at high temperatures (~2600 ^oC). As first step the exact composition and configuration of the foam had to be optimized for maximum energy transfer to heating the water. Foams of varying densities and composition were manufactured. The produced foams were fully characterized to ensure high conductivity graphite foams with large surface areas were produced. It was found that the foams had to be subjected to a slight oxidative treatment to open the pores and fully expose the foam structure for maximum heat transfer.

The foams were tested in a variety of configurations to determine the maximum concentration ratio and hence minimum collector area, as well as the minimum collector depth required for efficient heat transfer. The energy transfer of the foam under concentrated sunlight conditions to a water medium was monitored to determine the efficiency. Testing demonstrated a reduction in efficiency with thickness and an independence of concentration ratio. This indicates that the least amount of foam is used at the highest concentration ratio. The maximum ratio achievable is dependent on manufacturing limitations, in this case the smallest size the foam can be cut to without fracturing, around 1 cm^2. The overall efficiency of the foam for energy transfer to the water was found to be around 40%, similar to conventional flat plate collectors. Given the cost of the high temperature heat treatment this value is disappointingly low.

A stable carbon black nanofluid was developed that had to be fully characterized and tested for the optimal concentration at maximum energy transfer to the water thermal fluid. The non-toxic surfactant Tween 20 was used to produce nanofluids with varying composition. These fluids were fully characterized in terms of radiation absorption, radiation transmission, thermal depth and photo-thermal properties. The results of this testing indicated that at a concentration of between 0.001 and 0.005 vol % the fluid could achieve 100% absorption in a flow channel as shallow as 3 cm. This was used to design a baffled flow cell for field testing of the nanofluid. The flow cell was modelled in detail to take into consideration design issues such as the material of construction, number of baffles, flow distribution and heat losses. Coupled with the experimental results it followed that an overall efficiency for the flow cell of around 75% can be expected.

To estimate the yields which would be achievable from the two types of absorber materials a complete system model had to be designed and simulated. It is envisioned that the unit will operate in a batch mode where it is loaded with a charge of seawater in the morning, a continuous circulation rate is set and the system gradually achieves steady state through the day. In addition, a heat recovery device is incorporated in the form of a heat pump to recover some of the energy present in the flash produced water vapour. The operation of this system throughout the day and its sensitivity to key design parameters was thoroughly evaluated. Due to the nature of the operation it was found that only when flow cell and heat recovery efficiencies exceeded 80 and 40 % respectively could the system achieve the production rate expected for the ideal case of pure evaporation.

The unit operates with a fixed feed rate for ease of operation. In addition, the flash temperature is fixed (based on atmospheric conditions, vacuum not considered) as well as the maximum feed temperature due to material and cost considerations. This fixed delta temperature in essence determines the system behaviour and limits the vapour production rate. As a realistic operating point, a heat recovery efficiency of 33% was assumed along with the experimentally determined efficiencies of 40 and 75% respectively for the foam and nanofluid collectors. This indicated that the system could achieve yields of around 5.8 and 10.8 litres per day (per m^2 aperture) for the surface (foam) and volumetric (nanofluid) absorbers respectively.

Despite their drawbacks the efficiencies of traditional solar stills have recently been improved through modern innovations. Examples of this are the use of thin-film designs and energy storage media to enhance efficiency. As a benchmark for comparison it was decided to also develop a modern traditional still design. Prior lab work indicated a thin liquid film greatly improves evaporation if the system can be operated stably without dry spots. To achieve this a wick based evaporator was designed and tested. Jute cloth was used based on easy of availability and low cost, which were the objectives for the whole system. The system was built and tested eight times over the period of a month. In the best case experimental result the still was found to be capable of delivering 2.4 litres per day (per m^2 aperture).

It was initially intended to couple the wick based still to a multi-stage, external condenser which incorporated phase change materials as energy storage. This would enable the still to operate well into the night when the driving force for condensation is at its maximum. For this reason the wick still was also operated in a pure evaporator mode. This involved the use of a double pane window as the still aperture. Experimental results were encouraging and the still achieved markedly higher operating temperatures of up to 95 ^oC. In addition, it was shown that in this mode the still could operate even more effectively at elevated ambient temperatures. To enable a preliminary assessment a multi-stage condenser with and without energy storage was modelled. It was found that due to the low cost of solar energy it is not sensible to increase the capital cost of the device using a multi-stage design. In addition, the simulation did indicate that the incorporation of a phase change material, when coupled to a suitable evaporator could achieve a meaningful yield increase. This information is currently being used to design and build a combined system for future testing.

The final objective of the investigation was to assess all three designs in terms of economic and operability considerations. Currently available small-scale solar evaporator designs achieve yields of between 3 to 4 litres per m^2 per day at a cost of around R 0.08 / litre. The thin-film design has not quite achieved this production rate but several improvements have been suggested which, with coupling to the external energy storage condenser may be significantly improved. The cost of the system however compares well at an estimated R 0.11 / litre. This does however indicate that extremely cheap energy storage media must be identified for the improved yield to offset the additional costs. As expected the concentrated solar, flash based designs significantly outperform the traditional stills. However, this comes at a drastically increased cost of around R 0.92 and R 1.71 / litre using the carbon nanofluid and graphitic foam respectively.

From a maintenance and operability perspective the concentrated solar platform has performed well over the past year despite its complexity. Aside from a few issues which can be corrected in future designs the system has been operating autonomously for almost two years. The only manual effort required is cleaning of the mirrors, no electricity has ever been used. Despite this benefit however, it is not recommended that the platform

be pursued further as an option for solar desalination. The additional costs of concentrating the sunlight, mainly through the tracking system, are overwhelming despite the low cost nature of the current design. Instead it is recommended that the option of achieving the high temperatures required for flashing using other methods be explored, perhaps through superior insulation options. Or alternatively, the option of a high efficiency but high cost solar collector such a multi-junction photo-voltaic cells, coupled to reverse-osmosis, should be investigated.

Despite its simplicity the thin-film design still has some issues for continuous operation, mainly the maintenance of an even distribution of liquid throughout the still in the face of variations in solar irradiation. It is recommended that the option of a bottom-up feed system is considered. This would require the use of a wick material that has a strong enough capillary action to draw moisture up the inclined still. This system would not require any costly process control as it would be self-regulating depending on the rate of evaporation. Such a design, using a double pane cover and coupled to an energy storage condenser, appears to be the most attractive option for small-scale, solar desalination.

Papers published and conference presentations:

H. Badenhorst, N. Fox, A. Mutalib. “The use of graphite foams for simultaneous collection and storage of concentrated solar energy”. Carbon (2016) 99:17-25. DOI: 10.1016/j.carbon.2015.11.071 (Journal IF 5.9)

J. Bester, H. Badenhorst “Concentrated solar power for sea water desalination in a direct absorption solar collector using carbon black additives” South African Solar Energy Conference, Stellenbosch, Nov 2016.

ACKNOWLEDGEMENTS

The project team wishes to thank the following people for their contributions to the project.

Reference Group	Affiliation
Mr M Van Dijk	University of Pretoria
Dr A Madhlopa	University of Cape Town
Mr W Pierce	Aurecon
Prof A Jimoh	Tshwane University of Technology
Dr K Craig	University of Pretoria
Dr T Roos	Council of Scientific and Industrial Research
Mr P Thompson	Umgeni Water

CONTENTS

LIST OF FIGURES

LIST OF TABLES

ACRONYMS & ABBREVIATIONS

CF	Concentration Factor
CPV	Concentrated Photovoltaic
DASC	Direct Absorption Solar Collector
DMA	Dynamic Mechanical Analysis
DNI	Direct Normal Irradiance
DoE	Department of Energy
ED	Electro-dialysis
EG	Expandable Graphite
IF	Impact Factor
IRP	Integrated Resource Plan
MSF	Multistage Flash Distillation
MED	Multi-effect Distillation
MP	Mittal Pitch
PCM	Phase Change Material
PMMA	Poly Methyl Methacrylate
PV	Photovoltaic
RO	Reverse Osmosis
RO-PV	Reverse Osmosis coupled to Photovoltaic
RVC	Reticulated Vitreous Carbon
SEM	Scanning Electron Microscopy
TGA	Thermogravimetric Analysis
TMA	Thermomechanical Analysis
VC	Vapour Compression
XRD	X-ray Diffraction

CHAPTER 1: BACKGROUND

1.1 INTRODUCTION

Water consumption is always increasing due to population growth. It is projected that close to 70% of the world population will face water shortage issues by 2025. South Africa has utilized virtually all of its fresh water resources so it is imperative that alternatives be found. The South African Human Rights Commission and Department of Water Affairs have reported that [1, 2]:

- “Only 85% of households have access to clean water”
- “75% of households do not have access to acceptable sanitation or are at high risk”
- “South Africa already uses 98% of its available fresh water supplies.”

Furthermore, acid mine drainage threatens water supplies in and around the primary economic centre of Gauteng. Something must be done to rectify the situation and ensure long term water security for South Africa. Some communities have access, but to unusable sources such as, seawater, brackish water and contaminated rivers and dams. Historically, desalination has been the most expensive way to produce drinking water at the commercial scale because of the high energy requirements. In addition, all over the world government and industry are turning to renewable energy resources to achieve a more sustainable energy supply [3, 4]. Environmental pressure is increasing and conventional energy reserves are declining leading to higher prices [5, 6]. Solar is arguably the most abundant and readily available form of renewable energy, with the sun providing the energy needs of the entire planet for one year in a single hour [7]. The Department of Energy (DoE) developed the Integrated Resource Plan (IRP) as a road map for the future, indicating that solar energy will make up a significant portion of South Africa's future energy mix [8, 9].

Because seawater desalination or brackish water recovery are such energy intensive processes [10-15], it makes sense to look to ways of using renewable resources directly at the point of use and avoid the inefficiencies of electricity generation and grid losses. The de facto industrial standard for this is reverse osmosis coupled with photovoltaic systems (RO-PV) [16]. The low costs of these systems are made possible by the exceptionally high capacity of such units at around 10000 m^3 / day. It is fairly indisputable that it is difficult to improve on the performance of this approach using other, capitally expensive, solar options [17]. However, in South Africa many communities are still not connected to the electricity or water supply grids, thus a gap exists in the market for small or micro scale <0.1 m^3 / day, off-grid, desalination/water purification units.

For these smaller size units costs are invariably higher [17] which can be utilized for solar augmentation. Solar stills have been around for a long time; however, this is a slight misnomer. Traditionally these designs do not incorporate the boiling and condensation of water, thus they are not true distillation units. Instead they make use of direct sunlight to heat a collector plate which in turns heats water above ambient temperature to enhance the level of evaporation. Whilst the energy input has very little operating cost, this approach suffers from a significant downside, namely low efficiency and yields. In addition, these units neither achieve the high purity of distillation, nor the disinfection benefits of boiling. To achieve true distillation however, the water must be heated to high temperatures and this requires high levels of solar concentration.

A novel, off-grid, solar concentrator platform has been developed at the University of Pretoria. The system uses only existing technology and cheap, off the shelf components to achieve high levels of concentration. It is a modular structure ensuring scalability to community needs. The concentrator can be coupled to a suitable collector to heat water to a suitable temperature for distillation. A lab scale version of the concept has been tested using graphitic foams and a carbon black suspension as two potential collector options, with promising results. For comparative purposes an improved traditional evaporator, using a thin-film concept to be coupled

to a phase-change material (PCM) for energy storage was also developed. This system can be used a benchmark for comparison to the prior two concentrated solar options based on efficiency, economics and operability.

1.2 PROJECT AIMS

The following are the aims of the project as laid out in the original proposal:

1. To extend the prior lab testing of the three methods (concentrated solar energy coupled to a graphitic foam target and a carbon black suspension respectively, as well as the thin-film solar evaporator concept), to field testing using real, concentrated in two cases, sunlight as input. The objective is to overcome the issues identified and develop practically implementable systems.
2. To compare all three methods and determine which is the most efficient and cost effective for desalination/brackish water recovery.
3. To determine which of the three methods will result in the design with the lowest maintenance and operator input.

1.3 SCOPE AND LIMITATIONS

The foam study was limited to in-house developed graphitic foam. This foam is the most economical option available and its physical properties have been compared to alternatives in other studies within the group. Furthermore the aim is to optimize the foam configuration specifically for this application; the optimal parameters would change for different foams. The carbon black used in this study is procured from the Cabot Corporation to ensure a reproducible material is obtained. In future it is planned to use carbon black from recycled scrap tyres. However, the properties of carbon black obtained from scrap tyres vary significantly depending on the source; this may obscure clear conclusions from the current investigation. Water utilised in this investigation is limited to tap water obtained at the University of Pretoria from the Tshwane local government. Conventional sea salt is dissolved in the water to reach equivalent levels found in seawater for desalination testing purposes. This is only to confirm the potential influence of dissolved salts on the operation. In future this may be extended to real water samples from a suitably chosen deployment site once the design is proven and finalized.

Prior investigations into the different options were limited to laboratory scale testing under electrically simulated sunlight. All field testing was performed using real sunlight on the University of Pretoria's concentrated solar platform located at the Experimental Farm, the design and operation of which is described elsewhere in this report. The exception is the thin-film evaporator which did not require concentrated sunlight but was tested at the same location. The location is well established and very flat with no buildings or obstructions. The solar irradiation and other meteorological information is monitored extensively which allows the results to be easily generalized to alternate locations for implementation. The system size is limited to small scale, defined as delivering a yield of less than 0.1 m^3/day. System modelling was either first principles based in the Python programming language or using the finite volume method in the Fluent platform within commercial software package ANSYS. Solar ray-tracing was done using the SOLTrace program for the solar platform [23].

CHAPTER 2: LITERATURE REVIEW

2.1 INTRODUCTION

Contaminated drinking water is one of the major health hazards responsible for almost 90 % of the wellbeing problems in areas not connected to the water network. Women and children are very vulnerable to water borne diseases. Generally, women are also responsible for fulfilling the requirement of water in their household and thus spend a large portion of their time on procuring water. Out of the 40–50 litres per capita per day (lpcd) water requirement for domestic consumption, only 2 lpcd is the drinking water. A total amount of 5–10 lpcd water is needed for drinking and cooking purposes and thus this is the only quantity of water that needs to meet the stringent quality standards of potability prescribed by World Health Organization [1], whereas the remaining amount of water needed for washing and cleaning can be of intermediate quality. Intensive use of chemical fertilizers in agriculture and other industrial activities cause natural and inorganic pollutants to leach down to the sub-surface water and hence the drawing of water through hand-pumps may not be safe for drinking purposes [17].

Keeping in view the poor paying capacity of disadvantaged communities, water supply to remote areas through pipelines could be uneconomical and moreover, it also encourages wasteful use of high quality water in washing, cleaning and lavatories [9]. Therefore, for economical and sustainable water management systems, it is important to supply water at the point of use, at an appropriate level of quality, which is suitable enough for the intended use. Water and energy are two inseparable items that govern our lives and promote civilization. South African is still in the midst of an energy supply crisis. The transportation of drinking water from far-off regions is usually not economically feasible or desirable. In addition, power supply to these regions carries equally high costs. Thus it makes sense to attempt to solve these two problems simultaneously using sustainable and readily available resources.

Hence, there is a clear need for small scale (<than 0.1 m^3/day), off-grid, desalination options using solar energy. The following segment details the literature background surrounding conventional solar desalination. A key to achieving higher yields and better water quality through renewable energy may be the use of concentrated solar power, which is the subject of the next section. In order to harvest the solar energy however, a collector is required. The final chapter reviews the existing literature on carbon foams and carbon black, with a view on their use as solar collectors.

2.2 CONVENTIONAL SOLAR DESALINATION

2.2.1 TRADITIONAL SOLAR EVAPORATORS

A traditional solar still, consists primarily of a shallow basin with a transparent glass cover. The sun heats the water in the basin, causing evaporation. Moisture rises, condenses on the cover and runs down into a collection trough, leaving behind the salts, minerals, and most other impurities. Solar stills can be classified into passive and active categories based on energy supply. Passive systems are those which receive no energy from non-solar energy sources while active systems receive some energy from an external source to raise the temperature and consequently the evaporation rate of the undistilled water. This external energy can be supplied by solar collectors or the thermal energy wasted in industrial units. Passive and active setups are also sometimes referred to as direct and indirect. In the current investigation the extra complexity of active/indirect systems, in addition to higher costs both from equipment and extra insulation have precluded them from

consideration [82]. This disqualifies the use of both conventional flat plate collectors, as used in solar water heaters, and evacuated tube systems.

Basin stills are the most common direct systems and come in a variety of configurations, according to their cover designs such as; single slope, double slope, V type and hemispherical. The average distillate production rate of a standard single-basin still is between 0.005 and 0.011 $m^3/(m^2.day)$ depending on the insulation quality [83]. Several aspects of the fabrication are important including glazing, liner, sealant, construction material, condensate channels and side walls. All of the stills mentioned typically rely on the glazing, i.e. still cover to serve as the condensation surface. However, this has numerous drawbacks; the most significant of these are high heat losses and light scattering. An alternative approach is the use of a separate condenser. This decreases the convective heat loss through the still cover and provides an effective heat sink for the condensing vapour, increasing the yield by 50-70% [83]. Some of the evaporating water still condenses on the cover surface and a fraction of the vapour passes to the condenser chamber by the effect of a pressure difference causing the pressure in the still chamber to drop. Lowered pressure decreases the formation rate and number of the vapour droplets on the inside surface of the still cover which allows more solar radiation to reach the water in the still basin and improves evaporation.

Conventional basin type solar stills have significant disadvantages; the horizontal water surface inevitably causes cosine loses especially at higher latitudes and the large thermal capacity of the water in still basin limits fresh water output. It has been demonstrated with a single basin experiment that the thinner the water bed, the higher the yield obtained [84]. Stills with inclined absorber surfaces are reported to have significantly higher productivity compared to basin-type stills. In an inclined still, water flows from the top to the bottom of the absorber surface. This can be achieved by a flat plate over which the liquid flows in a thin-film or a weir system which has a more complex construction. The thin water film allows easy absorption of the incoming radiation by the underlying plate, rapid heating and consequently high evaporation rates. Even distribution of the water on the plate is an issue, as are dry spots. To correct for this and maintain uniform thickness of water and an even distribution, a wick can be used to draw water by capillary effect. In a wick still, the feed water flows slowly through a porous, radiation-absorbing pad (the wick). Capillary suction of the cloth fibres used as wick produces a thin water film which can easily be evaporated by the incoming solar radiation, at the same time avoiding dry spots. Wick stills have less feed water in the still at any time and so the water is heated more quickly and to a higher temperature [85]. Inclined stills usually operate without separate condensers rather using a shaded portion of the cover. There is a small distance between the cover and absorber plate which quickens the saturation and condensation processes. A critical consideration which is highlighted for the productivity of a solar still is the temperature difference between the water vapour and condensing surfaces. A higher temperature difference between these surfaces yields higher productivity [86]. An alternative design is the combination of a glass cylinder and a tray or trough inside the cylinder or inside a sphere. While these stills do offer advantages in terms of the condensation area per evaporation surface, they require custom built and expensive glass components which are prone to breakage. For these reasons they are not considered for this application.

Three different wick designs were found in literature [87]. First, a single wick still with a water reservoir inside the still where the wick floats inside the reservoir and exits at an angle. This angle creates a driving force for capillary effects and sucks the saline water through the cloth. Preliminary tests indicated that this method did not provide a sufficient dispersion of water. The second option, a multi-wick configuration did not show any clear benefit above the prior arrangement. Finally a single wick with an external feed system was examined. This arrangement offers the most flexibility and control over the introduction of water into the still and onto the wick. A simple gravity feed system with variable flow and a perforated pipe as distributor may be used to control the liquid distribution onto the wick.

The material properties which are of the utmost importance when selecting wick materials are: porosity, water absorbency, water repellence, capillary rise and heat transfer coefficient. A very large variety of materials have been tested in the past [88]. From this water coral fleece was identified as the best wicking material.

Comparative tests between jute cloth, polystyrene sponge, water coral fleece and wood pulp paper were performed. Jute cloth is cheap and easy to find whereas wood pulp paper is not reusable, polystyrene sponges have no capillary rise and bad absorbency while water coral fleece is an expensive material. The distance between the basin (wick cloth) and the glass cover has an optimum and is considered more important than the still angle. Several tests were performed by research groups [19] and it was found that reducing the depth will reduce the shadowing effect of the walls and thus improve the still performance. Reducing the gap from 13 to 8 cm the output increased by 11% in the case of an inclined still with condensation on the still cover.

2.2.2 RECENT IMPROVEMENTS TO SOLAR EVAPORATORS

To achieve optimal performance a system coupled to external condensers performs the best. For this reason alternative external condenser arrangements were also considered. Phase change materials (PCMs) are superior energy absorbing and releasing materials, utilizing sensible as well as latent heat [89]. Energy absorbed during daylight hours is stored and then released after sunset. The release of energy is facilitated by the decrease in ambient temperature causing the water temperature within the still to drop. Due to the energy release the water within the still remains at a constant temperature while ambient temperature continues to decrease, taking full advantage of the increasing temperature difference/driving force [90].

Prior investigations into the use of PCM's and heat storage [91] resulted in an increase in productivity when added as a heat reservoir beneath the solar still basin. Achieving increased productivities of 36% and 13% for Lauric acid and sand, respectively. Results also suggest that productivity increases with an increase in mass of PCM. Other research [90] compared the effects of various PCMs on the productivity of a single stage basin still. PCMs usually have a large latent energy and low thermal conductivity while having a melting point within normal operating temperatures of the system [92]. The choice of PCM according to its melting point is crucial as it is dependent on the maximum temperature that can be achieved by the water within the still [89]. This is to ensure the use of the latent energy of the material at roughly constant temperature. Other characteristics of PCMs include non-toxic, non-corrosive, chemical and thermal stability. Hydrated salts, paraffin waxes, fatty acids and eutectics of organic and inorganic compounds are materials that have been considered over the years. Inorganic salts and organic fatty acids are commonly used PCMs. While organic fatty acids are non-corrosive, chemically and thermally stable they do not exhibit phase change enthalpies and thermal conductivities as large as inorganic salts [92].

In multistage systems the existing stage passes energy from the process vapour to the subsequent level by means of condensation. This transferal of energy reduces the wastage of heat energy that would otherwise be disregarded [93]. Work has been done [94] to monitor the output of distillate for each stage of a multistage solar still comprised of four stages. It was found that stages 1-4 produced 36%, 26%, 20% and 18% of the total distillate yield. Reasons for this non-ideal transfer of energy from one stage to another include heat losses from still walls, heat energy removed by produced distillate, condensed droplets that cannot be collected or which drop back into evaporating liquid. Although results revealed that the productivity of existing stages decreased when a subsequent stage was added, the overall distillate yield increased. Non-continuous heating modes indicated that adding a 6th stage would not significantly increase the total distillate yield. Experimental investigations [95] show that a minimum incline of 5 degrees is needed to insure formation and collection of water droplets on the condensing plate. An increase in the concentration of salt within the water decreases the rate of evaporation [96]. This is due to the reduction of water vapour pressure at the liquids surface. Evaporation can therefore cause a reduction in rate as the local salt concentration increases. For these reasons a multistage, PCM filled condenser, coupled to a thin-film based evaporator presents the best modern system for traditional still-based desalination.

2.2.3 LARGE SCALE SOLAR DESALINATION

Industrial desalination processes based on distillation involve phase change [79]. These are multistage flash distillation (MSF), multi-effect distillation (MED) and vapour compression (VC), which could be Thermal VC (TVC) or Mechanical VC (MVC). MSF and MED processes consist of a set of stages at successfully decreasing temperature and pressure. The MSF process is based on the generation of vapours from seawater or brine due to a sudden pressure reduction when seawater enters an evacuated chamber. The process is repeated stage by stage at successively decreasing pressure. This process requires an external steam supply, normally at temperature around 100 ºC. The maximum temperature is limited by the salt concentration to avoid scaling and this maximum limits the performance of the process. For MED, vapours are generated due to the absorption of thermal energy by the seawater. The steam generated in one stage or effect is able to heat the salt solution in the next stage because it is at lower temperature and pressure. The performance of the process is proportional to the number of stages or effects. MED plants normally use an external steam supply at a temperature of about 70 ºC. For TVC and MVC, after initial vapour is generated from the saline solution, this vapour is thermally or mechanically compressed to generate additional production [80].

On the other hand the membrane processes such as reverse osmosis (RO) and electro-dialysis (ED) do not involve phase change. The first one requires electricity or shaft power to drive the pump that increases the pressure of saline solution to that required. This required pressure depends on the salt concentration of the saline solution, which is normally around 70 bar for sea water desalination. Both of these non-phase-change processes have very high energy requirements under these conditions. Thus to treat highly brackish waters these options become uneconomical on small-scale. In addition, in the presence of certain salts which precipitate easily the RO approach may be entire unsuitable due to blockage formation. Thus from a flexibility perspective thermal flash distillation is the most attractive option despite lower overall efficiencies compared to RO. This approach has the additional benefit of producing, water of exceptionally high purity irrespective of the source, which has been fully disinfected through the boiling process. This, in addition to its improved suitability for energy recycling (due to high temperatures), make it more attractive than traditional solar evaporators. The issue facing small scale flash distillation is the attainment of the required temperatures.

2.3 CONCENTRATED SOLAR POWER

In order to achieve the high temperatures and intense energy requirements of flash distillation, it is critical to have a high quality heat source, thermodynamically speaking. Conventional basin stills cannot achieve temperatures close to the boiling point of water under continuous flow; this necessitates the exploration of alternatives. Concentrated solar power (CSP) technologies have received a lot of attention in recent years, both in terms of concentrated photovoltaic (CPV) as well as thermal systems. In CSP systems optical equipment (mirrors or highly reflective metals) are used to focus the direct normal irradiance (DNI) component of the solar irradiation on a small surface. This increases the intensity of the solar radiation because it is focused on a smaller surface, it however does not change the amount of energy. The optical reflective systems are combined with a solar tracking system to follow the sun’s trajectory and thereby maintain optimal efficiencies. The four main CSP technologies available are parabolic trough collectors (PTC), linear Fresnel reflectors, parabolic dish systems and central tower systems.

Many different approaches exist for concentrating solar energy [56], broadly classified as line focus or point focus. The latter is capable of achieving much higher concentration ratios and hence higher temperatures, making it attractive for a wide variety of applications. Over the past decades, extensive effort has been placed on developing suitable receivers for solar energy capture [57-60]. However, the extreme conditions present at the focal point of such systems places very stringent requirements on the material properties. PTCs are the most mature CSP technologies, but in recent years there has been several megawatt scale central tower systems built. Linear Fresnel reflectors also show better performance as well as easier operability and maintainability, because of its modular reflection system, than PTC systems.

Concentrated systems offer certain advantages over non-concentrating systems. The two largest being smaller collection areas, that relates to smaller heat loss areas, especially infrared losses, and “higher-quality” or more intense energy that relates to higher temperatures that can be reached. This higher temperature results in a higher temperature difference over the energy collection surface area and therefore higher thermodynamic efficiencies are possible. The concentration process does, however, have some distinct disadvantages: inherently all concentrating systems has energy losses in the optical concentration steps, how significant these losses are, is dependent on the concentration setup, the nature and accuracy of the solar tracking system as well as the reflecting surface material’s quality and cleanliness. The success of using CSP is dependent on the trade-off between the collector efficiency and the optical losses. The applicability of CSP will be determined by weighing the improved efficiency to the additional capital costs. As of yet, CSP has not been directly applied to desalination, mainly due to the lack of a suitable receiver.

Traditionally, ceramic materials are used to construct solar receivers because of their ability to withstand extreme temperatures. However, ceramic materials have several drawbacks, namely low thermal conductivity and brittleness. Graphite on the other has excellent thermal conductivity and good ductility. In addition, graphite has a very low thermal expansion coefficient making it highly resistant to thermal shock, a property which is critical in solar receiver design. For the current design however, the desired solar collector must not only have a high capture efficiency and good heat transfer but it must also have a low cost. Thus it is crucial to explore carbon materials and designs which use local raw materials and reduce costs.

2.4 SOLAR COLLECTORS

A solar collector is a device that uses solar thermal energy by absorbing incident solar radiation and converting it to heat. There are two types of solar collectors: surface and volumetric absorbers. A surface solar collector absorbs the solar radiation on a surface (usually treated with an absorbent coating), this heats the surface and the surface subsequently heats a working fluid. This type of collector’s efficiency is therefore limited not only by the solar irradiation absorption efficiency, but also by the efficiency of the heat transfer between the surface and the working fluid. To overcome this, a material with a high surface area for exchange of energy with the fluid is needed. In a volumetric absorber solar collector or a direct absorption solar collector (DASC), the solar irradiation is directly absorbed in the working fluid. This reduces the number of steps in the heat resistance network and therefore results in a more efficient system being possible. The efficiency of a volumetric absorber is however directly dependant on the solar irradiation absorption properties of the working fluid. Both surface and volumetric absorbers will be explored through the use of graphitic carbon foams and carbon black nanofluids respectively.

2.4.1 GRAPHITIC CARBON FOAMS

Carbon foams are classified as either, amorphous and thermally insulating, or graphitic and thermally conductive. The first variety is generally prepared by carbonizing foamed thermoset polymers [24, 25]. The final product is typically a glassy carbon with a pentagonal dodecahedron structure [26] and thermal conductivities lower than 1 W/(m.K) [27-29]. Conductive foams are important in thermal management applications and as thermal energy storage materials [25, 30]. Although conductive foams were only recently developed the amorphous carbon foam materials date back to 1960’s when Walter Ford developed what was known as reticulated vitreous carbon (RVC) foam [31]. Being non-graphitic these foams were not used in heat management applications beyond serving as thermal insulation but rather their industrial applications included: impact absorption, catalyst support, and metal and gas filtration. Although not thermally conductive, these foams possessed other desirable material properties such as being thermally stable, low in weight and density, chemically pure, resistive to thermal shock and stress and having low thermal expansion that paved the way for further research into the field of carbon based foams [31].

It was not until the 1990s that researchers at the Wright Patterson Air Force Base Materials Lab pioneered the production of graphitic foams from alternate precursors such as coal and pitches. These foams were oxidatively stabilized and then graphitised to a thermally conductive state after foaming and are thus the real predecessor to all graphite foams currently in development and production today. These foams were foamed by introducing an inert gas to a pressure vessel containing a pressed article of pitch and then elevating the temperature to just above the melting temperature of the pitch. After holding the vessel for a period of time at this state of elevated pressure, the vessel is vented thereby providing a porous foam which can be taken to the successive steps of oxidative stabilisation otherwise known as cross-linking and then graphitisation. The patent of Kearns [32] explains this process in great detail.

Klett and co-workers [33] at Oak Ridge National Laboratory later developed a foaming process requiring much fewer steps than the Kearns method while producing foams that contain more highly aligned graphitic ligaments that are responsible for achieving higher thermal conductivities in these foams after graphitisation. Furthermore this foaming process does not require the introduction of pressurised inert gasses which can be costly in large scale production as well oxidative stabilisation which can be time consuming. The Klett method involves foaming by means of volatile release when mesophase pitch precursor is heated at a controlled rate. With elevated temperatures mesophase begins to pyrolyze and in a polymerisation reaction, forms and releases additional volatiles to those already present in the pitch. As the volatiles are released an associated increase in the molecular weight of the precursor causes an increase in the melt viscosity allowing the precursor to hold the bubbles in place inducing a foam structure into the precursor. As the temperature increases, further pyrolysis causes further increases in viscosity to the extent that the material is effectively coked thus eliminating the need to cross link the material in an oxygen atmosphere. These foams [34] have an open cell structure and feature high thermal conductivities (up to 182 W/(m.K) at a bulk density of 0.61 g/cm^3 [31]), low density, relatively large surface area and a low coefficient of thermal expansion [25]. The specific thermal conductivity is the thermal conductivity divided by the specific gravity. Klett et al. [31] consider this to be an important measure for conductive graphite foams in applications where weight savings are vital. The value for copper is ca. 45 W/(m.K) [29]. Graphite foams can have specific thermal conductivity values that are six times higher than that for copper.

As mentioned, carbon foams can also be produced using other low-cost precursors, such as coal, coal tar pitch and petroleum pitch [35]. However, high thermal conductivity foams are not achieved through this approach. Mesophase pitch is the preferred raw material for graphite foam production as it can be graphitized to a thermally conductive state. Mesophase pitch is a liquid crystal and comprises of polyaromatic hydrocarbons. The highly aligned molecular structure allows the mesophase pitch to be easily graphitised [36]. The most common method of producing mesophase pitch is by heat treating coal tar pitch. When coal tar pitches are heated to temperatures ranging from 620 to 800 K, the optically anisotropic mesophase appears in the isotropic matrix in the form of liquid-crystalline spheres. The spheres grow in diameters up to 100 μm and take up to 5 to 20 % of the mass of volume depending on the temperature as well as the chemical nature of the starting material. They finally coalesce to form a bulk mesophase. Mesophase pitch finds many applications in the production of carbon materials such as in the production of carbon fibres [37] as well as being a precursor in the delayed coking process [38].

In the Klett approach, the graphite foams are produced by foaming a mesophase pitch by volatile gas released from the mesophase pitch itself [39]. However, Yadav et al. [25] also produced high thermal conductivity graphite foam using a sacrificial template method. They impregnated polyurethane foam with mesophase pitch and converted it into graphite foam by suitable heat treatments. Open pore structure foams with density in the range 0.23 - 0.58 g/cm^3, compressive strengths in the range of 3 - 5 MPa and thermal conductivity values up to 60 W/(m.K) were obtained. Zhu et al. [40] showed that the compressive strength of mesophase-based foams can be improved significantly by addition of graphite flakes. Adding just 5 wt.% graphite improved the compressive strength from 3.7 MPa to 12.5 MPa. This foam had an apparent density of 0.757 g/cm^3 and a thermal conductivity of 110 W/(m.K).

New ways of producing carbon foams have recently been proposed. The foams are prepared using expandable graphite (EG) together with a coal tar pitch that was partially converted to the mesophase state. Although pure mesophase pitch is preferred for foam production it is a rare commodity. Hence coal tar pitch may be selected owing to its lower cost and general availability. Expandable graphite refers to natural graphite that has been intercalated with an intercalating compound capable of suddenly volatilising when heated. Expandable graphite is most commonly intercalated with sulphuric acid based compounds and the preparation of such expandable graphite involves the use of sulphuric acid with a strong oxidising agent such as nitric acid, chromic acid, ammonium peroxodisulphate or an electric current. A rich intercalation compound is thus obtained, which is then washed thoroughly. The resulting material is expandable graphite [41].

By heating this solid, the residual intercalate and the water molecules inserted during the washing process vaporise, pushing the graphite layers apart: a low-density material that roughly resembles worms is obtained. This heating process is known as graphite “exfoliation” and the material formed is known as “exfoliated” or “expanded” graphite. The minimum temperature at which the graphite exfoliation may take place can be altered by changing the intercalating compound. At temperatures much higher than the minimum or onset temperature for exfoliation one can achieve a more unidirectional expansion of graphite flakes due to the intercalating compound volatilising more rapidly. A key property of expandable graphite is its tendency to exfoliate when heated to high temperatures [42]. During exfoliation it expands rapidly in a worm-like manner to form vermicular graphite with a low density [43-45]. The bulk density can be as low as 0.006 g/cm^3 [46]. The exfoliation of the expandable graphite provides the “foaming” action to produce the required porosity. Afanasov et al. [46] previously prepared exfoliated graphite-coal tar pitch composites but they did not prepare foams.

Graphite foams can have a low density and high surface area making them ideal for flow through, heat transfer applications. Very high thermal conductivity foams can be produced from mesophase with potential for this application. However, low cost alternatives are now available as noted earlier [68]. The thermal diffusivity of these low density foams are 1.2x10^{-4} m^2/s^1 which is very close to that of pure copper, however the density of the material is 25 times less. These properties make them ideal candidates for use in solar receiver design [69].

2.4.2 CARBON BLACK NANOFLUIDS

Carbon black is an aggregate of graphite microcrystals that can have large differences in size, because of this carbon black can be seen as polycrystalline graphite [66]. Carbon black is made by the burning of hydrocarbons in an insufficient amount of air. The graphite crystallites that make up the carbon black particles can usually not be detected by diffraction techniques because of their small size [66]. The two basic methods to create carbon black are known as:

1. Channel process: Many tiny natural gas flames hit a cool metallic surface, the carbon black then forms on this metallic surface before being oxidised at a high temperature. The small spheroid particles formed using this process have the highest surface area, smallest particle size and the highest volatile content of any carbon black particle.
2. Thermal process: The carbon black is formed in a preheated firebrick-lined chamber due to the thermal decomposition of natural gas in the absence of air. This creates coarser carbon black with a lower surface area and larger particle sizes [66]. The properties and composition of carbon black [70] are shown below.

Morphology	Aciniform (grape-like) aggregates and agglomerates
Nodule size	15-300 nm
Aggregates size	85-500 nm
Agglomerate size	1-100+ micrometre
Total carbon	97-99 %
Elemental carbon	>97 %

Organic Carbon	< 2 %
Hydrogen to carbon ratio	<0.008
Trace inorganic species	<1 %
Solvent-Extractable Organic Matter	0.02-0.14%
Total PAH content	0.1-330 (mg/kg)
Surface Area	12-240 (m^2/g)
Density	1.7-1.9 (g/cm^3)

Carbon black is mainly used in rubber to increase the strength, hardness, stiffness, wear resistance, and heat resistance. Carbon black is also used in typographical inks, paints, enamels, lacquers, etc. Lampblack is a soft, amorphous and flocculent type of carbon black that is used as a black pigment. It is made by combusting coal tar and petroleum oil, before the particles are calcined in the flue gas where it is carried to a large chamber, this expansion then causes the particles to settle. Different feed-to-air ratios have a large effect on the characteristic and properties of the formed lampblack [66]. Acetylene black is made by the thermal decomposition of acetylene. In this strongly exothermic reaction the acetylene gas as put into a retort at 800 ºC in the absence of air where it decomposes. This reaction does not require additional heat. Acetylene black can be compared to high grade lampblack but with a higher liquid-absorption capacity, higher electrical conductivity and overall greater purity than that of lampblack. This makes acetylene black useful when electrical conductivity is needed; it is also used as filler in rubbers and plastics and in the making of dry cells [66].

It is clear that the method that is used to make the carbon black has a big impact on the properties of the final carbon black. The thermal conductivity of carbon black in the bulk phase is quite different from that of the individual carbon black particles [71]. The density of carbon black is 1900 kg/m^3 according to Maquin et al [71]. The apparent conductivities of acetylene black was found to be 45-60 mW/(m.K) under atmospheric air pressure and 3.5-5 mW/(m.K) under primary vacuum. Carbon black helps keep the cost of synthesized composites down because of their very low cost (10-20 % that of purified natural graphite) and their big production volume (9 times that of natural graphite) [72]. Carbon black is a fine powder of a quasi-graphitic form of almost pure elemental carbon. Specific grades of carbon black can be produced by varying the conditions under which it is made. This allows carbon black with a certain surface area, particle size, structure and conductivity to be made for specific applications [70].

Carbon black has very little inorganics or extractable organic compounds. The particle morphology of carbon black is described as aciniform (grape-like) aggregates which are made out of fused spherical particles. These aggregates are then also clustered into larger agglomerates [70]. In 2008 approximately 9.8 million metric tonnes of carbon black was produced. More than 95 % of carbon black is produced by the oil furnace process: a continuous process where carbon black is produced by the pyrolysis of heavy aromatic petroleum oils at temperatures between 1400 ºC and 1800 ºC. A big advantage of this process is that the manufacturing conditions can be well controlled to get a specific grade of carbon black. Carbon blacks are usually found as complex particle aggregates and agglomerates and not as free individual particles. Carbon black can also be produced from vegetable products (as opposed to petrochemical feedstock), carbon black produced from these vegetable products tend to have much larger particle sizes.

Carbon black is mainly made up out of particle aggregates and agglomerates with sizes larger than 100 nm and up to hundreds of microns. The carbon black aggregate is considered the smallest indivisible entity. Long et al [70] defines the carbon black aggregate as: “a discrete, rigid, colloidal mass of extensively coalesced particles, it is the smallest dispersible unit”. The basic building blocks of carbon black products are called primary particles or nodules, these particles have a turbostratic arrangement and are made up of randomly stacked, concentric sheets of graphite platelets. These nodules are usually only found within the reactor vessel because of their very quick and irreversible fused aggregate formation. Thermal blacks can however have some nodules in between the aggregates, but these nodules made from thermal blacks are usually larger than those of other carbon blacks (larger than 100 nm). The nodules form first, followed by aggregation and then

finally agglomerates (large clusters) are formed. These agglomerates can range in size from 1-100+ micrometre. Agglomerates can be made up of many thousand aggregates clinging together by Van der Waals forces. There are no chemical bonds or welding holding the agglomerates together, but these agglomerates are regarded as the predominant carbon black entity since they are not usually broken by normal manufacturing conditions or use. Manufactures usually further pelletize these agglomerates to reduce dust and to make handling and shipping easier, leading to a final product with diameters of 100-1000 micrometre.

Carbon black can be described as a nanostructured material (its internal or surface structure is in the nanoscale, but the strongly fused aggregates can be much larger) rather than a nanoparticle or nano-object. Smaller carbon black particles have larger surface areas. The surface area affects the intensity of the black colour, the conductivity and the UV absorption. A larger surface area leads to better absorption because of the larger area that is available. Carbon black absorbs energy from all wavelengths of light; this is what gives it its black colour. To obtain the maximum absorption of light carbon black particles with a high surface area should be chosen. The primary particle size is the most important factor that determines UV absorption efficiency, the UV absorption increases, with a decreasing particle size, until 20 nm is reached [73]. Carbon black also shows excellent absorption in the visible and infra-red ranges [74]. Preliminary investigations have demonstrated that carbon black is excellent for heating water [75]. Solar illumination of carbon nanoparticles dispersed in water produced vapour without the requirement of heating the fluid volume. When particles are dispersed in water at ambient temperature, energy is directed primarily to vaporization of water into steam, with a much smaller fraction resulting in heating of the fluid. This makes the material an ideal candidate for solar based desalination.

Carbon black from recycled tyres significantly reduces the cost and energy required to make carbon black and reduces the overall environmental impact. This process can be self-sufficient with regards to its energy requirements since the gases from the pyrolysis of the tyres can be used to add the heat necessary for the process [76]. According to Hita et al [77] 7×10^6 tons (or more) of waste tyres are created every year. The big increase in tyre consumption in Asia and Oceania will make them the main source of waste tyres for the next two decades, with China producing 5.2×10^6 tons of tyres in 2010 alone. Tyres are mainly made out of carbon black, steel, natural rubber and synthetic rubber. The carbon black reinforces the rubber and increases the tyres resistance to fracture and abrasion. There are 4 billion tyres in landfills and stockpiles with an additional 1.5 billion tyres sold each year. Pyrolysis of tyres can be used to create useful products like carbon black (called pyrolytic carbon black). The pyrolysis of tyres creates carbon black, a non-condensable gas mixture and a liquid fuel made up of aromatic and aliphatic compounds. Carbon black makes up 30-40 % of tyres, this carbon black comes from fossil sources and recycling this product would greatly help the profitability of tyre valorisation by pyrolysis. The carbon black obtained from this process was found to have comparable properties to commercial carbon blacks, with regards to their BET surface area [78].

Nanoparticles are defined as particles with a dimension in the 1 nm – 100 nm range. The term nanofluid describes a system where nanoparticles are added to a base fluid to create a colloidal suspension. Because there are a vast number of different types of nanoparticles, all with different material properties, it is possible for a nanofluid to be engineered for a specific purpose by merely changing the type of nanoparticles used. Millimetre and micrometre sized particles added to a base fluid is known to improve the thermal conductivity of the fluid, but their applications are limited by their instability that leads to sedimentation, mainly because of size effects. Nanoparticles show better stability in fluids because of their smaller size and increased Brownian motion of the nanoparticles in the fluid. A lot of research has been done to improve specific properties of nanofluids with the majority of research focused on improving the thermal conductivity of working fluids in heat transfer systems. Lately a lot of research around the optical properties of nanofluids has been done with nanofluids being extensively researched specifically for the use in DASCs.

Solar collectors' efficiency is limited by low solar radiation absorbance and low thermal conductivities of conventional working fluids. Various metals have been researched, predominantly for the use of improving the thermal conductivity of heat exchange fluids, but research has been done with multi-wall carbon nanotubes

(MWNT), single-wall carbon nanohorns (SWCNH), graphite, graphene and carbon. From the fluids typically employed as heat exchange fluids in solar collectors, water shows the highest solar radiation absorbance at only 13 %. Compared to water, all nanofluids have shown a significant improvement in the solar radiation absorbance. Carbon based nanofluids have excellent photo-thermal properties with graphite nanoparticles in water as base fluid found to absorb 96 % of solar radiation and SWCNHs found to absorb 95 %. This shows the possibilities in improving the efficiency of DASC's using carbon based nanofluids.

The biggest limitation to using nanofluids in any application is the stability of the nanoparticles in the fluid. Nanoparticles have a very high surface area to volume ratio that relates to a high surface energy and strong van der Waals forces acting between the particles attracting each other. This results in a tendency to agglomerate and lower the surface energy of the particles. The agglomerated particles have larger sizes that increase the settling rate and decrease the stability of the nanofluid. In previous studies, nanofluids are characterised as stable without a standardised definition of stability. Therefore, a "stable nanofluid" in this study is described as the negligible settling of nanoparticles from the base fluid that does not negatively affect the efficiency of the system.

CHAPTER 3: SUMMARY OF PRIOR WORK

3.1 INTRODUCTION

This chapter briefly summarizes all the prior work done as justification for the current project. The design, operation and characterization of the solar concentrator platform are given. Next the key aspects of the low cost foam material are highlighted both in terms of production and testing, as well as initial efforts to create a stable nanofluid. Finally the first attempt at achieving a thin-film evaporation unit is recounted.

3.2 NOVEL SOLAR CONCENTRATOR

A novel solar concentrator platform has been developed at the University of Pretoria. The system uses only existing technology and cheap, off the shelf components to achieve high levels of concentration. It is a modular structure ensuring scalability to community needs. A small scale prototype of the novel solar concentrator was built for proof of concept and configuration testing. The device uses a circular Fresnel lens which traditionally requires very accurate tracking to maintain its focal point. In addition, the lens requires a collimated light source, making the use of conventional electrical lighting impossible. For most practical purposes sunlight can be considered collimated making it ideal.

The use of sunlight has the additional benefit of replicating the electromagnetic spectrum exactly, instead of the approximation afforded by for example metal halide lamps. Unfortunately due to the trajectory of the sun across the sky, even if the lens tracking is impeccable the focal point will not be horizontal and its position in space will move as the sun moves. For these reasons the opposite approach was adopted: the lens is kept fixed and instead sunlight is reflected through a series of mirrors, shown schematically in Figure 1.

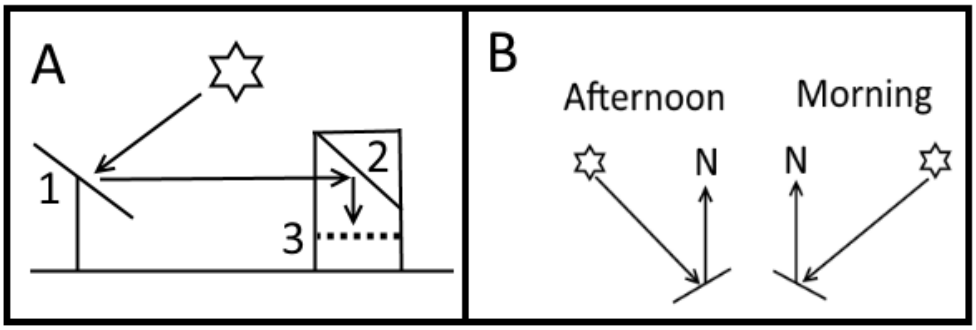

Figure 1: Schematic of tracking system (A) side-on and (B) from above.

The platform is oriented in a North-South direction (facing North given the current location in the southern hemisphere) with mirror 1 tracking the sun and mirror 2 being stationary. As can be seen from Figure 1 B, when viewed from above, mirror 1 maintains an angle perpendicular to the direction given by the centreline of the angle between the sun and true North. In this way sunlight is reflected in a northerly direction throughout the day independent of the azimuth angle of the sun. The elevation of the sun is compensated for by adjusting the angle of the mirror with respect to the earth's horizontal level. Thus the system uses a simple two axis tracking method which has been employed extensively in photovoltaic implementations.

The secondary mirror is not required if a horizontal beam of light can be used. However, for this investigation a vertical beam of light was preferential for the experimental setup. In this manner a downward directed, beam of collimated sunlight is produced, perfect for use with a Fresnel lens positioned at the dotted line in Figure 15,

i.e. location 3. The height of the focal point can be adjusted by varying the height of the lens. The system is shown in operation in Figure 16.

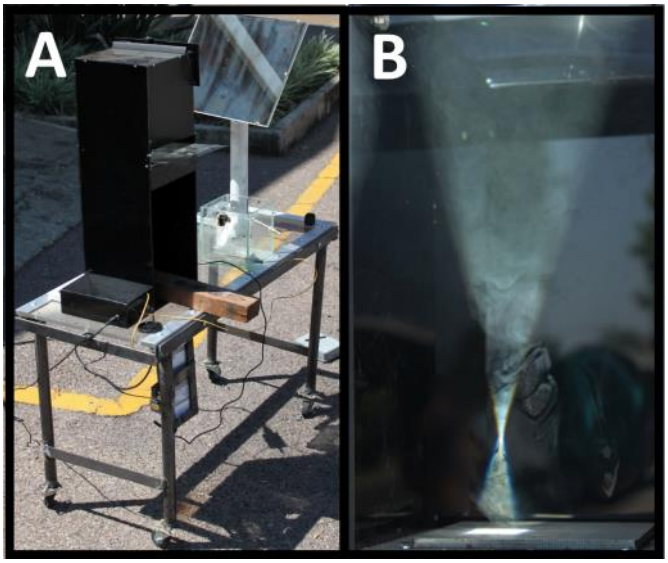

Figure 2: (A) Operational solar concentrator and (B) focal point.

As can be seen from Figure 2 B the assembly produces a concentrated beam of sunlight with a clear focal point. The lens is made from a polymer (PMMA) and results in only a small spectral loss, as demonstrated in Figure 3, where the solar spectrum above and below the lens is compared.

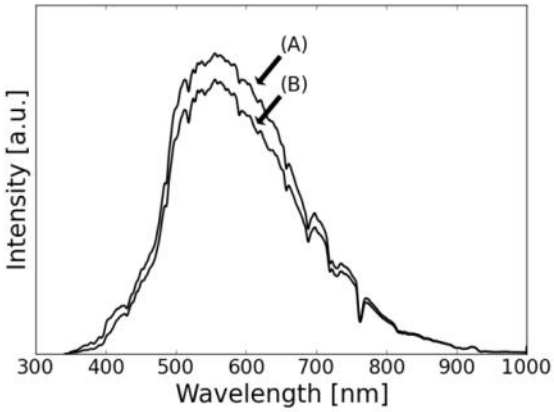

Figure 3: Solar spectrum comparison (A) above and (B) below the lens.

An Apogee Instruments PS-100 spectro-radiometer with a spectral range of 350 to 1150 nm and spectral resolution of 1 nm was used to measure the electromagnetic spectra. In addition the spectro-radiometer is calibrated to measure the total incident solar radiation in W/m^2, thus the total energy incident on a test sample can be accurately calculated. The lens leads to a reduction of 24% in the transmitted solar energy.

The laboratory scale prototype provided the validation and operational inputs required to design and build the pilot scale prototype. Most significantly it was found that the use of an automated tracking system created operational issues. During winter the system was unable to track the sun correctly due to the lowered intensity of the sun. The light dependant resistors had to be recalibrated and the tracking code rewritten.

For this reason the pilot scale design was not fitted with a tracking system but is instead pre-programmed with a fixed trajectory depending on the geographic location and time of day/year. Thus the system is independent of the yearly light intensity and this design has the added benefit that the tracking is not impeded by periodic cloud cover. The mirror will continue to track the sun despite lacking line of sight. The downside of this is the potential for slight misalignment of the mirror compared to online tracking correction. However the mirror was slightly overdesigned thus this has no impact on the achieved flux density. Based on the operational

experience and testing completed on the laboratory scale system the pilot scale unit was developed as shown in Figure 4.

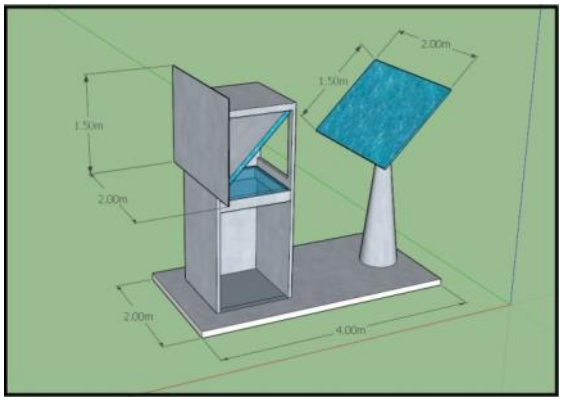

Figure 4: Pilot scale concentrator design.

The unit was then fabricated by a local renewable energy company, Netshield, who specialise in tracking systems for large photovoltaic units. The concentrator has its own power supply and battery storage, thus it is capable of fully independent, off-grid operation, making it suitable for deployment in off-grid areas. In this implementation a Fresnel lens with a diameter of 1 m was procured from China. This implies that the average power of the unit, at its current location in Pretoria will be 2200 kWh/yr. The expected peak output during summer will be approximately 1.1 kW. As mentioned earlier this system is not fitted with an on-line tracking system but is instead fitted with a built-in, pre-programmed tracking pattern. The tracking platform is fitted with two slew drive motors for accurate positional control, the completed concentrator if depicted in Figure 5.

Figure 5: As-built concentrator platform.

As mentioned, the mirror is over-sized, this has two benefits: firstly any small alignment errors due to tracking are negated since the lens will still have full solar coverage. In addition, this drastically extends the systems operational hours. By increasing the width of the mirror to 2 m the system can operate even during the early hours of the morning, in both summer and winter. During the former, the sun rises behind the perpendicular at an azimuth angle of ~116°. Based on the mirror width and lens width the current system can achieve tracking at an azimuth angle of 120°, thus it can potentially be used from sunrise to sunset. The mirror height of 1 m enables operation even at the maximum elevation angle of the sun ~92°.

The location was chosen as the Experimental Farm since this location offers a ground based position with no interference from any terrestrial objects during the entire year. The Fresnel lens was chosen based on availability, it is a circular lens i.e. point focus, with a diameter of 1 m and a focal point of 1.3 m. If the system proves commercially viable, it may be attractive to increase the mirror size. By increasing the size it may be possible to achieve four times the throughput in virtually the same tracking platform. The tracking platform and motors are designed to carry much heavier photovoltaic systems, thus it is capable of handling a much larger

mirror with virtually no additional cost. In the case of commercial operation the current over-sized mirror design may however not be cost effective. Thus a cost benefit analysis would have to be done determine the optimal mirror size and calculate the trade-off between mirror cost and increased operational hours.

As a preliminary estimate of the system performance a simulation of the platform was constructed in the SolTrace software package [23]. The Fresnel lens is replicated through the use of a segmented parabolic lens which is shifted, exactly as in the basic design of a Fresnel lens. However, to confirm the assumptions regarding lens geometry and fabrication technique, a small cross section of the lens was analysed using optical microscopy as shown in Figure 6.

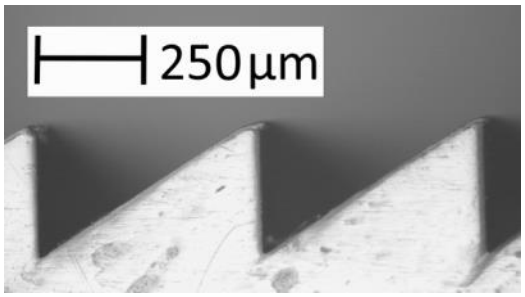

Figure 6: Lens cross-section.

The angles and distance to the centre-point were accurately measured which enabled confirmation of the fabrication accuracy and the lens focal point of 1.3 m. The model configuration is displayed in Figure 7.

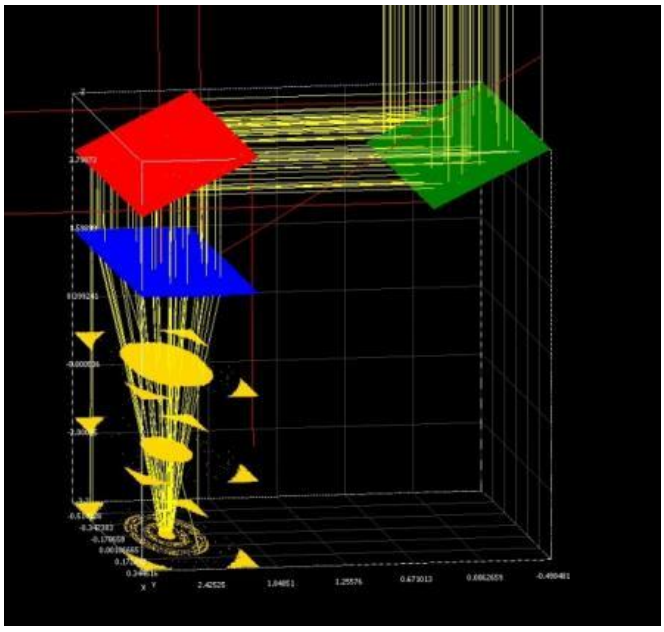

Figure 7: SolTrace model of concentrator platform.

Based on visual inspection of the operational system, it is estimated that the smallest achievable focal point has a diameter of around 10 cm. This was done by placing a black metal target at different heights until the minimum was found. Naturally this height coincides with the focal point of the lens but due to fabrication and physical limitations this point is never infinitely small but has some measureable dimension. Using the lens size this places the theoretically achievable concentration ratio at 100. This is confirmed by the simulation for which the results are presented in Figure 8.

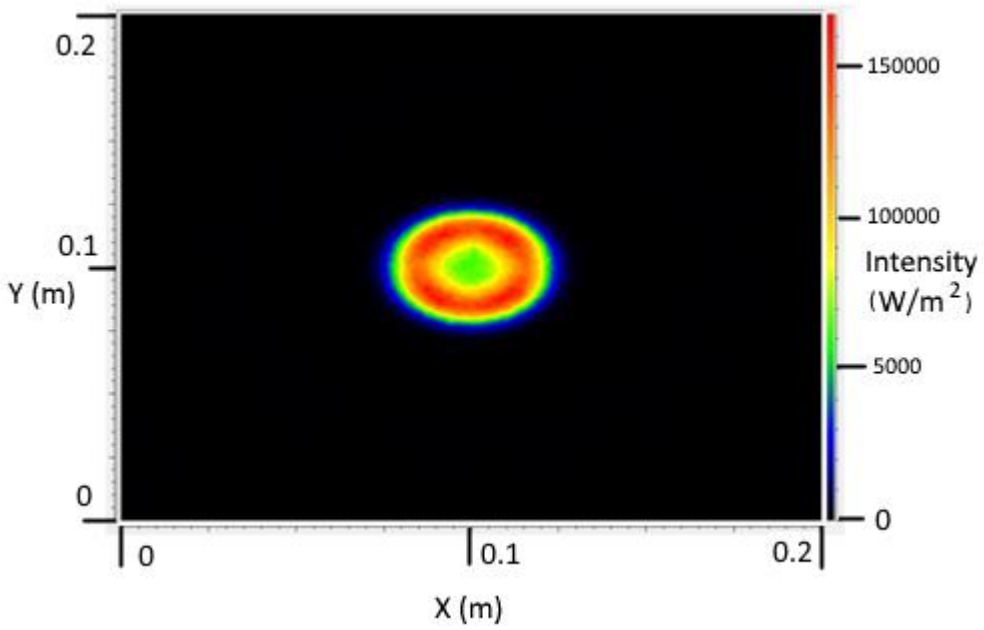

Figure 8: SolTrace concentration prediction.

The flux intensity output shown is for a solar irradiation level of 1000 W/m^2 on the primary mirror. It is interesting to note however that the model predicts an uneven flux distribution. The flux intensity at the inner and outer edges of the focal point are estimated slightly below the theoretical value of 100 000 whilst the annular region in the middle is estimated as being slightly higher. To confirm this distribution the flux intensity was physically measured at a distance of 20 cm below the lens using an Apogee Instruments MP-200 Pyranometer. These measurements are compared to the SolTrace prediction as shown in Figure 9.

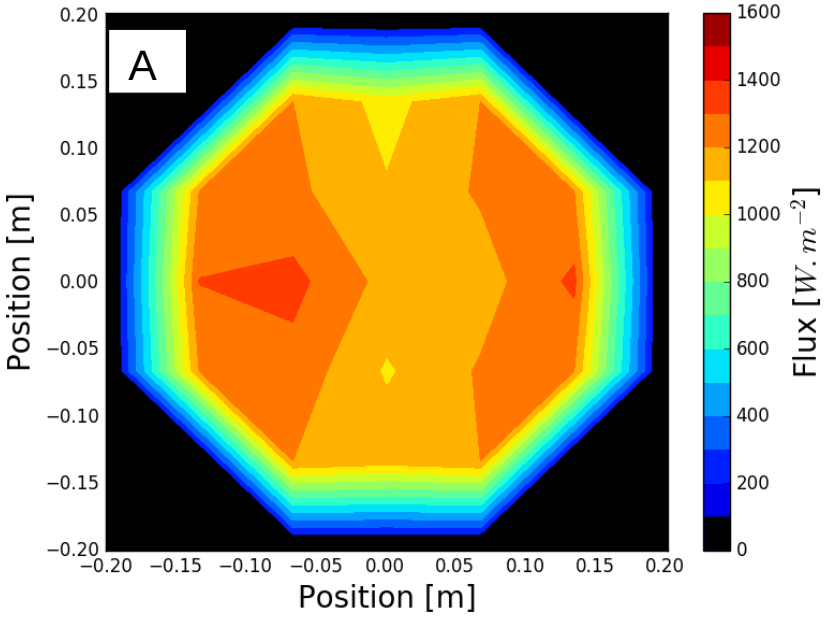

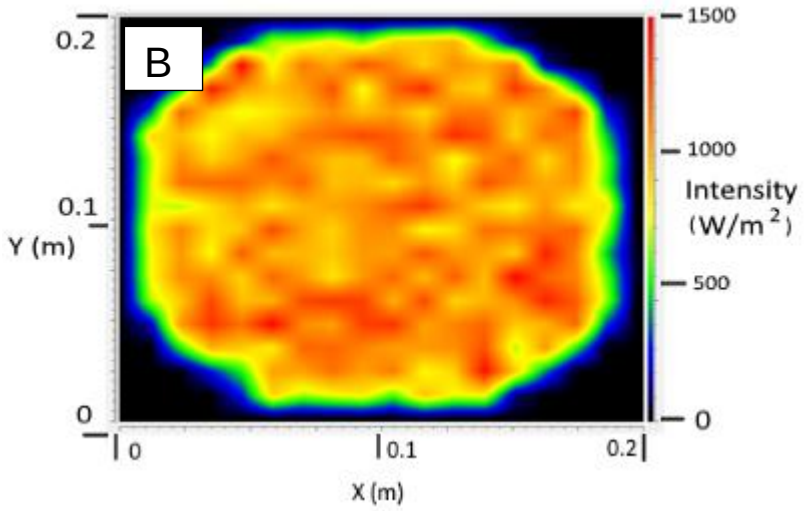

Figure 9: a) Measured and b) predicted solar flux concentrations.

This confirms the general randomized, evenly distributed behaviour at low concentration and gives an indication of the expected flux distribution on the flow cell. The predicted random distribution and concentration levels were used as the basis for the system and flow cell design taking into consideration the real lens geometry.

3.3 FOAM PRODUCTION AND PRELIMINARY TESTING

For the production of the foams coal tar pitch (110MP) was obtained from Arcelor-Mittal (South Africa) with a softening point of 63 ºC and a coke yield of ~44 wt %. The quinoline insolubles and toluene insolubles are 9 and 34 wt %, respectively. The Aromaticity Index is 0.53 and the C/H atomic ratio is 1.83. The expandable graphite (EG) grade ES170 300A (onset temperature 300 ºC) was obtained from Qingdao Kropfmuehl Graphite (China). According to the manufacturer, it produces >170 millilitre/gram exfoliated material when heated above 300 ºC. This implies that a gram of material expands to fill a volume of 170 millilitre upon heating, achieving a bulk density of (0.006 g/cm^3).

In short the foam production process is as follows:

- Pitch is heat treated at 437 ºC for 6 hours to produce mesophase pitch
- The pitch is ground and dry mixed with expandable graphite
- The mixture is foamed in air at 460 ºC and cross linked at 250 ºC
- The foams are then carbonized (1200 ºC) and graphitized (2600 ºC)

The foams and precursors were extensively characterized using the following techniques: Mastersizer particle size, BET surface area, skeletal and bulk density, thermogravimetry (TGA), thermomechanical analysis (TMA), dynamic mechanical analysis (DMA), rheometry, optical microscopy, scanning electron microscopy, Raman spectroscopy, X-ray diffraction and thermal diffusivity.

A key property of expandable graphite is its ability to exfoliate in a narrow temperature range as confirmed by the TGA mass loss and the TMA expansion occurring during the exfoliation process. The TGA indicated a single-step exfoliation event with an onset temperature above 250 ºC. By 600 ºC the sample has lost 10% of it mass owing to the CO_2 and SO_2 gas released during the exfoliation. The TMA onset temperature for the exfoliation is about 300 ºC. However, the TGA curve shows that mass loss commences at a lower temperature. The XRD diffractograms (shown in Figure 10) of the expandable graphite in the neat and exfoliated form showed a reflection that corresponds to the same d-spacing as pure natural graphite. The neat expandable graphite sample also feature an additional reflection located at a lower angle. This reflection is due to the

sulphuric acid intercalated graphite phase. After exfoliation, it disappears and only a pure graphite reflection is evident.

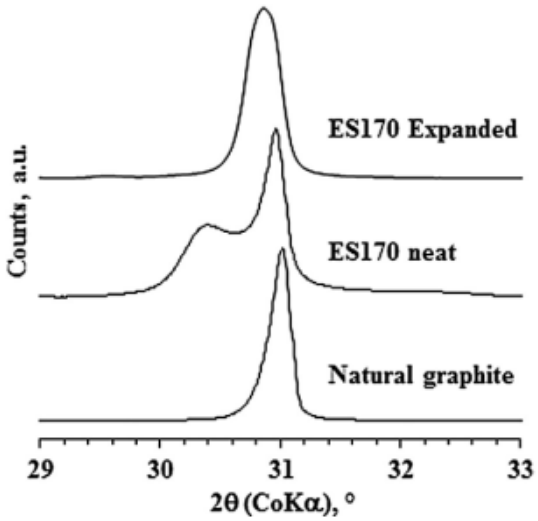

Figure 10: XRD diffractograms**.**

A polished surface of the heat-treated pitch under reflected light, shown in Figure 11, revealed a high concentration of quinolone insoluble particles aggregated around the spherical mesophase spheres. The presence of these particles probably prevented coalescence of the mesophase spheres into larger drops. The mesophase content was estimated at 47 volume% from image analyses. Mixtures of mesophase powder and expandable graphite (EG) were made starting at 1 wt.% EG and increasing in 1 wt.% increments up to 10 wt.% EG. The 2% mixture did not really produce a foamed structure and visually appeared to be a piece of solid mesophase while the 7 wt.% EG mixture produced foam that had little structural integrity. Homogeneous foams were obtained for samples that contained 3, 4, 5 and 6 wt.% EG. The mixtures containing higher concentrations of EG produced foams that were not homogenous: the top layer was much less dense than the bottom part of the foam.

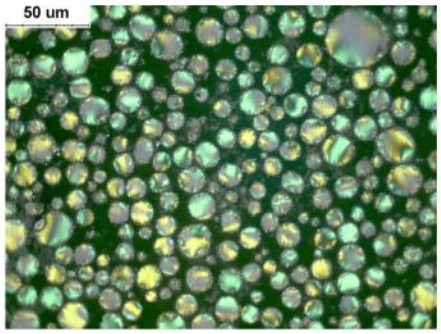

Figure 11: Optical micrographs of heat-treated pitch**.**

Figure 12 A shows photographs of a green and a graphitized foam sample obtained with the addition of 5 wt.% expandable graphite. Figure 3 B shows a close-up of the microstructure of this foam. It illustrates that the porosity of the foam derives from the loose packing of the flexible “worms” as well as the porosity of these “worms”. Thus the porosity is not uniform and there is a wide distribution of pore dimensions. The outer surfaces of the graphite “worms” are coated by a thin layer of residual pitch. However, regions rich in pitch are also visible. When the foam is cut or fractured, the “worms” are strongly bound to the pitch network.

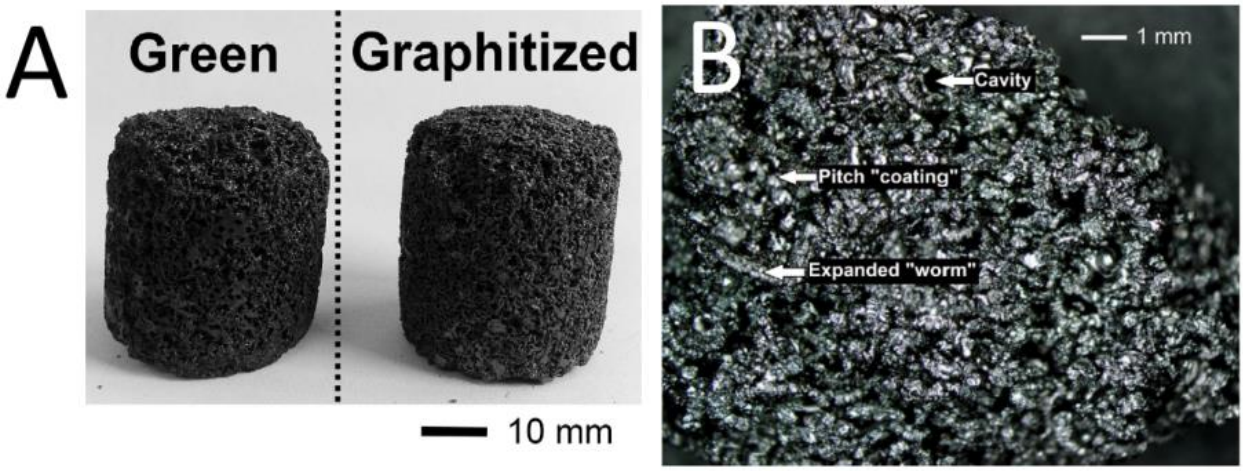

Figure 12: Optical micrographs of heat-treated pitch**.**

The characterization demonstrated that the foams are highly porous. The density of the graphitized foam prepared with 5 wt.% expandable graphite was 0.249 g/cm^3. Considering the volume expansion of the expandable graphite, the volume shrinkage of the foam and the mass losses on heat treatment, the theoretical lower limit for the foam density is estimated at 0.112 g/cm^3. This implies that the presence of the liquid pitch must have impeded the expansion of the expandable graphite. The thermal conductivity of conventional glassy carbon foam is usually less than 1 W/(m.K). Testing showed that even the “green” foam featured a thermal conductivity that was an order of magnitude higher. This is attributed to the highly graphitic nature of the vermicular exfoliated graphite phase that forms the 3-D network in these novel foams. Carbonization improves this value slightly but it increases by almost an order of magnitude when the foam is graphitized. This suggests an oriented microstructure in the foam that facilitates efficient heat transfer through the network. For these reasons the foam was considered an ideal starting material for the transfer of solar energy to heat a medium.

A solar simulator was constructed for the purposes of testing the solar efficiencies of the foams. To house the graphite foams a box was constructed out of glass. The box was constructed with the intent of it being filled completely with water with the foams submerged there in and to allow for as little air as possible to remain in the box during operation as air will allow for evaporation of the water and subsequent condensation on the lid of the box which can lead to unwanted scattering of the light before reaching the foam sample. To overcome this problem the possibility of air entering between the minute gaps created between the box lid and box itself during operation was minimised by sealing the lid as tightly as possible to the rig through the use of side clamps and lining the lid edges with rubber. Furthermore, two holes were constructed towards the top of the box and on either side to aid in the process of filling the box with water by tilting the box to the side so that one hole is facing downward and the other upward. Water was pumped from the downward facing hole and the air trapped in the rig released from the upward facing hole. Once the box was pumped full of water the holes were sealed by means of cork. A thermocouple was inserted in a third hole at the bottom of the glass box. A computer aided design of the glass box is shown in Figure 13.

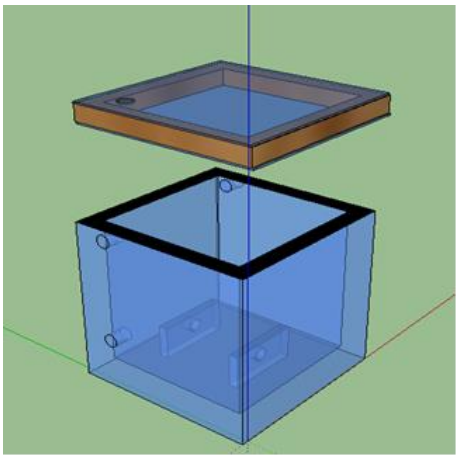

Figure 13: Water filled box for heat transfer tests**.**

Another problem that this rig was designed and built to overcome was the problem of the foams floating in the water. Because concentrated solar radiation is to be used, it is undesirable for the foams to float away from the point at which the radiation is being concentrated during a solar simulation. In order to anchor the foams in place, string was attached to the foams and then fastened to the box by threading and tying the string ends to the two holes that were drilled into each of the glass rectangles protruding from the floor of the box as shown in Figure 13. A double glass lid design was incorporated to thermally insulate the top of the glass box when a stagnant zone is created between the two layers. The glass box was then placed in a larger box made out of wood with a square base allowing a clearance of 14 cm between the wall of the wooden box and that of the glass box. This clearance was filled with fibre glass to provide insulation.

This system was used to conduct heating trials of water under an electrically simulated solar lamp. To simulate solar radiation a Phillips Master MHN-SE 2000W metal halide lamp was used. The spectrum of the sun and that of the halide lamp obtained by means of the spectro-radiometer is shown in Figure 14. A comparison of the two spectra reveals a decent amount of accuracy possessed by the halide lamp in simulating the sun's spectrum.

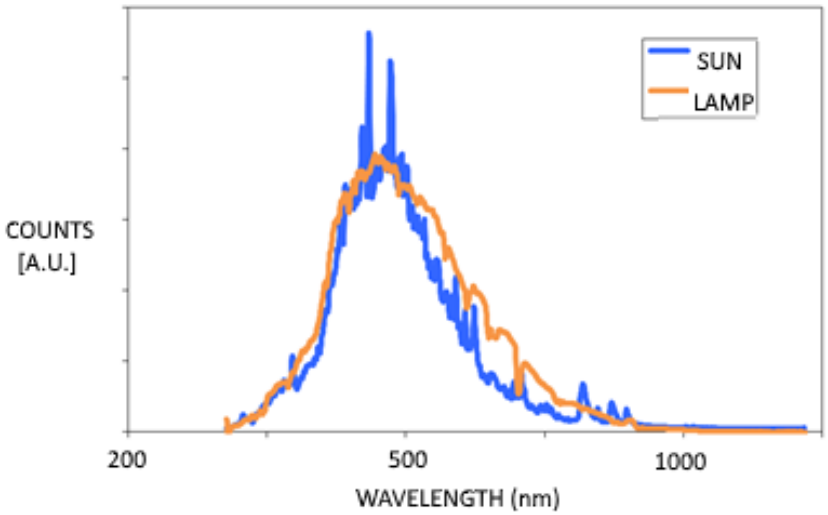

Figure 14: Radiation spectra of both the sun and the halide lamp**.**

The foams were placed in the sealed container with a measured amount of water. The container and insulating box were then placed beneath the solar lamp and left to heat up. The temperature of the water is continually measured and used to calculate the amount of heat transferred to the water. An example result of one such heating trial is shown in Figure 15.

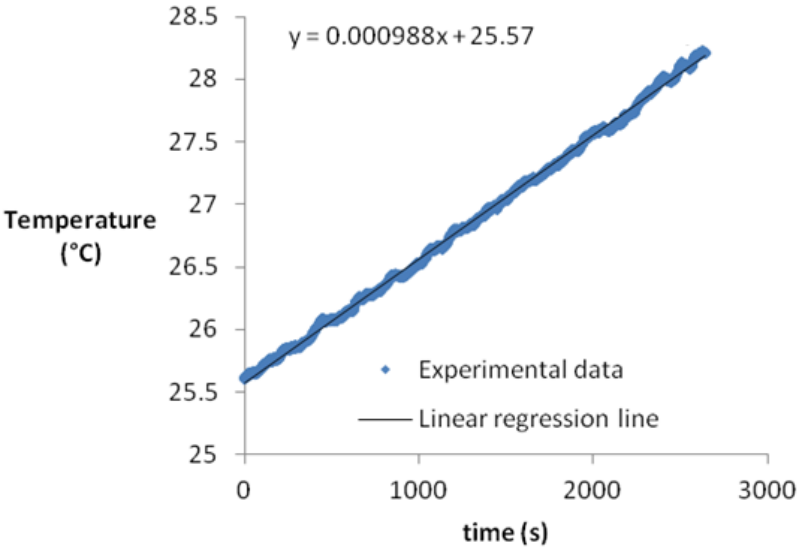

Figure 15: Water temperature over time during heating test**.**

Only the data for the period where the system had achieved a steady temperature increase was used, amounting to roughly one hour of heating. The incident radiation level above the box is measured using the spectro-radiometer, which allows the thermal efficiency of the foam to be calculated. Based on these tests efficiencies of around 70 % were calculated. Thus highly thermally conductive, low-density and inexpensive carbon foam was successfully prepared from a coal tar pitch and expandable graphite with a high exfoliation onset temperature. The foams demonstrated good heat transfer efficiency under simulated conditions and for these reasons they were selected for this project.

3.4 CARBON BLACK SUSPENSION DEVELOPMENT

This section details the development of a suitable carbon black suspension material for use as a solar absorber. The initial issue with carbon black was achieving a good dispersion of the particles in water without subsequent settling over time. The as-received carbon black was found to be extremely hydrophobic and tended to agglomerate in lumps which immediately settle out of the water. After much experimentation sonication was shown to be a suitable method to break up the agglomerate groups and fully disperse the carbon black in the solvent. The carbon black demonstrated excellent radiation absorption capability at low concentrations as can be seen from Figure 16.

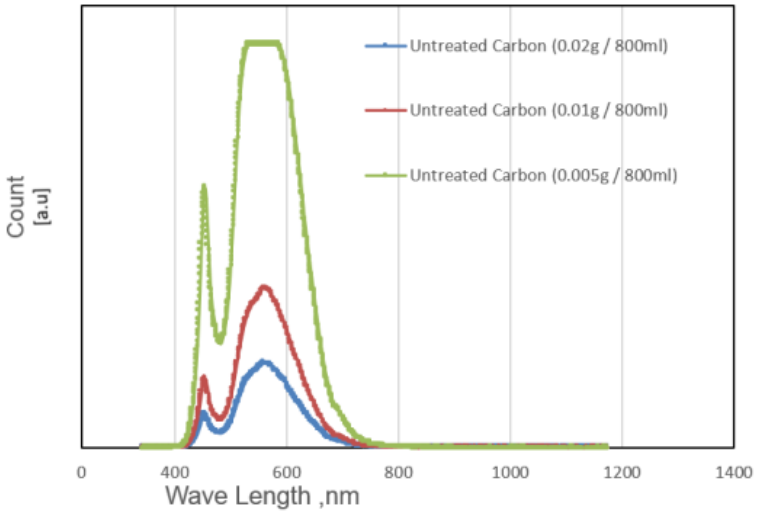

Figure 16: Settling behaviour of carbon black.

Even at concentrations as low as 0.003 wt% the sonicated suspensions demonstrated an over 95% drop in the amount of transmitted radiation over a 5cm path length. Unfortunately however the particles would still rapidly settle out. The same situation was not found for ethanol as a solvent, this lead to the conclusion that the surface groups on the carbon black may be affecting the dispersion stability. To explore this phenomenon a photodiode was used in combination with the spectro-radiometer. This allowed the transmission of light through a suspension to be monitored over time, across the entire visible range. No preferential absorption reduction was found as can be seen from Figure 17.

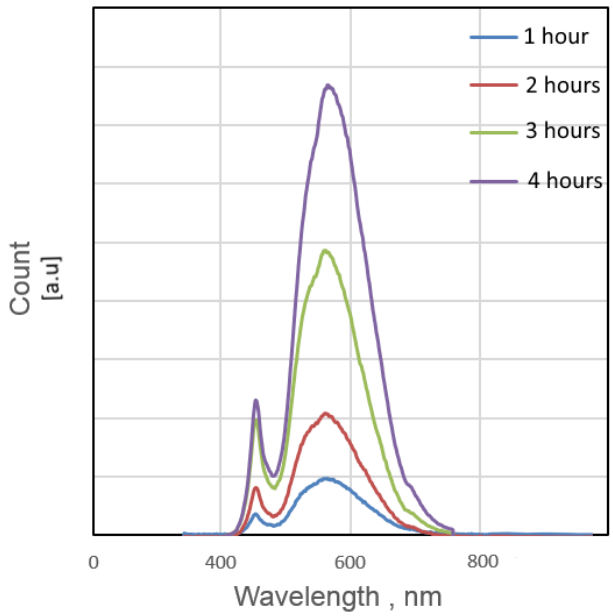

Figure 17: Settling behaviour of carbon black.

As can be seen from the figure the carbon black rapidly settles out with an even increase in the amount of radiation transmitted over time. Within only four hours virtually all the material had settled and an intensity corresponding to pure water was obtained. To combat this a wide variety of oxidative surface treatments were explored, including sulphuric acid, nitric acid, hydrochloric acid, sodium hydroxide, hydrogen peroxide and strong oxidizers like potassium dichromate. A selection of concentrations and soak times were explored with little success. As can be seen from Figure 18, settling occurs within hours of dispersion.

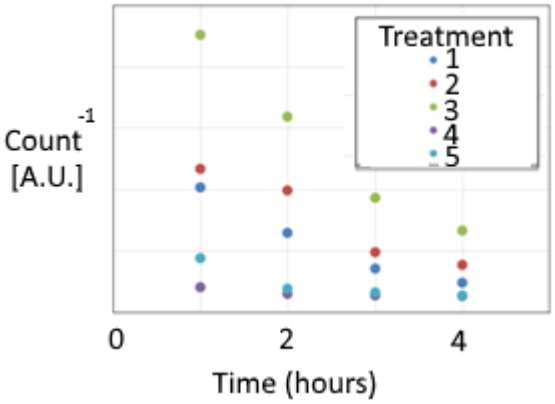

Figure 18: Settling behaviour of surface treated carbon black.

From temperature desorption experiments coupled with mass spectrometry, it was clear that the surface oxygen groups of the carbon were indeed modified but evidently not in a manner that aided dispersion stability. This can be seen from a comparison of the untreated desorption spectra and treated spectra in Figure 19.

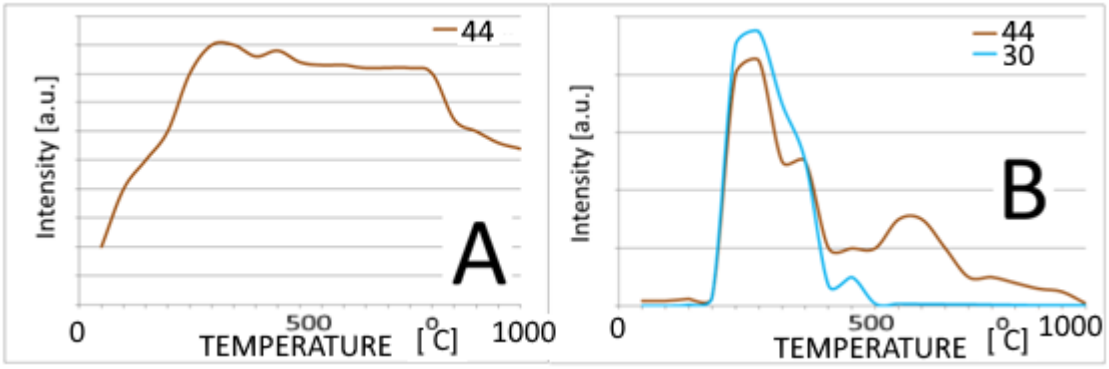

Figure 19: Mass spectrometer analysis of (A) untreated and (B) nitric acid treated carbon.

An additional factor which was observed was that the surface groups tended to degrade or transform over time. This is evident from Figure 20 which demonstrates the thermal desorption behaviour of the nitric acid treated material after soaking in water for a week.

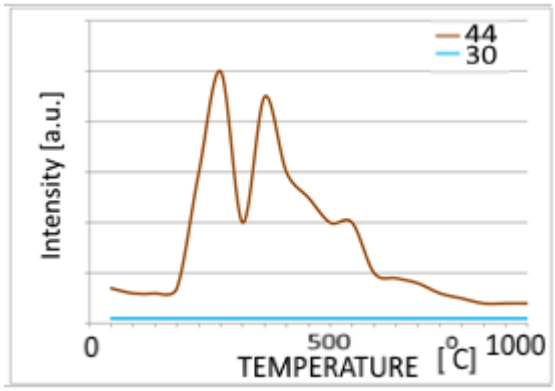

Figure 20: Mass spectrometer analysis of nitric acid treated carbon after one week in water.

Ultimately however a treatment was found which resulted in carbon black suspensions that were stable indefinitely. Carbon materials treated with 15 g of potassium permanganate, 150 ml nitric acid and 50 ml water per 5 gram of carbon were successfully dispersed. The carbon remained in suspension; however, if the carbon was dried it could not be dispersed again. It is probable that the carbon surface groups react to bind the particles together when the water is evaporated. Scanning electron images of the dried samples did in fact show a large degree of agglomeration. Furthermore it was discovered that when the sample is heat-treated to moderately high temperatures the suspension again becomes unstable. This is highly undesirable for heating applications where elevated temperatures will invariably be achieved.

As an alternative, a variety of surfactants were explored including the commercial product Tween or polysorbate 20. The stability and relative nontoxicity allows it to be used as a detergent and emulsifier in a number of domestic, scientific, and pharmacological applications. Tween successfully resulted in a stable dispersion of carbon black in water without any surface treatments. It was also demonstrated that the mixture of Tween, water and carbon could be boiled without any degradation of the Tween or the dispersion stability. For these reasons and the relatively low cost of Tween it was decided to this surfactant rather than surface treatments to disperse the carbon black in water. A variety of carbon black suspensions and Tween were prepared and tested as demonstrated in Table 3.1.

Table 3.1. Carbon black and Tween suspensions.

Path length	Energy transmittance at 600 nm	Elapsed time	% Transmittance
(mm)	(Watt/m^2)	(days)	(%)
2	0.90	0	29

3	0.37	0	11
5	0.080	0	2.4
6	0.026	0	0.81
8	0.007	0	0.22
9	0	0	0.00
13	0.011	0	0.33
2	1.3	1	36
3	0.57	1	16
5	0.15	1	4.3
6	0.082	1	2.3
8	0.038	1	1.2
9	0.017	1	0.47
13	0.0083	1	0.23
16	0.0063	1	0.17
19	0.0061	1	0.17
25	0.0048	1	0.14
31	0.0053	1	0.16
3	0.63	3	18
6	0.086	3	2.4
8	0.043	3	1.2
9	0.0040	3	0.11
13	0	3	0.00
3	0.31	6	12
5	0.061	6	2.3
6	0.036	6	1.4
9	0.0080	6	0.31
13	0.0045	6	0.17
16	0.0039	6	0.15
19	0.0037	6	0.14

The results indicated that a carbon concentration of around 0.01 wt% was sufficient to achieve full absorption over path length of 13 mm. Additional testing was carried out and it was found that only 0.02 wt% Tween was needed to achieve a fully homogenous suspension without any agglomeration. These loadings are extremely low for achieving such marked benefits using additives. The tests were carried out over a period of a week and as can be seen from Table 3.1 the suspensions remained stable, retaining their excellent absorption properties. In the interim these results have been extended to time periods of several months. These results demonstrate that full absorbance can be obtained at a concentration of 0.01% wt carbon black over a very short path length and the suspension is stable for periods beyond a week. For these reasons a carbon black/Tween suspension was chosen for this project.

3.5 CONCEPTUAL THIN-FILM SOLAR STILL

During prior work a thin film evaporator concept was developed to theoretically enhance the efficiency of standard evaporator designs. It was initially proposed that if, in addition to having a thin film of liquid flowing

over a flat plate collector, it was possible to have a dry, fresh air stream flowing counter-current over the film, high evaporation rates could be achieved. To test this idea a lab scale test bed was designed and built, as shown schematically in Figure 21.

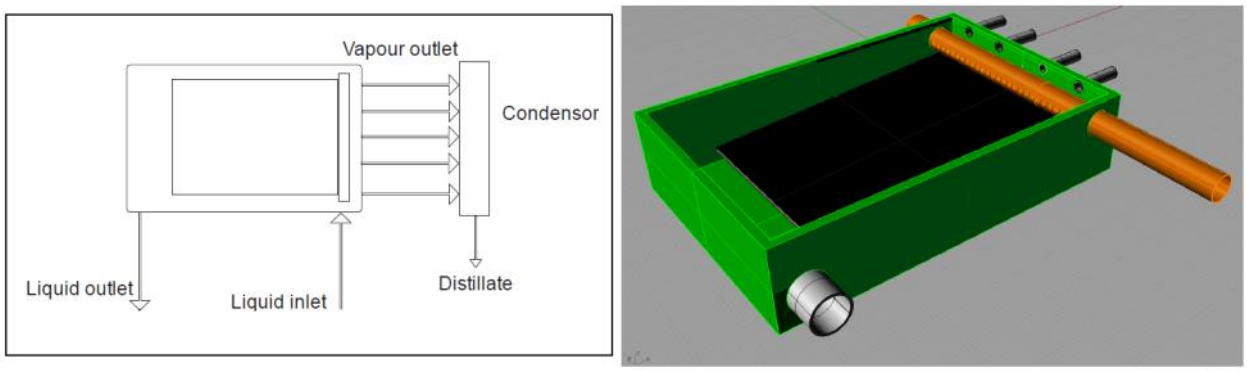

Figure 21: Thin-film evaporator design.

Water is pumped into the evaporator through a distributor constructed from a perforated copper pipe. It slowly flows over a flat plate solar collector at a very small angle. The flat plate is coated with a mixture of carbon black and paint to make it completely black and fully absorbent to light. The plate is enclosed in a sealed and well insulate container, while the top surface of the container is sealed using either glass or polycarbonate to allow radiation through. Sunlight onto the plate is simulated using two 400 W Haloline Eco lamps with a measured output of 1085 W/m^2 per lamp. The fluid heats up and a portion is evaporated. Air flow through the evaporator is achieved by a vacuum pump attached to the condenser outlet. The system operation is demonstrated in Figure 22, with the lid removed.

Figure 22: Thin-film evaporator operation.

From this image one of the initial issues with this design is clearly visible: uneven distribution of water over the plate. Despite the application of several thin coats of paint onto a very smooth surface, it was not possible to achieve an even distribution of water flowing over the plate. During operation this would result in regions where insufficient wetting took place and dry spots occurred. The water vapour from the plate must be condensed and collected as distillate. The flow of dry air across the evaporator plate should increase the driving force for evaporation by lowering the relative humidity above the plate. However, initially this system resulted in very low yields. It was determined that this was caused by condensation difficulties. This is mainly due to the relative humidity influence whereby the dilution effect of the air reduces the amount of vapour that can easily be condensed, as opposed to a pure water vapour stream which could be relatively easily condensed fully. To overcome this issue an oversized manifold was used to achieve maximum condensation. The entire condenser was placed in a cooled water bath to ensure condensation as demonstrated in Figure 23.

Figure 23: Submerged condenser.

Under these conditions it was found that the thin film receiver was capable of quite high distillation rates. Crucial operating parameters were still maintaining the thickness of the film and the even distribution of liquid across the plate. Unfortunately this is not a practically feasible system as the cost and cooling associated with the condenser would be prohibitively expensive. However, the work indicated that if a solution could be found which consistently achieves an evenly distributed, thin liquid water film on a black receiver, high yields are possible. In the absence of a flowing air stream the dilution effect would be drastically reduced and the condenser requirements would be significantly lower, making it achievable using simple air cooling. Such a modified design is indicative of a wick driven system for a traditional sealed basin still, which is the focus of this project. In addition, a review of literature included in the prior section has indicated that this design would be perform best when coupled to a multistage, phase changed based condenser.

3.6 CONCLUSIONS FROM PRIOR WORK

The prior work demonstrated that highly conductive graphite foams could be produced from low cost, locally available materials. In addition, it was shown that a stable carbon black suspension in water could be achieved using a simple, non-toxic surfactant. For this reason these two approaches we selected for comparative assessment as solar collectors under concentrated sunlight. The two methods represent fundamentally different mechanisms for absorption and as such would give a relative indication of the capture efficiencies possible using these techniques. First however these materials must be fully characterized and optimized for the specific application.

The thin-film solar still demonstrated that modern designs could indeed deliver higher yields, however several practical issues remain to be overcome. The primary issue is that of an even, thin distribution of water on the collector. A wick based approach was chosen as the most suitable to solve this problem. Secondly the identification of limitations either on evaporation or condensation remains difficult due to the coupling and inter-relationship of these two aspects. Thus as part of the project the aim was to use a system where these two could be decoupled, in the hopes of identifying and alleviating constraints within each separately.

CHAPTER 4: EXPERIMENTAL METHODOLOGY

4.1 OVERVIEW

This section and the subsequent results chapter are subdivided into three subsections. The first deals with the graphite foam surface solar absorber, the second details the direct absorption solar collector namely the carbon black nanofluid. Finally the experimental testing of thin-film solar still is reported.

4.2 GRAPHITE FOAM TESTING

4.2.1 Materials

Foams of differing density and surface area were produced by varying the amount of intercalated graphite in the starting mixture at 3, 4, 5 and 6 wt%. After production the foams were carbonized and graphitized in a TTI furnace (Model: 1000–2560–FP20) for 1 hour at 1500 ºC and 6 hours at 2750 ºC respectively. This process removes any hetero (non-carbon) atoms from the structure and converts the material into a highly crystalline version which is critical for achieving high thermal conductivity.

4.2.2 Methods

The production of the graphitic foams used in this investigation has been detailed in the previous section.

To measure the heat transfer capability of the foams a simple, water based calorimeter was constructed. The device is built from extruded polystyrene foam (ISOboard, South Africa). Water is not capable of penetrating the closed cell structure of the polystyrene foam. This material was chosen due to its particularly low thermal conductivity ~0.024 W/(m.K), which keeps heat losses to a minimum. Structurally it is simply a rectangle of polystyrene foam (13 cm x 13 cm x 8 cm) with a small square cavity (3 cm x 3 cm x 3 cm) in the centre of its top surface. The top surface is covered with a thin square of double pane glass (3 mm thickness). For this work standard window glass was used. To account for any spectral losses an Apogee Instruments PS-100 spectro-radiometer with a spectral range of 350 to 1150 nm and spectral resolution of 1 nm was used. The device is also calibrated to measure the total incident solar radiation of a given spectra in W/m^2.

When conducting an experiment, a fixed volume of water is placed in the polystyrene foam cavity. The graphitic foam is then submerged in the water and time allowed for the water to penetrate and fill the pores. The cavity is then topped up with a measured amount of water and sealed to ensure no leakage and no air gaps. The initial water temperature is measured and the sample is then exposed to concentrated sunlight for a fixed time period. The assembly is removed and thoroughly shaken to ensure a homogenous final temperature is measured for the water. Using the mass and heat capacity of the water, the captured energy is calculated. This ensures a representative result is achieved for the average heating rate of the water for the entire test. The cavity is significantly larger that the foam, such that the thermal capacity of the foam itself is negligible. The incident radiation on the foam (compensated for any path losses) is measured using the spectro-radiometer for each test allowing computation of the thermal efficiency.

In order to determine the optimal foam configuration several geometric parameters were varied in addition to the foam density. These include the foam thickness and upper area (i.e. the two dimensions other than thickness). When the area is varied the height of the setup is changed to ensure that the entire surface of the

foam is irradiated. This ensures that each test receives the same amount of irradiation, without any loss, while at the same time varying the intensity of the radiation. As the smallest surface is exposed to the same amount of radiation, this represents the highest solar concentration factor or intensity. In this manner the optimal thickness can be determined along with the influence of concentration factor.

4.2.3 Characterization

To confirm the extent of graphitization the foams were characterized using a PANalytical X-pert Pro powder diffractometer (XRD) with variable divergence and receiving slits coupled to an X'celerator detector using iron-filtered cobalt Kα radiation. In addition the samples were visually inspected using polarized light microscopy.

The surface areas of the foams were determined with a Micromeritics Tristar II instrument. The bulk density was calculated and the skeletal density was measured using a Micromeritics AccuPyc II 1340 gas pycnometer. Scanning electron microscope (SEM) images were obtained using an ultra-high-resolution field-emission microscope (Zeiss Ultra Plus 55 FEGSEM) equipped with an in-lens detection system and operated at an acceleration voltage of 1 kV. A working distance of between 2 and 3 mm was used. The sample was lightly deposited on carbon tape and examined without any additional sample preparation. All thermal oxidation was conducted in a TA Instruments SDT Q600 thermogravimetric analyzer (TGA) under instrument grade oxygen flowing at 500 ml/min.

4.3 CARBON BLACK NANOFLUID TESTING

4.3.1 Materials

Based on the prior work it was found that a concentration of 0.01 wt% of carbon black suspended in water had excellent absorption properties over a length of 13 mm. This was achieved using a non-ionic surfactant Tween (Polysorbate 20) at a loading of 0.02 wt%. The mixture is sonicated in water for 60 min to ensure homogenous dispersion and produce the carbon black nanofluid. The carbon black used is Printex Degussa AG grade. Seawater is simulated by dissolving 35 gram/litre of sea-salt in tap water; this is used for all experiments. However, to obtain a more detailed knowledge of the thermal nanofluid (water + carbon black) additional testing is required to determine for example, the absorption coefficient and other important physical properties. These properties will then be used as input to design and optimize the flow cell to be used for solar radiation capture.

4.3.2 Methods

The absorption properties of the nanofluid were characterized as a function of path length. Fluids with varying concentrations of carbon black is added using a 3 ml pipette into a 100 ml beaker. The height of the fluid is measured as more liquid is added to increase the path length. This was done for carbon black concentrations of 0.0005, 0.001, 0.005, 0.01 and 0.05 wt%. The beaker was placed on top of the spectro-radiometer (Apogee Instruments PS-100) beneath a solar simulator (Phillips Master MHN-SE 2000W metal halide lamp) which closely replicates the solar spectrum and intensity. The objective is to determine the percentage radiation absorbed compared to a beaker with only seawater at the same loadings. In addition, the test was repeated after the nanofluid had been used in concentrated solar experiments and left to stand for three weeks.

The photo-thermal properties are an indication of the nanofluid's ability to absorb solar radiation and thermally heat the seawater. To characterize this aspect of the fluid a simple test was constructed using polystyrene foam (ISOboard, South Africa) and 50 ml glass polytop containers (similar to test tubes). The polystyrene was chosen due to its extremely low thermal conductivity which limits thermal losses. Several cavities, each large

enough to contain a single polytop, are cut into a rectangular section of the board (10x15x30cm). The cavities are spaced far enough from each other and the sides to ensure that each polytop is sufficiently insulated. The polytops are then filled with nanofluid at varying concentrations: 0, 0.001, 0.005, 0.01, 0.05, 0.1 and 0.2 wt%. Individual thermocouples are also placed in each polytop to monitor the temperature of each sample over time. All samples are simultaneously exposed to the same sunlight and the amount of energy absorbed is monitored. In this manner the optimal concentration for maximum photo-thermal conversion can be determined.

The thermal absorption depth is important to understand the penetration depth of sunlight into the nanofluid and as such the depths at which radiation absorption are taking place. Whilst prior experiments may indicate how much radiation is absorbed for a path length, this does not necessarily translate to the temperature increase at a given depth. This is mainly due to conductive and convective effects which occur due to the thermal gradient. A square container (10x10x10cm) was fabricated from ISOboard with a square cavity at its centre. The cavity extends through the entire depth of the container and is filled with fluid. A Perspex sheet is sealed to the bottom to allow any light making it through the fluid placed in the container to be observed. The temperature at 6 different depth locations is measured with thermocouples spaced 15 mm apart. The top of the cavity is open to atmosphere and is exposed to concentrated solar radiation. The temperature at each location was monitored for nanofluids at varying concentrations: 0, 0.0005, 0.001, 0.005, 0.01 and 0.05 wt%.

Once the freshwater has been recovered from the seawater the salty brine must be treated. Evaporation tests were conducted to determine to what extent it would be possible to separate the carbon black from the brine. Samples of carbon black at 0.01 wt% and seawater were prepared in 500 ml beakers and left open to atmosphere overnight to evaporate in a convection oven.

Based on preliminary design considerations a trial flow cell was constructed as shown in Figure 24 with a depth of 3 cm.

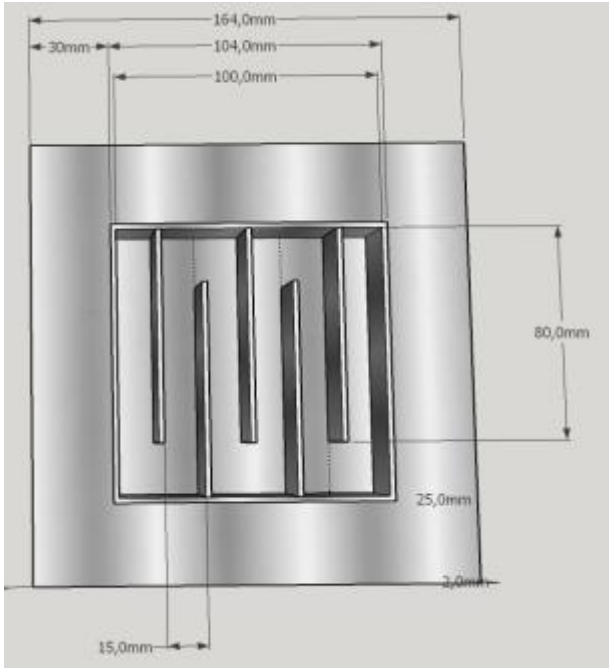

Figure 24: Preliminary flow cell design.

The operation of this flow cell was tested to be used as input in future designs. The flow cell was constructed from ISOboard polystyrene foam to limit any heat losses. The baffles and cover were constructed from Perspex. Perspex was chosen due to its low cost and excellent transmission of sunlight. Nanofluids with varying concentrations, 0, 0.0005, 0.001, 0.005, 0.01 and 0.05 wt% were pumped through the cell at a flow rate of 80 ml/min. This was achieved using a peristaltic pump operating at 10 r.p.m.

Evaporation tests where done to determine what the behaviour is when the carbon black based nanofluid is dried. This can be related to a recovery step of the concentrated brine solution after processing to recover the salt and possibly the carbon black. The nanofluid was placed in an open pan into a convection oven and evaporated overnight.

4.3.3 Characterization

A spectro-radiometer (Apogee Instruments PS-100) was used for characterizing the solar radiation incident and transmitted at different points in the path length as well as through the nanofluid itself. Temperatures were measured using K-type thermocouples linked to a National Instruments data acquisition system. Scanning electron microscope (SEM) images were obtained using an ultra-high-resolution field-emission microscope (Zeiss Ultra Plus 55 FEGSEM) equipped with an in-lens detection system and operated at an acceleration voltage of 1 kV. A working distance of between 2 mm and 3 mm was used. The carbon black nanoparticles were lightly deposited on carbon tape and carbon coated. The particle size of the carbon black particles in suspension was measured by using dynamic light scattering (DLS) principles with a Malvern Zetasizer Nano ZS.

4.4 SOLAR STILL TESTING

4.4.1 Materials

Based on experience gained during prior work and the review of existing literature it was decided to modify the thin-film design to a wick type approach. The wick design still achieves a thin-film of liquid by drawing the water through the thin wick fabric by capillary action. In addition, the system would not use dry air flow to achieve enhanced evaporation since this lead to issues with condensing the distilled water from the vapour stream at low concentrations. Indications from literature are that systems with multi-stage, PCM loaded condensers perform optimally. However, no study could be found linking a wick based, inclined still to such a condenser. For this reason it was decided to first build and test the wick based design before linking this evaporator to a secondary condenser.

The evaporator unit was designed and fabricated as dimensioned as shown from different perspectives in Figure 25 and 26. This unit can be closed and thus acts as a parallel single basin solar still. This design can however, be connected to an external condenser at a later stage.

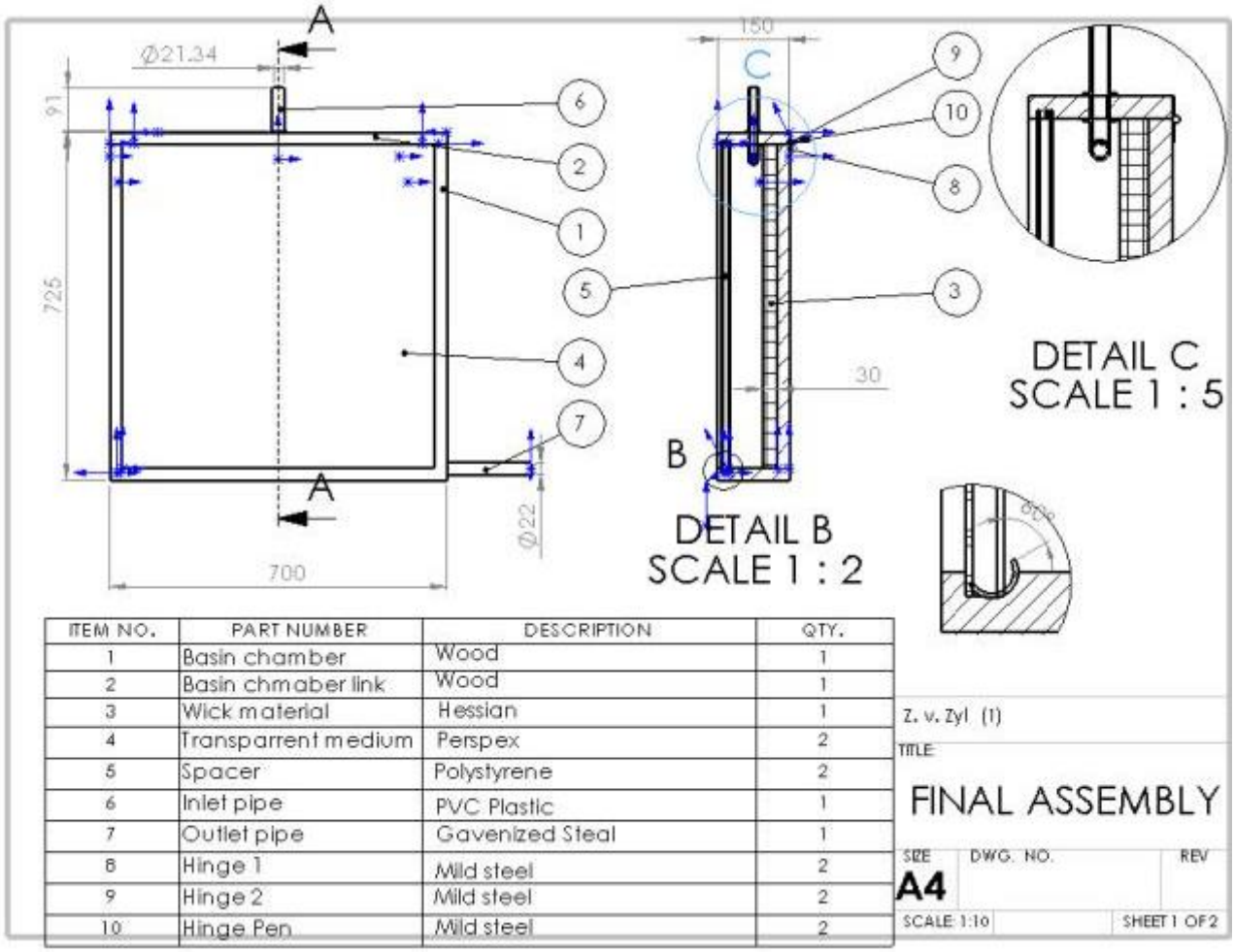

ITEM NO.	PART NUMBER	DESCRIPTION	QTY.
1	Basin chamber	Wood	1
2	Basin chmaber link	Wood	1
3	Wick material	Hessian	1
4	Transparrent medium	Perspex	2
5	Spacer	Polystyrene	2
6	Inlet pipe	PVC Plastic	1
7	Outlet pipe	Gavenized Steal	1
8	Hinge 1	Mild steel	2
9	Hinge 2	Mild steel	2
10	Hinge Pen	Mild steel	2

***Designed using Solid works**

Figure 25: Section view of designed solar still

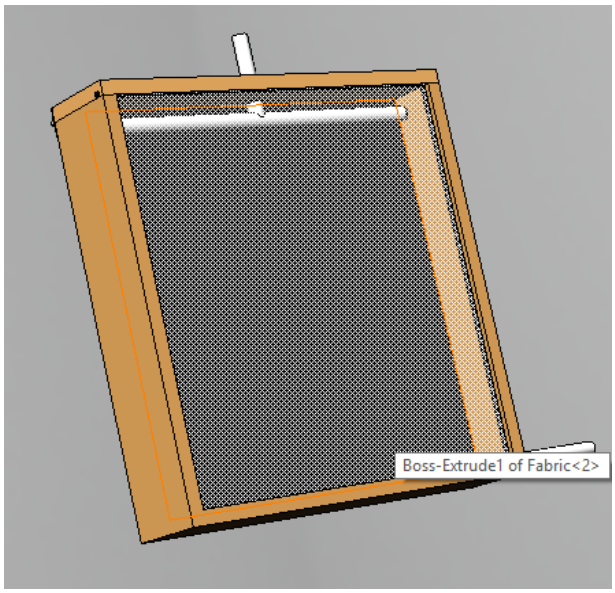

Figure 26: 3D View of designed solar still

The body of the still was built from readily available wooden materials. The upper window is constructed from Perspex due to its transmission properties. The distance between the wick surface and the Perspex was 9cm. Note that the wick is wrapped around a polystyrene foam base (ISOboard) as demonstrated in Figure 27. This

makes it easy to remove and replace the wick and the distance between the wick and the Perspex can easily be changed by inserting another layer of polystyrene.

Figure 27: Wick cloth attached to polystyrene base

In addition, the foam limits any heat losses to the bottom of the still which is the largest exposed surface. The wick area is 0.348 m^2. The wick material was already dark grey and therefore it was decided not to use carbon black to achieve the absorption. The Perspex segment closest to the wick, is pushed into the collection pipe opening, as water will condense on this surface and slide down into this tube as demonstrated in the insert in Figure 25.The collection pipe is a semi-circular section of stainless steel tubing with a diameter of 22 mm. The water distribution device is made from a section of PVC pipe, with small punched holes to facilitate even distribution across the wick as shown in Figure 28.

Figure 28: Hole for distribution pipe

The design is mobile and lightweight; it can be moved to different experimental locations. Additional material or equipment can be added to this design, like the use of silicon to seal all the connection points and thermocouple access points.

4.4.2 Methods

The unit has to be manually tilted at the desired angle and to allow the water that is collected inside the tube to flow to a collection bottle. Figure 29 illustrates the complete experimental setup with feed tank, pipe connections and product collector. The still was maintained at a constant 20º angle, consistent with the recommended angle for the latitude of South Africa. The orientation was also kept constant as North-South.

Figure 29: Front and side view of experimental setup

A suitable location was selected based on the requirement of an open area with no trees or buildings surrounding it, to ensure no obstruction with maximum sunlight at all times of the day. A tennis court was chosen as the experimental location, as it is relatively unobstructed in all directions.

The prior variables are independent while others like still angle, location and vapour gap (distance between wick and Perspex cover) are kept constant throughout the testing. The water is collected in a plastic container and the volume yield is measured in a measuring cylinder. This allowed determination of the single dependent variable, fresh water yield under different conditions.

Table 4.1 list a summary of all the parameters and variables of interest:

Table 4.1. Summary of parameters and variables.

Variables:		
Independent	Constant	Dependant
Ambient temperature (°C)	Still angle (°)	Fresh water yield (ml)
Inner still temperature (°C)	Location	
Solar radiation ($W.m^{-2}$)	Vapour gap (cm)	

Tests were conducted on 6 different days under varying conditions. Measurements of the independent variables were taken at the start of the experiment, after 20 minutes of operation and after one hour of operation. At this point the run was terminated and the total accumulated fresh water yield measured. During the initial stages of the investigation it was found that maintaining an even water distribution on the wick over the test period was difficult. Exactly matching the instantaneous evaporation rate to the water flow rate from the tank (with varying liquid level) through the valve into the distributor on onto the wick proved impossible. This either led to accumulation of liquid in the still or drying out of the wick. Therefore, to maintain conditions as consistent as possible during different runs, the wick was submerged in water at the start of each experiment. The amount of water absorbed was the same every time and this was then allowed to evaporate over the test period. For the time tested under the conditions, this never resulted in drying out of the wick, thus the still was operated in a batch fashion. This is very similar to any conventional basin still.

4.4.3 Characterization

A Major tech MT 24 thermocouple was used to measure the ambient and inner still or vapour temperature. All measurements were made in °C. To measure the solar radiation flux density, an Apogee MP-200 Pyranometer with a separate sensor and handheld meter was used to obtain a W/m^2 reading for the incident radiation.

CHAPTER 5: RESULTS

5.1 OVERVIEW

As mentioned previously this section is subdivided into three subsections. The first deals with the graphite foam surface solar absorber, the second details the direct absorption solar collector namely the carbon black nanofluid. Finally the experimental testing of thin-film solar still is reported.

5.2 GRAPHITE FOAM RECEIVER RESULTS

The graphitic nature of the foam is easily confirmed from the XRD diffractogram shown below in Figure 30.

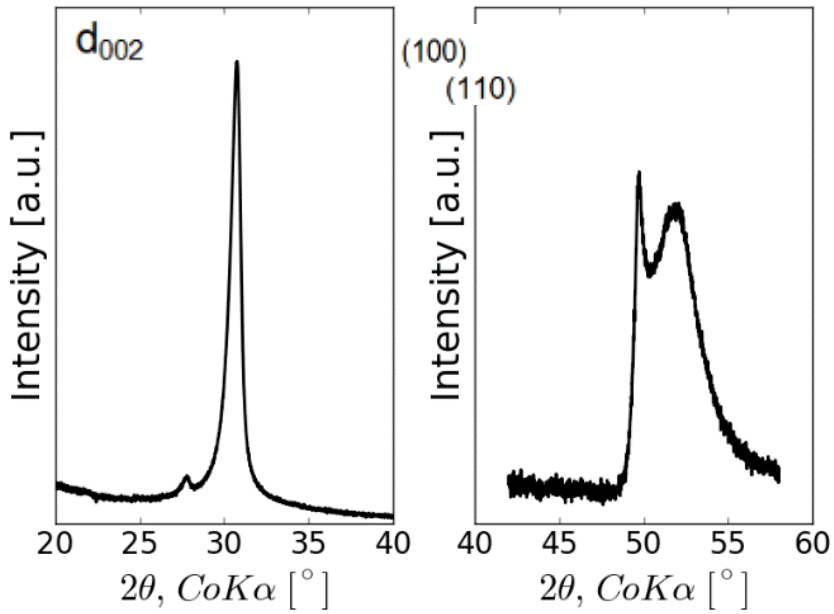

Figure 30: XRD diffractogram of selected regions for graphitized foam.

The graphitized foam clearly shows the characteristic d_{002} graphite reflection at 30.9º (CoKα) along with the (100) and (110) peaks at around 50º. Whilst this confirms the presence of graphite it indicates neither the size nor the extent of alignment of the graphitic subdomains. When the foam ligaments are examined closely under polarized light however, the graphite microstructure may be observed in Figure 31.

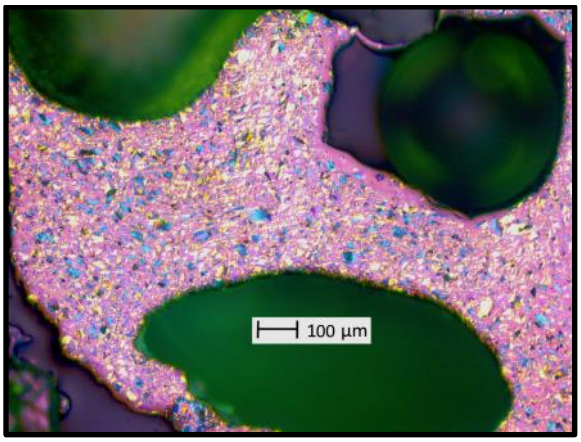

Figure 31: Optical micrograph of foam under polarized light at 50x magnification.

The sub-domains are very small and randomly oriented resulting in a fine mosaic texture. This is most likely due to the pitch milling step. Some alignment is visible near the edges of the foam ligaments but this effect is limited. This result explains the foams' fairly low thermal conductivity of around 21 W/(m.K). Initially however, skeletal density measurements were found to be on the order of ~1 g/cm^3. This is significantly lower than the theoretically expected graphite density of 2.26 g/cm^3. Thus it was concluded that the foams may have a significant portion of closed porosity. To overcome this issue a small sample was progressively oxidized in air and the results are shown below in Figure 32.

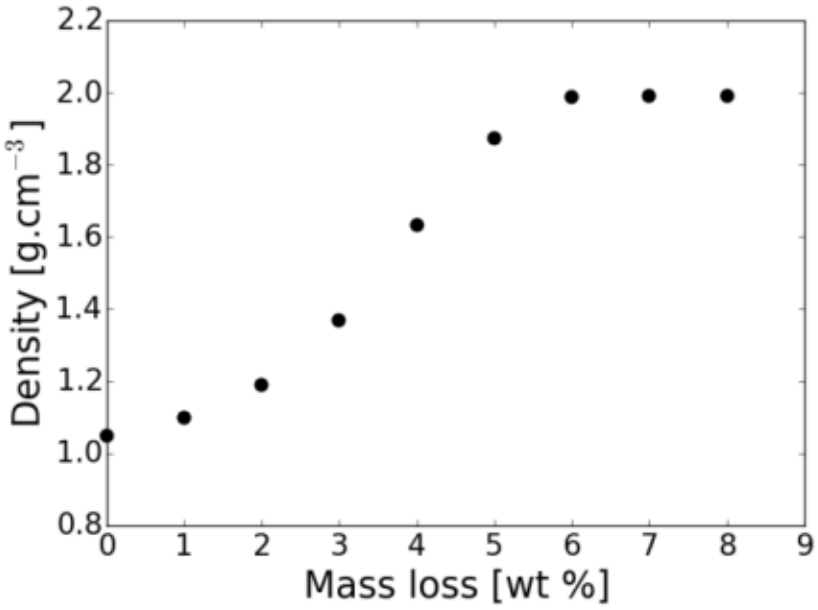

Figure 32: Foam skeletal density as a function of oxidation.

There is a steady increase in the skeletal density as the sample is oxidized and the pores are opened up. However, the value levels off beyond 6% mass loss, indicating that all pores have been opened and additional oxidation may erode the pore walls and degrade the foam structure. The final achieved density is around 2.00 g/cm^3, which corresponds to the skeletal density of the original sample measured when it is ground into a powder. The value is slightly lower than the theoretical value for a single crystal of graphite. This is in line with expectations since the microstructure of the material has a very fine mosaic texture indicating millions of small crystals with many grain boundaries and defects. In addition, given the maximum heat treatment is only 2600 ^{o}C, the transformation to graphite may not be complete.

Based on the oxidation results all foams were oxidized to a mass loss of around 6% before any heat transfer testing was done. This ensures maximum permeability of the fluid and maximum surface area for heat exchange. The foams were placed in water and heated using the solar concentrator. To compare the overall foam performance the efficiency (η) is calculated as:

$$\eta = \frac{m_W\,[kg] * C_P\,\left[{}^{J}/_{kg.K}\right] * \Delta T\,[°C] \,/\, t\,[s]}{incident\ radiation\,\left[{}^{W}/_{m^2}\right] * lens\ area\,[m^2] * loss\ \%} \qquad (5.1)$$

Where m_W is the mass of water, C_P is heat capacity of water, ΔT is the change in water temperature from the run start to finish and t is the run time. The achieved foam bulk densities as the amount of EG is increased are given in Table 5.1.

Table 5.1. Foam bulk density and surface area.

Expandable graphite [wt %]	Bulk density [g.cm^{-3}]	BET surface area [m^2/g]
3	0.419	4.13
4	0.384	3.14
5	0.355	2.04
6	0.299	1.40

As the loading of EG is increased the foam density decreases as expected. It is however interesting to note that this also leads to a substantial reduction in the BET surface area, as demonstrated in Figure 33.

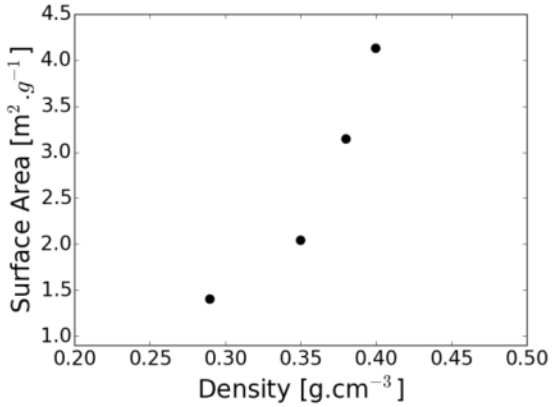

Figure 33: Variation of foam surface area with bulk density.

The reason for this reduction may be due to the fine pore structure present in the pitch derived graphite. Synthetic graphite is known to produce a fine microstructure and very small pores known as Mrozowski cracks, especially for materials with a mosaic precursor structure. As the EG loading is increased the amount of this micro-porous material decreases (for the same total mass) leading to an overall reduction in the surface area. It may be reasoned that this reduction in surface area would lead to a loss of performance, however as can be seen from Figure 34 this is not the case.

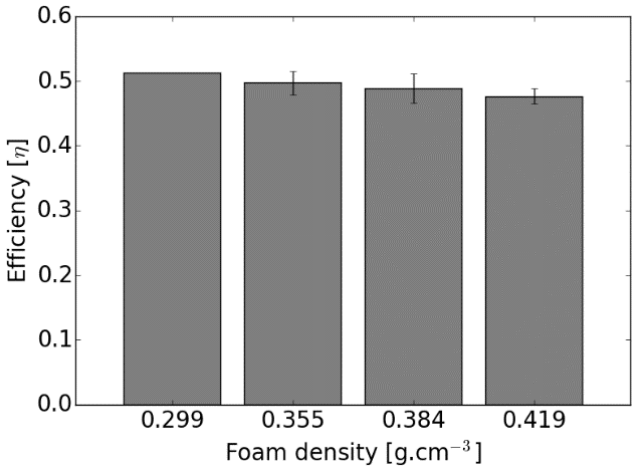

Figure 34: Foam performance as a function of density.

In fact, there is a slight reduction in the performance of the foam as the density, or equivalently surface area, increases. The reason for this is thought to be a decrease in the thermo-syphon effect whereby fluid is drawn through the foam. Due to the high heating rate at the top foam face, the water density is significantly reduced

in this zone leading to an updraft flow. Water is drawn from the surroundings and from within the foam structure to replace the outflowing material. As the density of the foam is reduced there is less resistance to this flow and more efficient transfer of energy to the water is achieved.

This concept is in accordance with the earlier assertion that the increased surface area is caused by micro-pores since these will not contribute significantly to the heating rate. For heating the bulk movement of fluid through the macro-porosity is relevant, rather than the slow diffusion of heat out of the micro-pores. As cooler liquid is allowed to flow more freely through the foam, the average driving force or delta temperature will increase, in addition to a higher convective heat transfer coefficient due to the thinner boundary layer.

Each experiment is repeated at least five times and the standard deviations are given by the error bars in the figures. The exception is the lowest density foam which degraded significantly after the first experimental run and could not be used again. For this reason the second best performing foam with a density of 0.355 g/cm^3 was chosen for subsequent analysis. In an effort to obtain the optimal foam configuration, the foam geometry was varied for the chosen foam, as detailed in Table 5.2.

Table 5.2. Foam geometry variation.

Experiment	Thickness (cm)	Area (Width x Breadth) (cm x cm)
1	2.9	2.3 x 2.3
2	1.3	2.3 x 2.3
3	0.6	2.3 x 2.3
4	0.9	1 x 1
5	0.9	1.5 x 1.5
6	0.9	2 x 2

The variation was done in two steps: first the foam thickness was varied while maintaining a constant upper surface area. Secondly the thickness was kept constant while the upper surface area was varied. In all cases the focal point of the lens, i.e. the focal size, was chosen to exactly cover the foam surface area. The reason for this choice is visible in Figure 35 below.

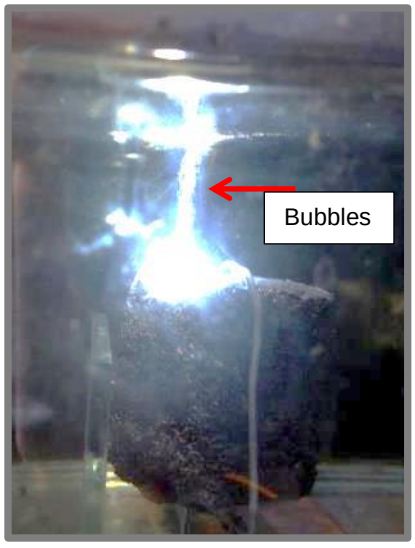

Figure 35: Nucleate boiling on foam at point focus.

When the focal size is reduced to its minimum value, nucleate boiling is observed. This leads to several complications, firstly the small bubbles tend to disperse the concentrated radiation, leading to increased losses. Secondly the bubbles themselves embody a significant energy flow which is not accounted for. They represent a large amount of heat in terms of the enthalpy of vaporization which is not quantified by measuring the water temperature. Thus to avoid any boiling the focal size is increased from point focus to the upper surface area of the foam. It should be noted that this does not affect the total incident radiation in any way since the size of the lens is fixed. The result of a variation in the foam thickness is demonstrated by Figure 36.

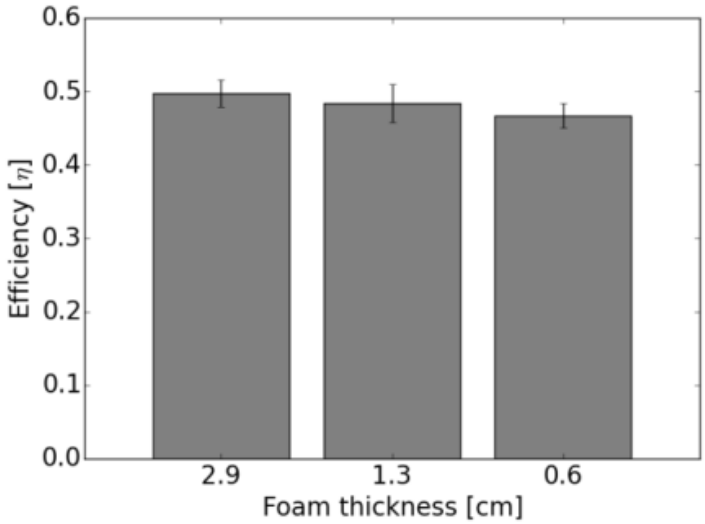

Figure 36: Foam performance as a function of thickness.

As can be seen from this figure the overall efficiency decreases as the thickness is reduced. This indicates that the entire foam surface area is being used for heat exchange. The implication is that as a result of the relatively high thermal conductivity of the foam, heat penetrates to well within the structure. This agrees with the thermo-syphon concept whereby water is being drawn into the foam from all directions and heat exchange is predominantly due to bulk convection. Thus any reduction in thickness, or that is to say the overall volume and surface area, reduces the heat transfer rate. The results of the upper surface area variation are shown below in Figure 37.

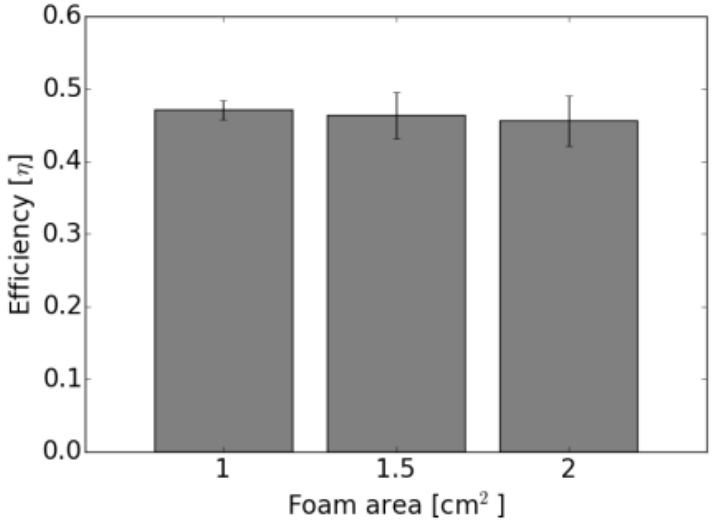

Figure 37: Foam performance as a function of upper surface area.

The data indicates a very small reduction in the efficiency as the focal size is increased. The smaller focal size has a higher concentration ratio which results in a substantially higher foam temperature. This leads to a much higher heat transfer rate due to the increased driving force and higher thermo-syphon flow rate (due to

increased buoyancy). Thus it can be seen in this case, despite a very large reduction in the foam volume (75 vol %) and associated surface area, the heat transfer rate remains more or less the same. This result indicates that for heat transfer in a flow through system, the optimal result is achieved for the highest concentration ratio. A result which also leads to a reduction in the receiver cost as its size is reduced to the minimum.

For evaluation the foam performance may be compared to that of traditional flat plate collectors. However, if this is to be done the path losses through the lens and the glass cover (to prevent evaporation) must be taken into account, which brings the overall system thermal efficiency to around 30%. Flat plat collectors operating under similar conditions generally have an efficiency of around 35 to 40%. Thus it can be seen that the foams achieve a slightly lower efficiency than traditional flat plate collectors. It is believed that the graphitic nature of the foam is responsible for this. When the foam is cut its surface exhibits a very shiny texture, consistent with other types of graphite. This may reflect a portion of the light instead of absorbing it. The reason the result is quite different from the initial testing completed during the prior work is that during these tests the samples were not cut. The ultra-fine cutting blade, which is required to avoid damage to the foam structure, results in a highly polished finish. This is quite different from the raw foam; unfortunately the structure of the raw foam is quite erratic, making density and upper surface area measurements impossible unless it is cut into shape.

This investigation demonstrated that it is possible to rapidly screen different options and optimise the receiver geometry for maximum efficiency. In this case the foam with the lowest density and smallest upper surface area, or rather highest concentration ratio, should be chosen since both imply a reduction in material cost. However, care must be taken that the area is not reduced excessively, which may lead to the formation of nucleate boiling or foam breakage during cutting. In addition, the foam thickness must be chosen large enough to ensure that sufficient surface area is present for maximum heat transfer.

Overall the foams deliver an efficiency similar to a flat plate collector thus no benefit is afforded by the porous nature of the foam and the flow of the water through this structure. This may be due to the fact that the porosity is not low enough or the thermal conductivity is not high enough. The former cannot be decreased as this leads to structural failure and the latter is a function of the raw material used. Nonetheless, using the data gathered during this investigation and a suitable system model, the potential yield of a foam based still can be calculated. This is done in the next section for the optimal foam configuration, i.e. the arrangement with the highest efficiency at the lowest foam volume or by implication cost.

5.3 NANOFLUID CHARACTERIZATION RESULTS

5.3.1 Absorption properties

The absorption tests were carried out under simulated light to ensure consistent results. Shown in Figure 38 is the absorption immediately after production of the nanofluids compared to a reference radiation measurement of an empty beaker. Figure 39 shows the absorption of the nanofluids after three weeks and field testing in the flow cell under concentrated solar radiation (this can be seen as a worst case scenario) to a reference measurement of the radiation transmitted through a base fluid sample of salt water with no carbon black added.

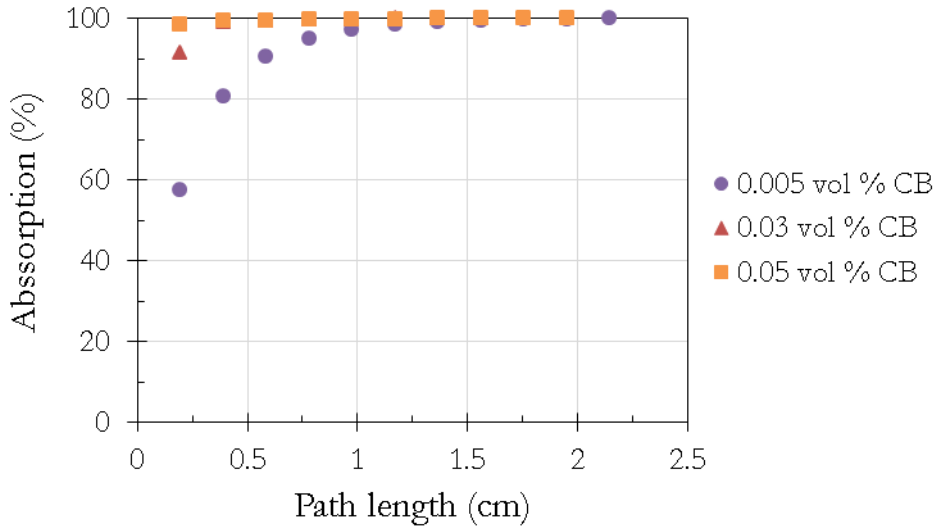

Figure 38: Absorption spectra of freshly prepared carbon black nanofluids

From Figure 38 it can be seen that at a concentration of 0.05 volume % as well as 0.03 volume % carbon black, all the incoming radiation is absorbed almost immediately. For a 0.005 volume % carbon black nanofluid all the radiation is absorbed in a 12 mm path length.

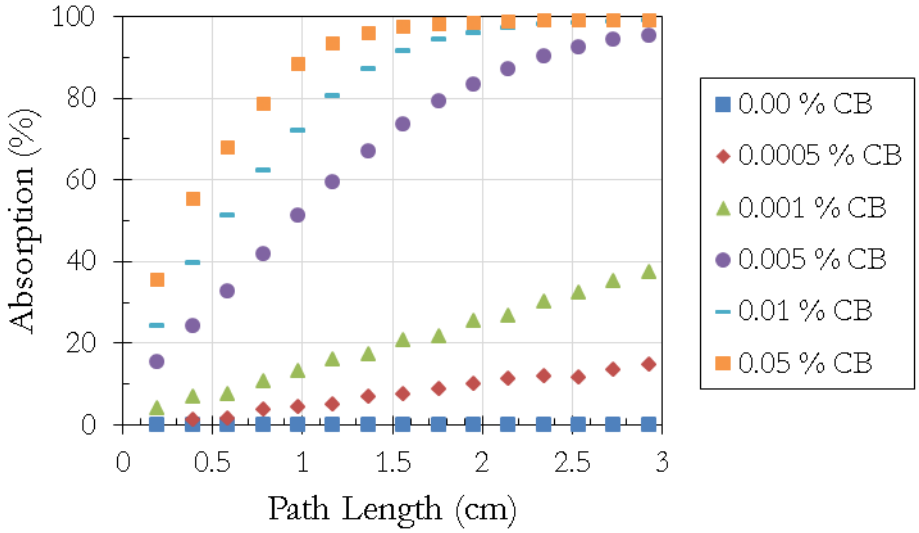

Figure 39: Absorption spectra of used carbon black nanofluids

From Figure 39 it can be seen that the absorption increases linearly at concentrations of 0.001 vol % and lower. At concentrations of 0.005 vol % and higher, the absorption efficiency improves exponentially towards

an asymptote. For a concentration of 0.005 vol % a 100 % absorption is achieved in about 30 mm. For 0.01 vol % and 0.05 vol % a 100 % absorption is achieved at about 20 mm.

Comparing the absorption spectra of Figure 38 and Figure 39 it can be seen that there is a drop in the absorption efficiency after use and a time lapse. But even in a worst case scenario situation the nanofluid still functions at very high absorption efficiency. This effect will also be significantly less in a continuous flow cell where the material is continually mixed through flow effects and pumping.

5.3.2 Photothermal properties

In an effort to characterise the photo-thermal properties of the nanofluids different concentrations of carbon black nanofluids were prepared and placed into glass polytop tubes. A thermocouple was placed through the cap into the centre of the polytop. The polytop tubes were placed in an insulating foam material and positioned in the sun, as can be seen in Figure 40.

Figure 40: Photo-thermal property experimental setup.

The temperature increase of the nanofluid was measured as a function of time on multiple days where all the days showed similar results. Two days' results are shown in Figure 41 and Figure 42 respectively. The data in Figure 41 was measured with an average direct normal incident (DNI) radiation value during the run time of 950 W/m^2. The data in Figure 42 was measured with an average DNI radiation value of 788 W/m^2. The radiation data was taken as minute averaged from the Southern African Universities Radiometric Network (SAURAN) at the UPR - GIZ University of Pretoria station.

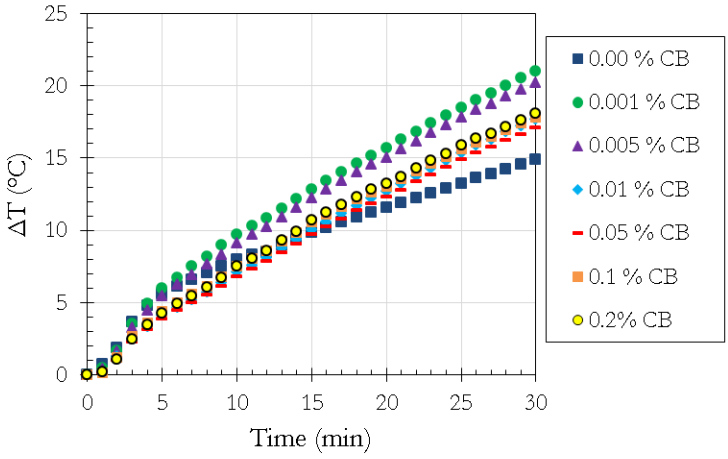

Figure 41: Photo-thermal properties of different weight %concentration carbon black nanofluids at an average DNI of 950 W/m^2.

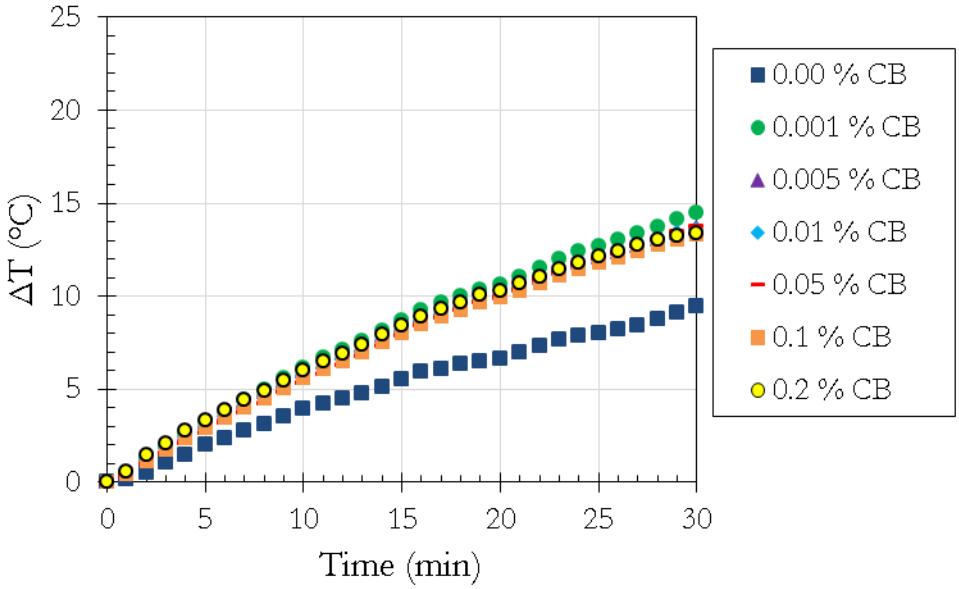

Figure 42: Photo-thermal properties of different weight % concentration carbon black nanofluids at an average DNI of 788 W/m².

From Figure 41 and Figure 42 it can be seen that the temperature increase reached in a 30 min run time is higher in Figure 41 because of the higher solar radiation value of 950 W/m² compared to the 788 W/m² in Figure 42. On both days it can be seen that there is not a very distinct difference between the photo-thermal properties of the different concentration of nanofluids. In both cases, more distinct in Figure 41, the lower concentrations performed better than the higher concentrations. This is due to the higher radiation absorption rate closer to the surface of the polytops that leads to higher radiative heat losses from the higher concentration nanofluids. The lower concentration nanofluids allow light to pass further into the fluid, heating the bulk of the fluid and not just the surface.

5.3.3 Thermal absorption depth

These measurements go hand-in-hand with the absorption properties experiments done under the solar simulator lamp. An experimental setup was designed to determine the penetration depth of the concentrated solar beam. An insulated foam container was made with six thermocouples spaced 15 mm from each other. The container has a depth of 105 mm and is open to the atmosphere on the top and enclosed with a Perspex sheet at the bottom. The setup is shown in Figure 43 A and B. The concentration of nanofluids tested included 0.00 volume %, 0.0005 volume %, 0.001 volume %, 0.005 volume %, 0.01 volume %, 0.05 volume % carbon black nanofluid as shown in Figure 22 C.

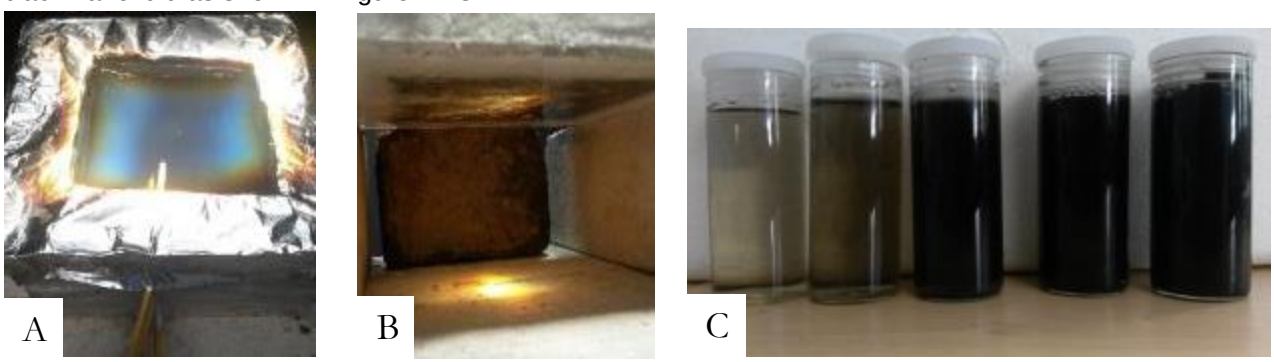

Figure 43: Absorption depth experimental container. A: Top of container, B: bottom of container, C: nanofluid concentration range used.

The absorption depth data for each concentration can be seen in Figure 44 to Figure 49. Where relevant the light that passed through the container is added as a secondary Figure.

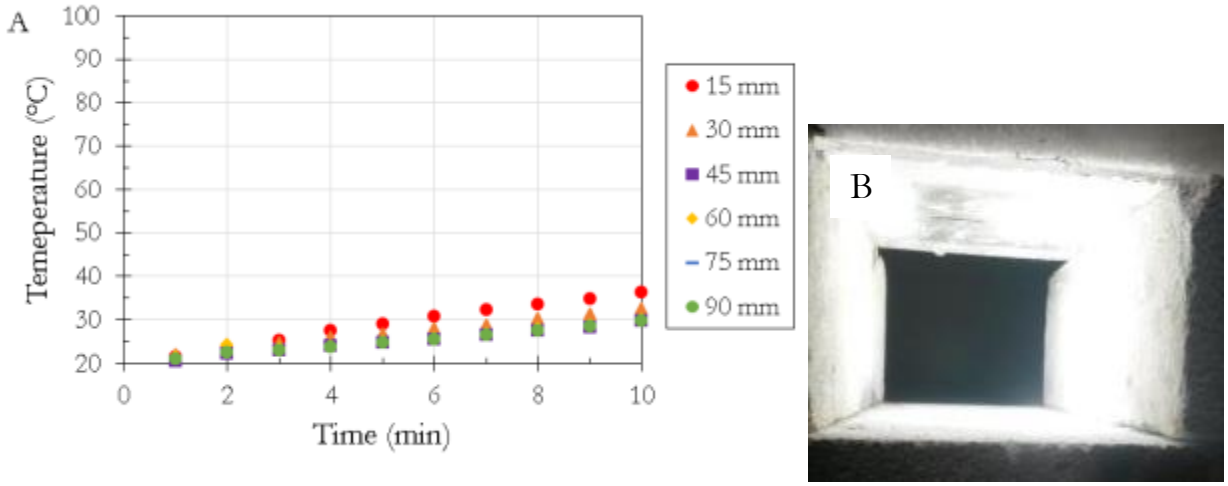

Figure 44: A: Temperature increase profile for salt water for an average DNI of at different depths 750 W/m2. B: Photo at bottom of container.

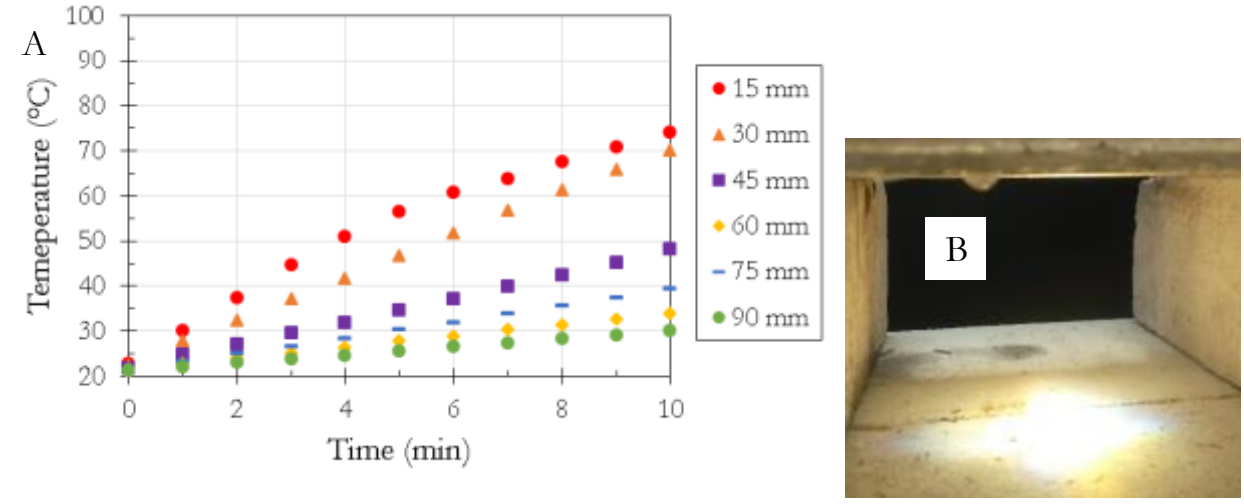

Figure 45: A: Temperature increase profile for 0.0005 vol % carbon black nanofluid at different depths for an average DNI of 800 W/m2. B: Photo at bottom of container.

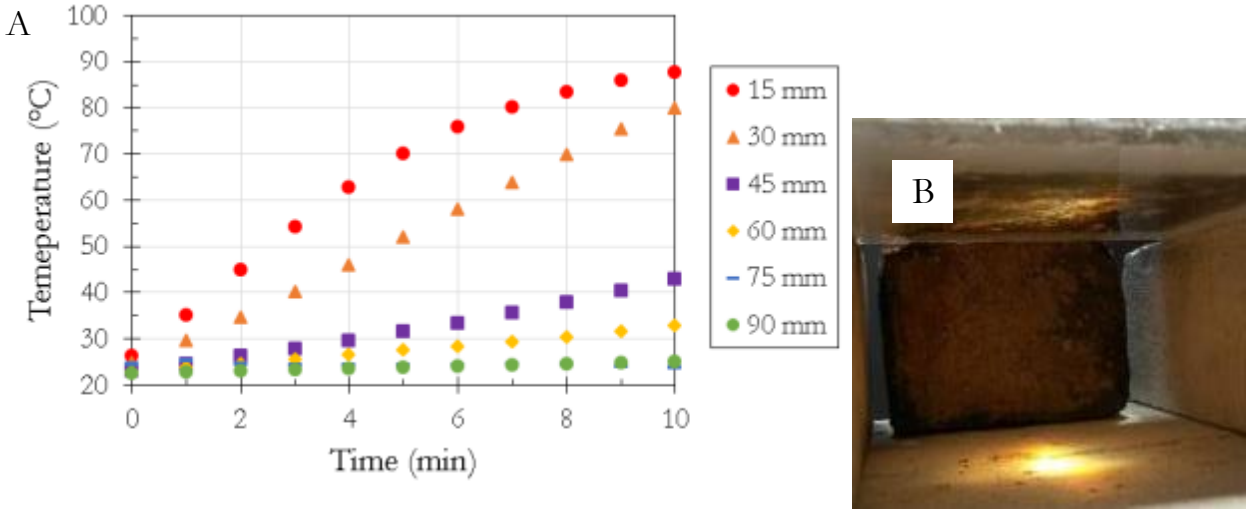

Figure 46: A: Temperature increase profile for 0.001 vol % carbon black nanofluid at different depths for an average DNI of 805 W/m2. B: Photo at bottom of container.

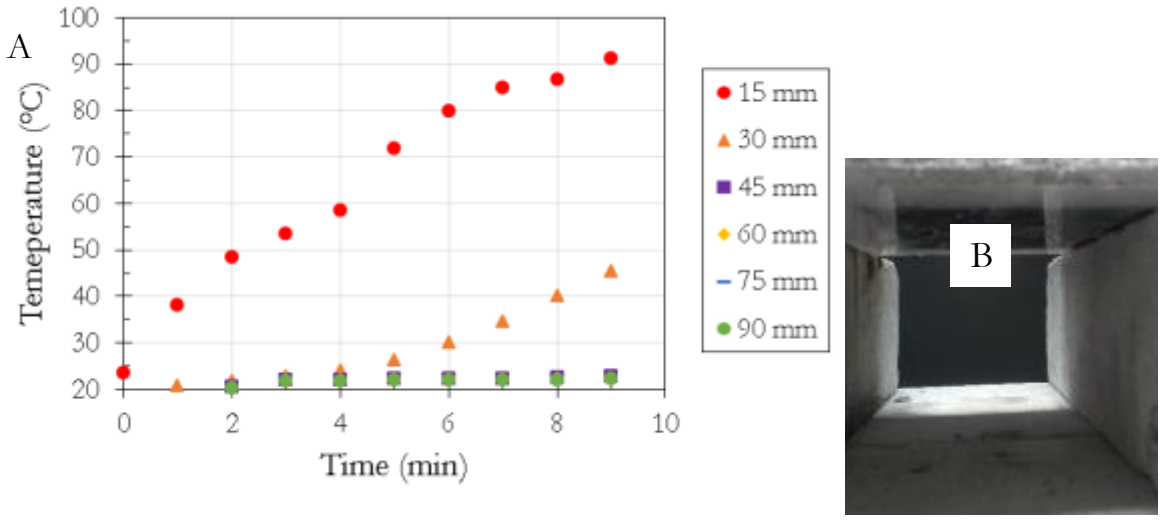

Figure 47: A: Temperature increase profile for 0.005 vol % carbon black nanofluid at different depths for an average DNI of 760 W/m2. B: Photo at bottom of container.

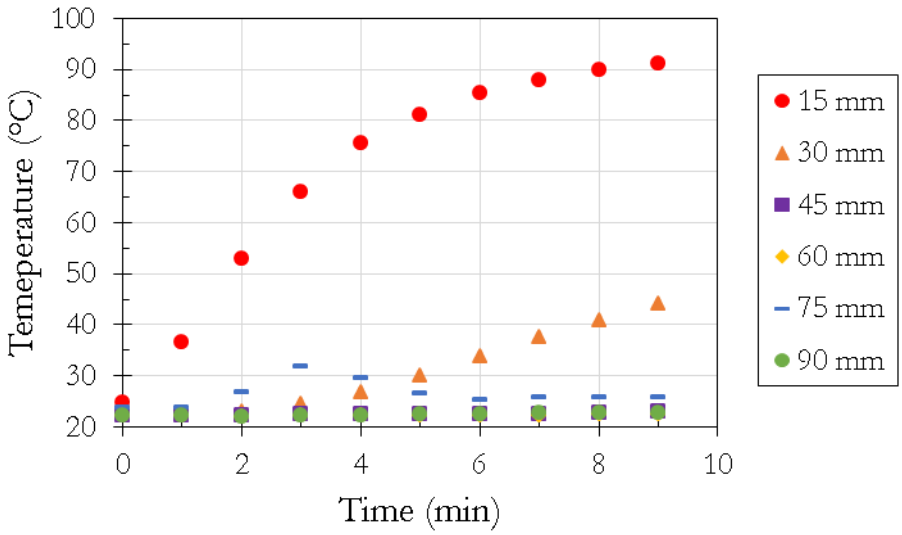

Figure 48: Temperature increase profile for 0.01 vol % carbon black nanofluid at different depths for an average DNI of 788 W/m2.

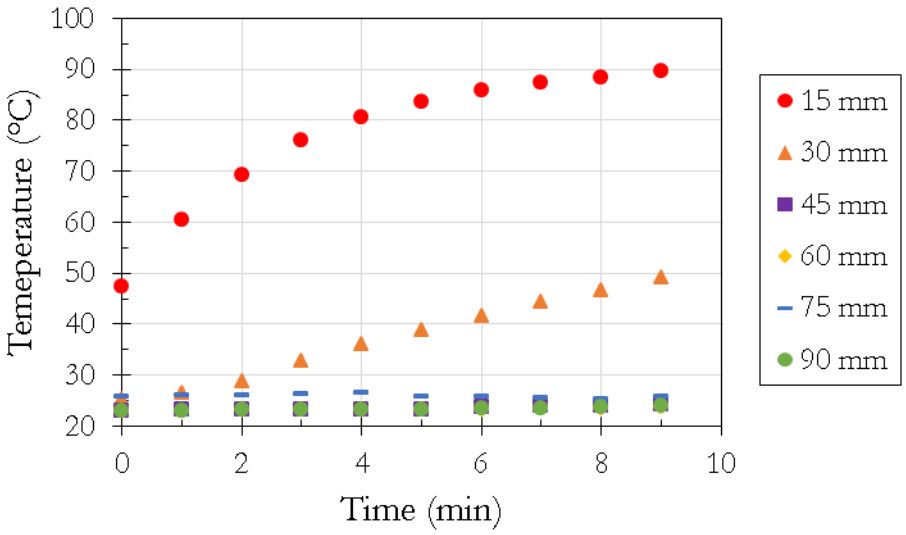

Figure 49: Temperature increase profile for 0.05 vol % carbon black nanofluid at different depths for an average DNI of 764 W/m2.

From Figure 44 it can be seen that the salt water does not absorb much of the solar radiation, as determined from Figure 44A because of the lack of temperature increase and in Figure 44B from the intense light that exits the container at the bottom. It should also be noted that the thermocouples at all the depths indicate temperature is increasing in a similar way.

From Figure 45 it can be seen that even at such low concentration as 0.0005 vol % carbon black the degree of energy absorption increases significantly where a maximum temperature of 75 °C is reached in 10 min. From Figure 45B it can still be seen that there is a lot of radiation exiting at the bottom of the container. Using the MP-200 pyranometer the exiting radiation was attempted to be measured but it exceeded the maximum reading of 1500 W/m^2. All of the depths show an increase in temperature, although different to the salt water the top liquid is heated faster than the bottom liquid as is expected because the radiation that reaches the bottom has less intensity. The top two thermocouples show similar temperature values after 10 minutes. From Figure 46 it can be seen that 90 °C was approached after 10 minutes at 15 mm as well as 30 mm. From Figure 46B it can be seen that there still exits light from the bottom of the container. Using the pyranometer an energy value of 1100 W/m^2 was measured. It is also seen that although light passes through there is not significant heating below 60 mm.

From Figure 47 it can be seen that there is a much higher temperature gap between the 15 mm and 30 mm thermocouple, where the temperature at 30 mm depth only starts rising at 5 minutes. It is believed that this temperature increase is more due to conduction from the top layer than from radiation absorption. It should be noted that for this configuration very little convection is expected due to the thermal stratification: i.e. the lower density, higher temperature water layers should be stable above the higher density colder layers. From Figure 47B it can be seen that no light passes through the nanofluid at this concentration or higher concentrations. There is no heating for the liquid below 30 mm that shows that all the significant energy is absorbed in the top 30 mm layer.

From Figure 48 it can be seen that the top layer heats up quicker and the second layer at 30 mm also starts heating at an earlier time (4 minutes). This could be an indication of a higher thermal conductivity because of the higher concentration of carbon black. There is no other significant heating in the layers below 30 mm. It should be noted that the temperature profile of the thermocouple at 75 mm is an anomaly and attributed to experimental error because there is no heating at 60 mm or 90 mm.

Figure 49 shows similar results to Figure 48 except that that the 30 mm layer starts heating at 2 min. This supports the theory that all the significant energy is absorbed in the top 15 mm layer and the second layer at 30 mm is heated by conduction and that at higher concentrations carbon black the nanofluid has a higher thermal conductivity that leads to faster heating of the second layer.

There was a very fast transition between 0.001 vol % and 0.005 vol % carbon black nanofluids in the penetration depth of the solar radiation. Where there is still unused light passing through at 0.001 vol % and at 0.005 vol % there is no distinct heating in the 30 mm layer. This suggests that the optimum concentration will be somewhere between 0.001 vol % and 0.005 vol % carbon black as this will absorb all of the concentrated radiation but still allow heating to be distributed into the bulk fluid reducing convective heat losses from the surface.

It is difficult to make conclusions regarding the overall absorption efficiency of the system from this data since a critical stream is unaccounted for, namely the amount of evaporated/boiled water. Presumably once the carbon black concentration is high enough to heat the upper fluid layers to temperatures approaching the normal boiling point, these losses are significant.

5.3.4 Evaporative test results

Evaporation tests where done to determine what the behaviour is when the carbon black based nanofluid is dried. This can be related to a recovery step of the concentrated brine solution after processing to recover the salt and possibly the carbon black. The nanofluid was placed in an open pan into a convection oven and evaporated overnight. The results can be seen in Figure 50.

Figure 50: Drying behaviour of nanofluid.

From Figure 50 it can be seen that the salt crystallises on available surfaces, while the carbon black remains suspended in the liquid as the level drops finally settling on the surface of the plate. This suggests that with adding surfaces for crystallisation of the salt, like fins, the salt will be separated fully from the carbon black offering a solution for harvesting the salt from the concentrated brine solution. The highly concentrated carbon black solution can then be recycled in the system for reuse.

5.3.5 Flow cell test results

As part of the design process it is critical to obtain the optical and physical properties of the thermal fluid. For this reason the first portion of this section is dedicated to characterization of the carbon black and water. The

next step is to gather operational data for a continuous flow system, as a starting point for testing a basic baffled flow cell was built, as depicted in Figure 51.

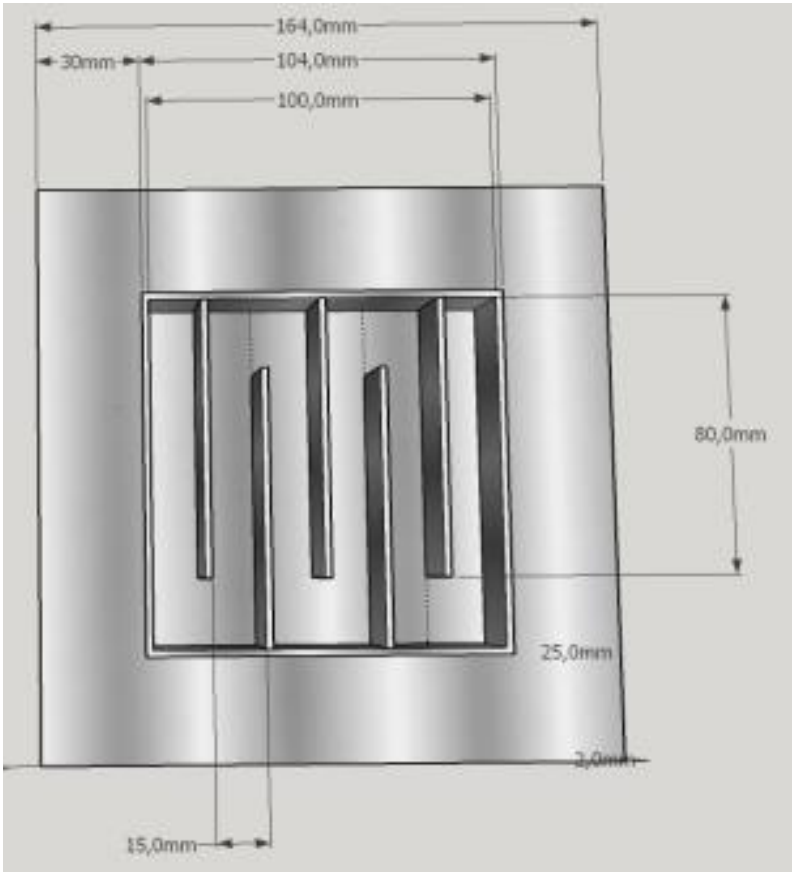

Figure 51: Baffled flow cell.

This cell was constructed based on the experimental absorption results and a basic concept for the overall system. The objective was to measure the achievable temperature increase of the nanofluid under real flow conditions. No specific targets were set for the design; instead the data will be used as input into a more detailed model for design optimization. The temperature increase measurements were taken on the solar concentrator platform on the Experimental farm at the University of Pretoria. The nanofluid was run at a pumping rate of 10 rpm on a peristaltic pump which relates to approximately 80 ml/min throughput. The nanofluid was pumped through a 3 cm deep collector with a 10 cm x 10 cm collecting surface and 5 baffles positioned with 1.5 cm between each baffle as shown in Figure 51. The experimental configuration and actual flow cell are presented in Figure 52.

Figure 52: Solar collector design and in operation.

The different concentration nanofluids used are shown in Figure 53, these are the same ranges used during the prior photo-thermal testing.

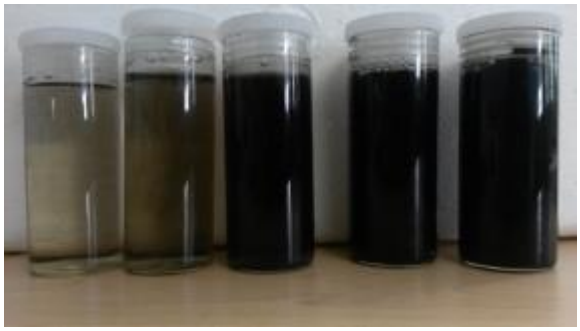

Figure 53: Different nanofluids used, from the left 0.0005, 0.001, 0.005, 0.01, 0.05 volume % carbon black.

The measurements were taking during the course of the day for the different concentrations of nanofluids. The temperature difference (ΔT) values were normalised by dividing the minute averaged ΔT values with the minute averaged DNI values collected from the SAURAN database to get sensibly comparable data. The results are shown in Figure 54.

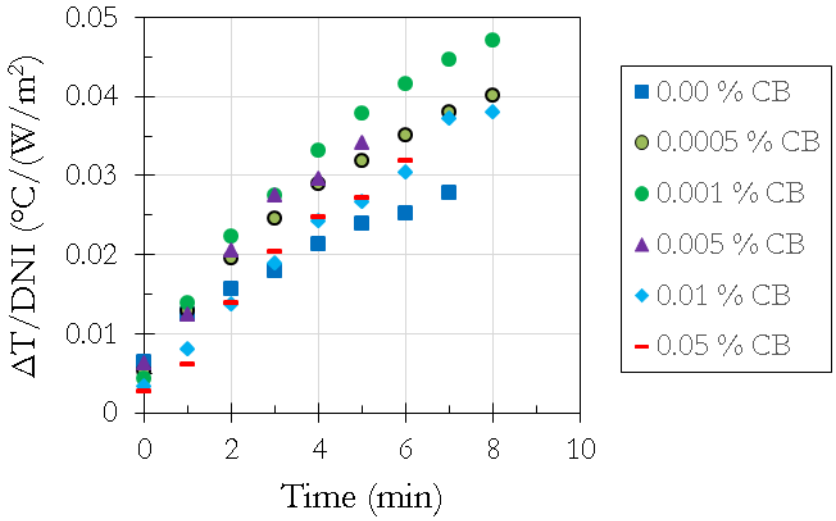

Figure 54: Temperature increase data for different volume % concentration carbon black nanofluids.

The boiling temperature for the nanofluids is approximately 90 °C at atmospheric pressure in Pretoria. For the salt water and the 0.0005 vol % carbon black nanofluid no boiling occurred during the run, but from the 0.001 vol % carbon black concentrations the runs started forming bubbles on the surface of the collector which lead to early termination of the runs (as shown for example in Figure 55).

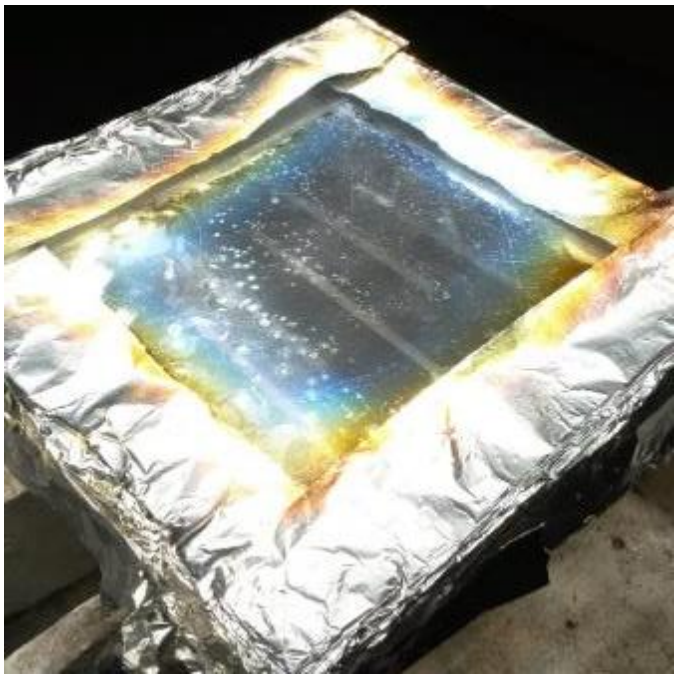

Figure 55: Bubble formation during processing on surface of collector for higher concentration nanofluids.

It was seen that the boiling occurred while the outlet temperature was as low as 38 °C for 0.05 vol % carbon black nanofluid. This indicates that the bulk fluid is not heated evenly though and there is rapid boiling occurring at the surface of the collector. To compare the heating rates of the different concentration nanofluids only the first 5 minutes of operation are used as all the nanofluids have data for this timespan. Each set of data was fitted with a linear trend line and the slopes compared, as shown in Figure 56 and Table 5.3.

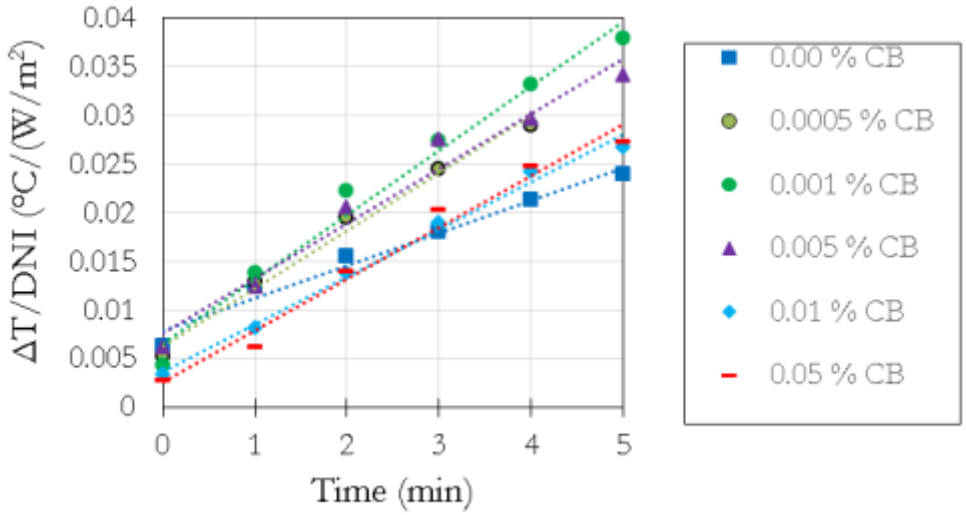

Figure 56: Temperature increase data for different volume % concentration carbon black nanofluids with fitted trend lines

Table 5.3. Comparison of heating rates at different concentrations compared to that of salt water.

Sample	Improved efficiency (%)
0.00 % CB	0
0.0005 % CB	55.88
0.001 % CB	94.12
0.005 % CB	67.65
0.01 % CB	44.12
0.05 % CB	55.88

From Table 5.3 it can be seen that the thermal efficiency is a maximum at 0.001 volume % carbon black with an efficiency improvement of 94 %. This concentration is low enough to allow transmittance of the sunlight into the bulk fluid. The 0.0005 % carbon black nanofluid does not absorb all of the radiation leading to a lower heating rate. For the concentrations higher than 0.001 vol % carbon black all of the radiation is absorbed close to the surface of the collector, this causes higher convective heat losses from the surface rather than heating of the bulk fluid.

From the absorption properties tests in Figure 39 it can be seen that at 3 cm depth approximately 40 % of the light is absorbed. The depth of the collector is 3 cm, however, this offers a path length of 6 cm for absorption before the reflected radiation (from the bottom of the cell) is lost.

The maximum efficiency found at 0.001 vol % carbon black correlates well with the results from the depth absorption experiment. Although based on that test not all of the energy is would be absorbed in the 60 mm path length of the collector (assuming non-diffuse reflectance), a significant proportion of the energy is absorbed and the bulk fluid is heated. It is expected however that the true maximum efficiency will be at a concentration between 0.001 vol % and 0.005 vol % carbon black as this will allow 100 % radiation absorption as well as bulk fluid heating.

Based on these results the flow cell operation can be estimated for modelling purposes. Following detailed modelling the cell can be incorporated into an overall system design to calculate the expected cost and yield. This is done in the next section.

5.4 SOLAR STILL RESULTS

The experimental results for the testing of the still unit are given in Table 5.4.

Table 5.4. Solar still with single sheet of Perspex test results.

Test	Date	Start Time	Conditions	Ambient temp (°C)	Solar Rad. (W/m²)	Still temp. (°C)	Yield (ml)
1	12/04/2016	15:40	Clear	28	990	28	
		16:00	Clear	27.6	990	60	
		16:40	Clear	26.8	990	66.7	80
2	05/05/2016	12:30	Clear	24	900	24	
		12:50	Clear	25.4	900	58	
		13:30	Clear	26	900	62	70
3	12/05/2016	11:55	Clear	26	1045	26	
		12:15	Clear	32	990	60	
		12:55	Clear	33	987	67	80
4[a]	16/05/2016	12:25	Cloudy	16	800-1100	16	
		12:45	Cloudy	16.4	800-1100	42	
		13:25	Cloudy	18	830	50	30
5	16/05/2016	14:30	Cloudy	20	870	20	
		14:50	Cloudy	19.5	870	43	
		15:30	Cloudy	20	850	48	40
6	17/05/2016	10:15	Clear	18	850	18	
		10:35	Clear	19	870	43	
		11:15	Clear	21	930	50	50
7	17/05/2016	12:15	Clear	20	930	20	
		12:35	Clear	20.5	850	63.6	
		13:15	Clear	22	950	78	110
8	17/05/2016	13:27	Clear	22	950	22	
		13:47	Clear	22	950	60	
		14:27	Clear	22	950	68	85

[a] For this run the is some uncertainty regarding the solar radiation measurement due to large fluctuations caused by cloud movement.

The following figures show the relationship between the effect of solar radiation, still temperature and ambient temperature on the yield after one hour of testing.

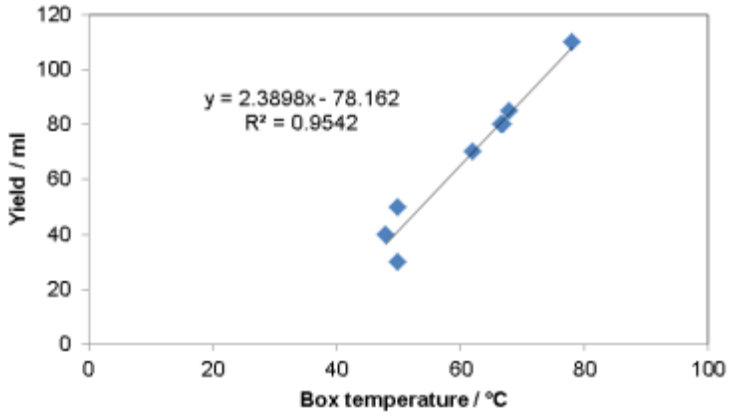

Figure 57: Yield vs. the still temperature over 1 hour for single sheet Perspex

From Figure 57 the trend is clear that as the box temperature is higher, the evaporation rate is higher and thus the overall yield is higher. The maximum temperature inside the still was 78 (°C) as shown in Figure 58.

Figure 58: Maximum temperature obtained in the box using a single Perspex sheet

Once clouds passed over the sun, an almost immediate drop in temperature is witnessed and because the solar radiation decreases, evaporation ceases for that time. It was observed that when the solar radiation is high, there is rapid evaporation, and this can be seen when a droplet of condensate rolls down the Perspex, it is immediately fogged up again. Figure 59 shows the yield after one hour and the instantaneous solar radiation at the same time.

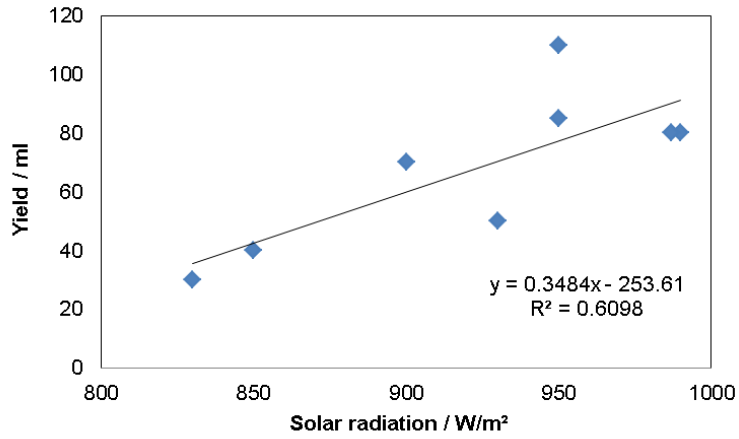

Figure 59: Yield vs. the solar radiation over one hour for single sheet Perspex

The correlation is not very good but it is clear that as the radiation increases the yield does too. If the average solar radiation can be measured, one will have a better insight to the effect of solar radiation on the yield and thus the evaporation tempo. The maximum solar radiation achieved was 1045 (W/m^2). An interesting observation was that high yields can still be obtained even when the ambient is quite low (below 25 °C see Figure 60). This can be owed to the fact that a cold wind passing over the outer layer of the Perspex, will help to cool the surface and thus creating a larger temperature difference between the inner Perspex surface and the wick (evaporation) surface.

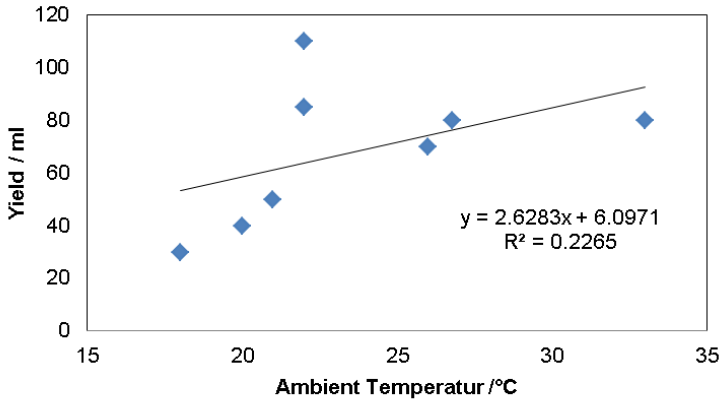

Figure 60: Yield vs. ambient temperature over one hour for single sheet Perspex

Unfortunately there is no clear trend visible and this may have been influenced by variations in wind speed. The box temperatures differed between 20 minutes and one hour of operation and the differences are shown in Figure 61. This just gives an indication as to how effective the still heats up at early stages and what the maximum potential is considering the current conditions. An effective still should rapidly heat up to a steady state value and then slowly increases over time.

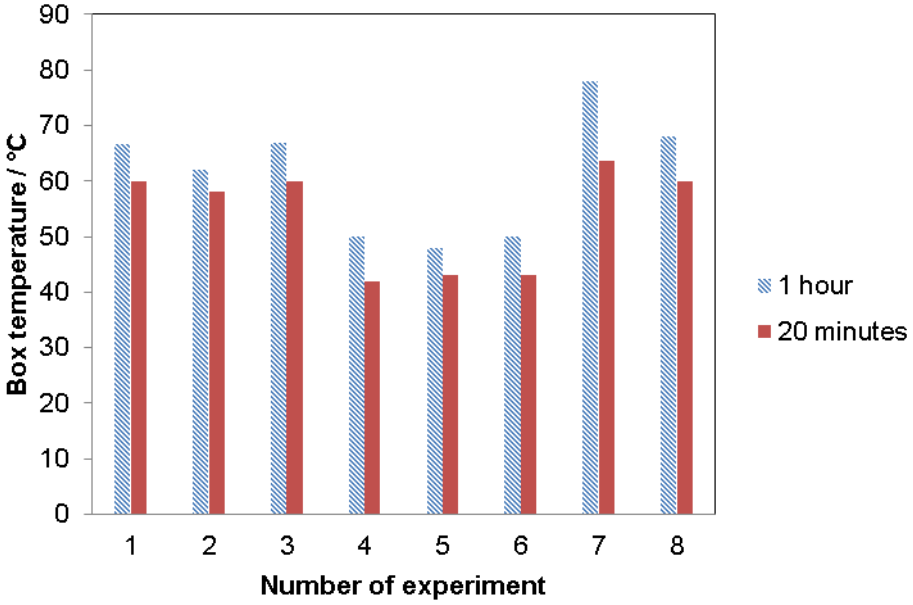

Figure 61: Different still temperatures at different operating times

This figure demonstrates that in most cases a large temperature difference is still measured during the initial and final portion of the run, in some cases up to 10 °C. This indicates that the still is still heating up during a large portion of the experiment and is not yet at steady state. Thus the experimental work conducted will provide a conservative estimate of the yield achievable with this wick-based, solar still design. For the best experimental case this is found to be 0.544 litres per day. This can then be compared to the results achieved for the concentrated system, as done in the following section.

However, the long term intention of this design is to operate it in conjunction with an external, multi-stage, PCM filled condenser unit. Under these conditions the still should be operated as an evaporator only. To develop a preliminary indication of what might be achievable under this operating mode, the still was slightly modified and the tests repeated, again over 6 days. An additional Perspex window was added to the top of the still to in

effect create a double pane window. The interior of the window will contain a virtually stagnant gas layer, providing insulation from outside conditions and preventing heat from escaping through this surface.

When the unit is operating in this fashion the objective would be for minimal condensation to take place within the evaporator unit itself. Instead the maximum amount of vapour should be heated at the highest achievable temperature. In addition, if no condensation is taking place on the surface of the innermost Perspex window, light scattering and absorption on this surface should be at a minimum, leading to better still efficiency. The experimental results for the use of the unit with a double pane window, i.e. as a feed unit for a condenser, are summarized in Table 5.5. An additional variable is tabulated namely the surface temperature of the innermost Perspex layer.

Table 5.5. Solar still with double-pane of Perspex test results.

Test	Date	Start time	Ambient temp (°C)	Solar Rad (W/m^2)	Inner Perspex surface temp. (°C)	Still temp. (°C)	Yield (ml)
1	12/05/2016	13:40	33	955	33	33	
		14:00	27.6	950	51.4	69	
		14:40	26.8	904	60	82	60
2	18/05/2016	11:47	16	700	16	16	
		12:07	16.4	640	36	40	
		12:47	17	690	43	54	20
3[a]	19/05/2016	11:20	16	900	16	16	
		11:40	16.2	915	50	57	
		12:20	16	942	83.4	95	30
4[b]	19/05/2016	13:20	21.2	908	21.2	21.2	
		13:40	22	816	63.4	70	
		14:20	24	772	60	72	40
5	16/05/2016	12:05	20.5	875	20.5	20.5	
		12:25	22	903	57	63.5	
		13:05	21	898	64	70.9	35
6	29/05/2016	12:34	21	950	21	21	
		12:54	22	967	63	67	
		13:34	22	987	72	84	38

[a] All water evaporated, but little condensed, possibly under an hour.

[b] Lower temperatures are witnessed on the same day, due to clouds passing.

The surface temperature of the innermost Perspex layer and the interior box or vapour temperature were measured during these experiments because the vapour temperature is the variable that will determine whether this heating unit will work successfully when connected to an external condenser. It was found that the temperatures were much higher than those achieved with only a single layer of Perspex. This is because of the stagnant gas layer that heats up and insulates the inner layer from colder ambient temperature and wind. Figure 62 shows the relationship between the inner Perspex surface temperature and the box temperature:

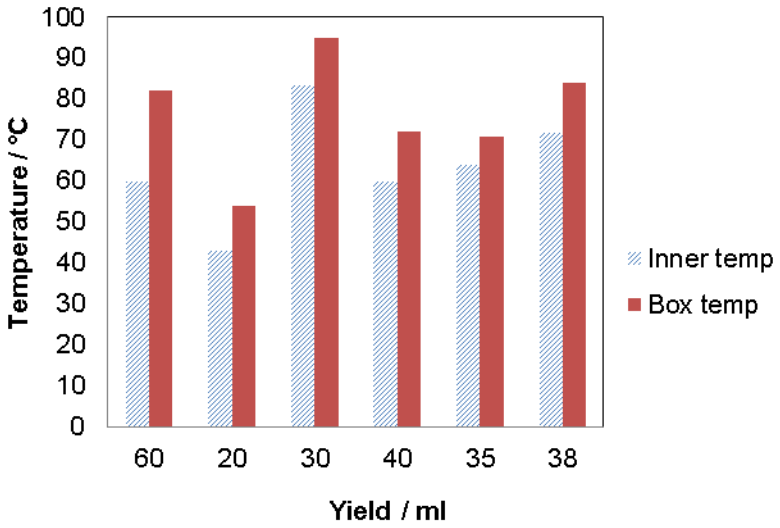

Figure 62: Inner Surface temperature and box temperature vs. yield after 1 hour

As can be seen from Figure 62, the temperature difference between the Perspex surface and the vapour varies during each experiment. When there exists a small temperature difference between the box temperature (vapour temperature) and the inner Perspex surface temperature, it is inevitable that the vapour will not condense on that surface; it would rather escape through small still leaks or condense on the sides of the still. This is more clearly seen and quantified in Figure 63 where the differences between inner Perspex surface and box temperatures are plotted with respect to the yield:

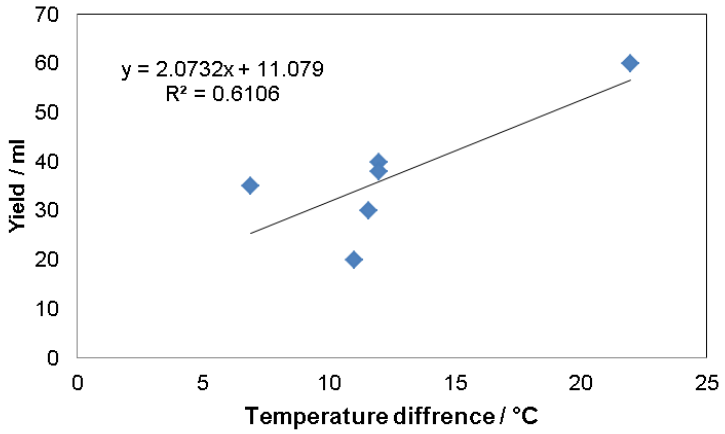

Figure 63: Temperature difference at one hour for double-pane Perspex

From Figure 63 it is seen that the higher the temperature difference, the higher the yield; thus when the condensing surface is sufficiently colder than the vapour temperature, then more condensation will take place. If the inner surface of the Perspex is too hot (close to the vapour temperature), almost no condensation will occur. Despite the potential vapour leakage it is clear that the fresh water yield is significantly less than achieved in the single pane experiment. Ideally the yield from the evaporator should be zero during this mode of operation with all the condensation taking place in the condenser. In this case no condenser is connected so this is not possible; nonetheless the achieved yield still provides valuable information regarding the operation of the still in this configuration. The box temperature increased quite fast, thus the differences between the box temperature at 20 minutes and one hour were not so large and this is a good result as higher temperatures will cause higher evaporation rates. In Figure 64 the difference in box temperatures after different elapsed times are shown.

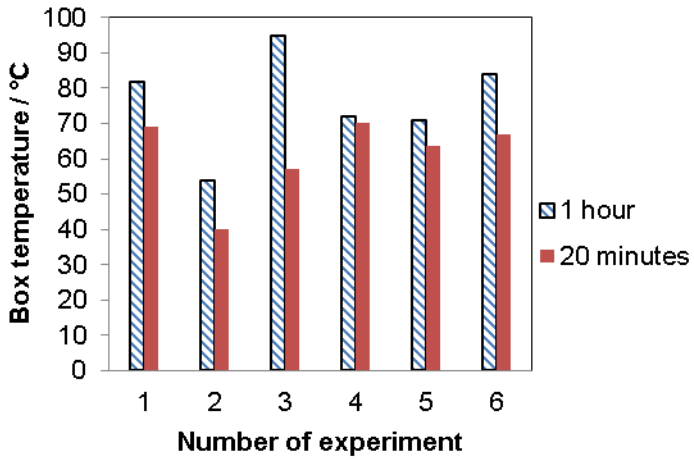

Figure 64: Box temperatures at different time for a double-pane Perspex setup

The maximum box temperature was 95°C, but the maximum wick surface temperature was actually 106°C as can be seen in Figure 65. This is a great result as the objective is to maximize the evaporation rate and achieve the highest possible temperature. However, maintaining an even distribution of water during this experiment is difficult and some hot spots do occur.

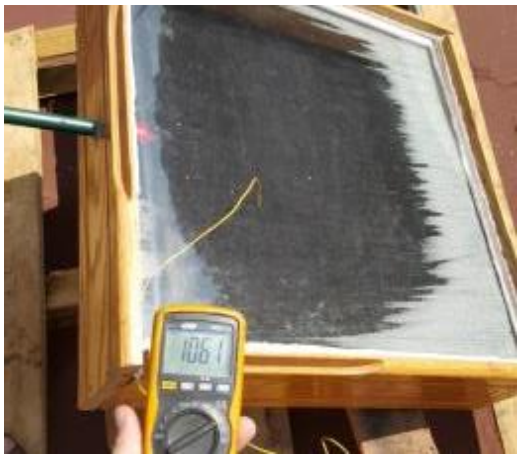

Figure 65: Maximum wick surface temperature obtained with double-pane Perspex

The ambient temperature had a much clearer effect on the yield during these experiments and it can be observed in Figure 66. This is due to the higher delta temperature developed between the still and ambient. The yield was higher for higher ambient temperatures whereas with the single Perspex layer, the result is not as clear. This effect is possibly because of the stagnant gas film that controls the condensation and not the unpredictable effect of wind and natural convection (as with the single layer of Perspex). In the current case higher ambient temperature simply results in a hotter box. It is also clear to see that the amount of condensation has visibly decreased when comparing Figure 65 and 58.

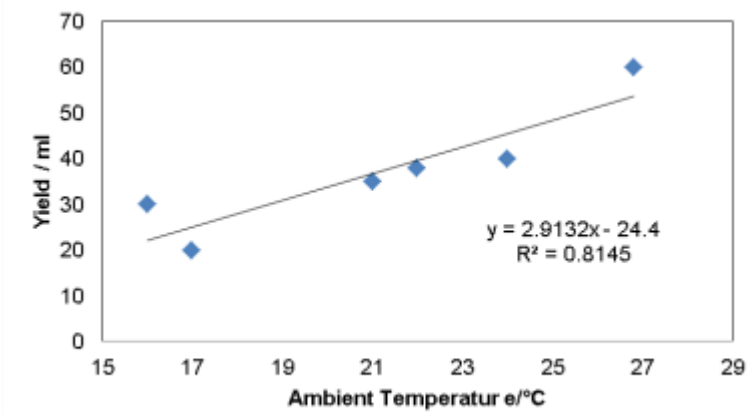

Figure 66: Effect of ambient temperature on the yield when using double-pane

When comparing the yields of the single Perspex layer to the double-pane Perspex, it is clear that with double-pane system the yield is lower for similar conditions. We want to also however compare the box temperatures. The average box temperature of 8 single Perspex layer runs was 61.21°C whereas with the double pane it was 76.32°C over 6 runs and the average yield of 8 single Perspex layer runs was 68.13 ml whereas with the double pane it was 37.17 ml over 6 runs.

Initially there is fog forming with the double pane Perspex until the stagnant gas layer is hot enough that no condensate will form. When this happens, less sunlight is dispersed by the droplets and thus more rapid heating is observed. With this higher temperature inside the box result and it is inevitable that more rapid evaporation of water from the wick should occur when using a double pane layer of Perspex. However in this case the yield is decreased because this vapour cannot be as easily condensed as in the single pane system. Thus the double-pane design will serve as a good configuration when combined with an external condenser.

CHAPTER 6: TECHNO-ECONOMIC MODELLING

6.1 OVERVIEW

The experimental results have provided enough information to proceed with a detailed, fundamental modelling of the flow cell. This is the first topic for this section. Since this collector was the only concentrated option to demonstrate high efficiency, only this option was selected for detailed modelling of the collector or in this case flow cell. Based on efficiency though, both options are incorporated into a complete flash desalination system. The full system model is explored in the second subsection to give an estimate of the achievable daily yields should the collectors be used for flash distillation. The potential integration of the thin-film solar still with a suitable multi-stage condenser is also explored. Finally, a techno-economic evaluation of all three options is considered together with an assessment of the operability requirements.

System modelling was either first principles based in the Python programming language or using the finite volume method in the Fluent platform within commercial software package ANSYS. Solar ray-tracing was done using the SOLTrace program for the solar platform [23].

6.2 DETAILED FLOW CELL MODELLING

The information obtained in the experimental section regarding the operation of the preliminary flow cell unit can now be used to simulate the cell in detail. This information in turn can be used to predict the cell performance when placed in a continuous flow system. A generic flow through cell with baffles is depicted in Figure 67.

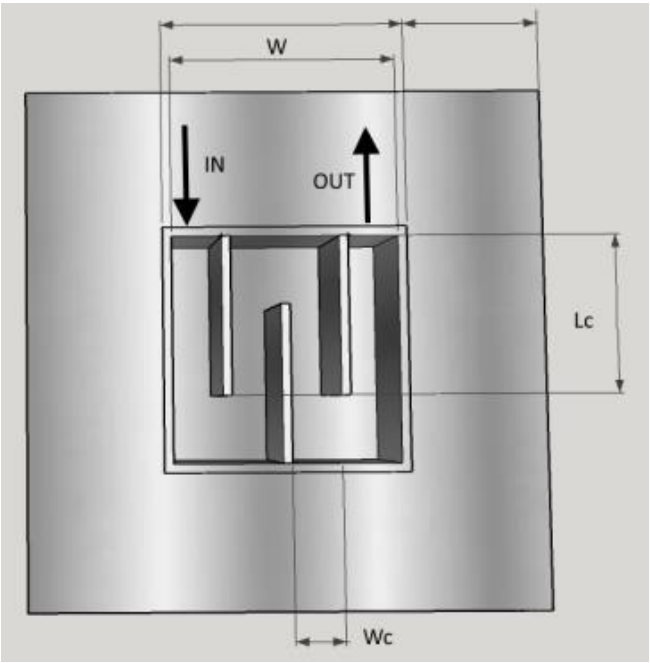

Figure 67: Baffled flow cell.

The baffles increase the flow path for the same cell area (W x W). However, increasing the number of baffles reduces the effective channel width (Wc), thus increasing the linear velocity which decreases the exposure time. Hence the temperature increase per pass is a trade-off between an increased flow length and an increased velocity. As a model starting point three baffles were chosen, but this will be optimized based on the desired operating conditions and the model predictions.

From the experimental work on the foams it was shown that from a cost perspective it is clear that higher concentration ratios, i.e. smaller cell sizes, are more economical. However, there are limitations and trade-offs, both from the achievable concentration ratio (due to lens imperfections discussed earlier) and increased losses (via reflection) as well as increasing absorptivity requirements to ensure all the light is captured. Based on the concentrator characterization results and achievable concentration ratios, cell dimensions of 10 cm x 10 cm were chosen for simulation. This places the concentration factor (CF) at 100, meaning that expected radiation levels are on the order of 100 000 W/m^2. At these high levels of exposure preliminary tests indicated that the materials of construction did not degrade. However at higher concentration ratios system degradation occurred which led to the choice of 100 as the maximum CF.

Preliminary testing of the carbon black dispersions, indicated that complete absorption could be achieved in as little as 1 cm using very low concentrations of carbon black. For this reason the simulated cell height was chosen as 1 cm however this may be modified based on physical measurements during testing. If this height results in excessive thermal stratification a lower carbon black concentration coupled with an increased cell height will be used to ensure uniform heating. The required mass flow rate can be roughly estimated from the expected water yield and operating time, for the model this was set to 500 ml/min[1].

Since the channel dimensions have been fixed, the linear velocity can be calculated. This in turn allows the Reynolds number to be determined as 10 000, which is well into the turbulent flow region. Thus it is likely that a lot of mixing will occur along the channel depth, leading to a more homogenous temperature distribution within the fluid. This effect is difficult to quantify theoretically and will be confirmed during field trials using thermocouple measurements at different heights and lengths along the channel. Based on these considerations a simplified theoretical model of the system can be formulated. The control volume for this analysis is shown in Figure 68.

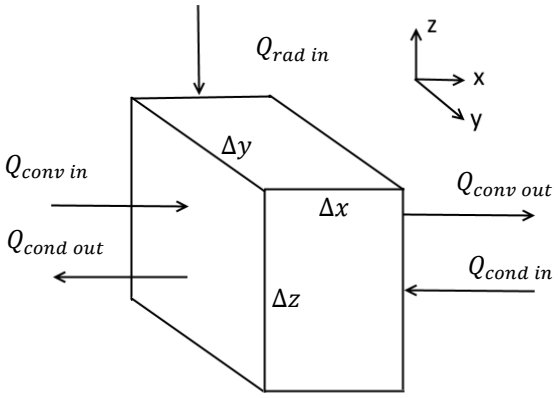

Figure 68: Model control volume.

As an initial estimate heat losses are neglected and the temperature distribution is assumed uniform in the z-direction. A simple, steady state energy balance for this system can be calculated as:

$$Q_{conv\ out} - Q_{conv\ in} + Q_{cond\ out} - Q_{cond\ in} - Q_{rad\ in} = 0 \quad (6.2.1)$$

This can be reformulated in differential form as:

$$\rho v C_p \frac{\partial T}{\partial x} - \frac{q_{rad}}{\Delta z} - k\frac{\partial^2 T}{\partial x^2} = 0 \quad (6.2.2)$$

Where q_{rad} is the incident radiative heat flux (assumed to be fully absorbed within the cell height). This equation can be discretised to give:

$$T_{n-1}\left(-1 - \frac{v\Delta x}{\alpha}\right) + T_n\left(2 + \frac{v\Delta x}{\alpha}\right) - T_{n+1} = 0 \quad (6.2.3)$$

The upwind scheme was used to implement the discretisation since the Peclet number can be calculated as 3000 which is significantly greater than one. The boundary conditions are both constant temperatures, where the initial temperature is set at 100 ºC (to represent good heat recovery) and the final temperature is assumed to be equal to the prior iteration value, since no additional heating occurs when the stream exits the flow cell. Using this simplified model both convective and diffusive effects can be taken into account and the resulting temperature profile can be calculated. This was done for the peak operating condition at an incident solar flux of 1 000 W/m^2 (unconcentrated) and the result is plotted in Figure 69.

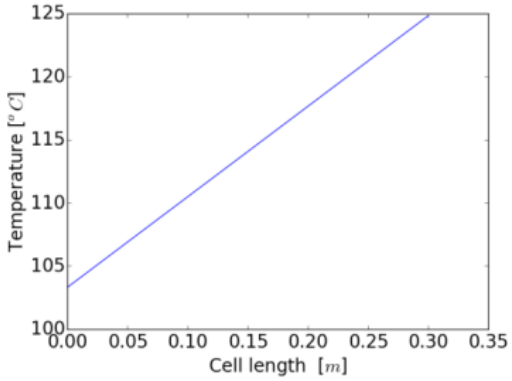

Figure 69: Temperature profile along flow cell.

As would be expected a simple linear increase in the temperature is observed along the flow channel since the high flow rate negates any diffusive effects. The temperature increase for a flow cell of this length is 125 ºC. Thus preliminary indications are that a 10 cm x 10 cm flow cell may be sufficient to achieve the required heating using three baffles. This model is not detailed enough to accurately reflect conditions in the cell and determine the optimum configuration. For this reason, a more comprehensive and accurate model was developed using the Fluent platform. A prototype flow cell was constructed to scale in the virtual environment, to reflect the preliminary design concept, as illustrated in Figure 70.

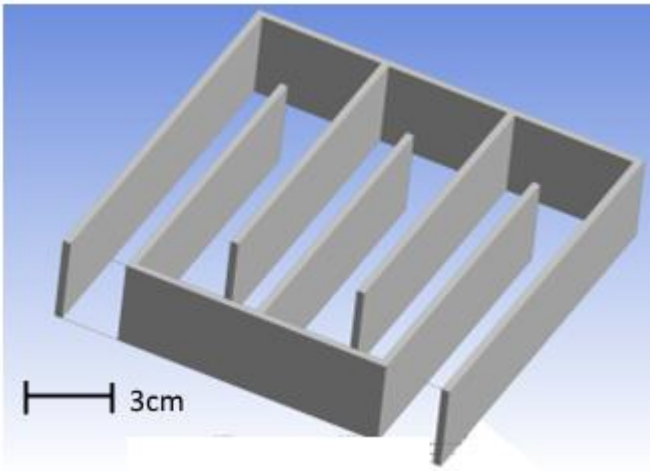

Figure 70: Flow cell isometric sketch.

The cell is constructed of a fluid zone and solid zone (aluminium) and meshed for the finite volume simulation. The results of the flow modelling are demonstrated in Figure 71 for laminar flow. Laminar flow was chosen due to its simplicity of configuration, in future however the simulation will be extended to turbulent flow conditions. This is expected to mainly influence the temperature distribution and loss calculations.

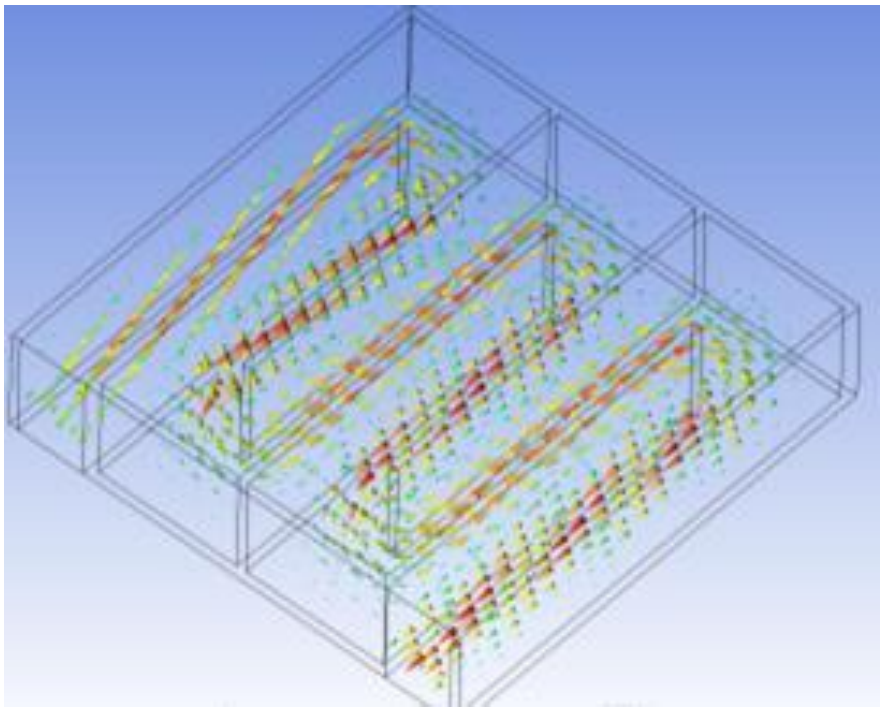

Figure 71: Flow cell flow pattern.

The arrows demonstrate the flow direction while their colour and size indicate the magnitude of the velocity. The flow pattern is more easily visualized by a contour plot of the velocity in the centre of the channel as demonstrated in Figure 72.

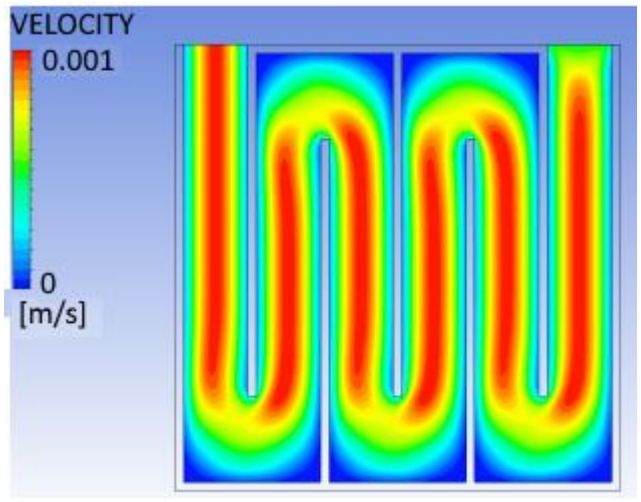

Figure 72: Flow cell velocity contour.

The model demonstrates the dead zones developed in the sharp corners of the current design, this indicates that the channel corners should be rounded to avoid stagnation points where the carbon black could settle out of suspension. This could be easily achieved using a circular/spiral coil; however constructing such a coil with a transparent upper surface would be very challenging. If the cells are constructed from an insulating material this could also lead to hotspots in these zones, as revealed in Figure 73 which shows the temperature distribution in a channel for aluminium compared to plastic.

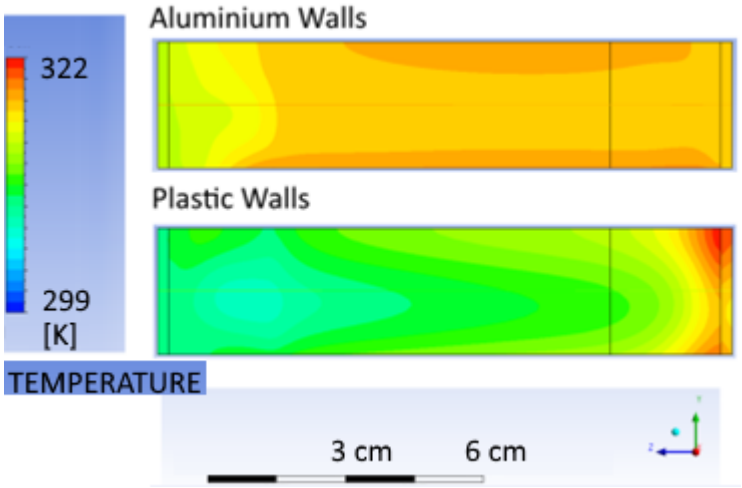

Figure 73: Flow cell channel temperature distribution for aluminium vs. plastic.

If the wall material is thermally conductive it allows heat transfer across it and a significantly more even temperature profile is established due to the heat re-distribution. Thus it was decided to construct the final cell from a suitable metal, which will be determined by cost and corrosion factors. Two key design considerations are the cell height and number of baffles. The cell height is intimately connected to the absorptivity of the water and the carbon black concentration. The mechanisms for absorption and scattering can be very complex. In the long term it is an objective of this work to develop a detailed model which fully accounts for radiation interaction with the thermal fluid. However, for the purposes of this investigation it is sufficient to qualitatively investigate the implications of the fluid absorptivity on the cell design. Field testing will nonetheless be used to confirm the conclusions and verify the design parameters. Figure 74 and 75 compare the temperature distributions within the flow cell for a high and medium absorptivity fluid.

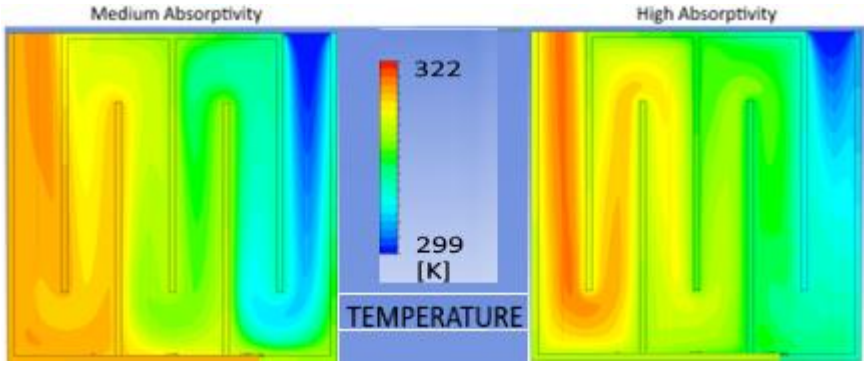

Figure 74: Flow cell temperature distribution for medium and high absorptivity.

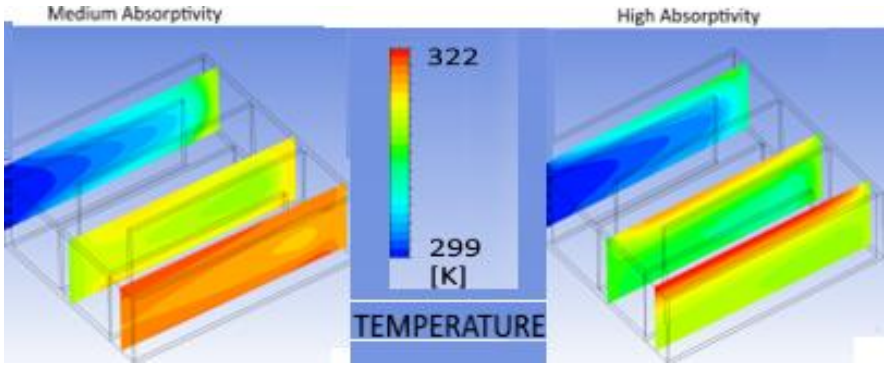

Figure 75: Flow cell channel temperature distribution for medium and high absorptivity.

For a low absorptivity radiation will simply be reflected back by the metallic flow cell bottom. However, it is important to note that this also happens for a fluid with an intermediate absorptivity, but in this case the radiation

can still be absorbed on the way back up before it exits the cell. Thus it is not necessary to have a cell which absorbs all the radiation in a single pass. In fact, as demonstrated by the figures, the use of a fluid with an excessive absorptivity clearly leads to thermal stratification. This is unwanted for several reasons, most importantly from an efficiency perspective this will lead to higher thermal losses as the primary loss mechanism is convection at the transparent cover surface, all other walls can be easily insulated. In addition, from an economic and recovery perspective it is preferential to use the lowest feasible carbon black concentration. As an additive this material will have a cost associated with it and if it must be recovered from the brine or salt product this will further increase expenses. The model and these considerations indicate that the lowest achievable carbon black concentration should be used; however the impact on the path length must be determined to calculate the influence on cell cost due to increased depth. A related issue which must be considered is the number of baffles in the design.

Traditionally baffles are usually installed in heat exchangers to increase the convection coefficient of the shell-side fluid by inducing turbulence and a cross-flow velocity component. In addition, the baffles physically support the tubes, reducing flow-induced tube vibration. For the current application the situation is quite different, the baffles are not needed for structural support and as previously highlighted they should be made of a high conductivity material, thereby adding to the cost of the flow cell. Thus from an economic perspective it is advantageous to reduce the number of baffles. As the number of baffles are reduced the flow path is decreased while the inlet size is increased and hence the channel cross-section as well (at constant depth). For the same mass flow rate this implies a lower linear velocity, as can be seen from Figure 76 which demonstrates the flow velocity for the two cases.

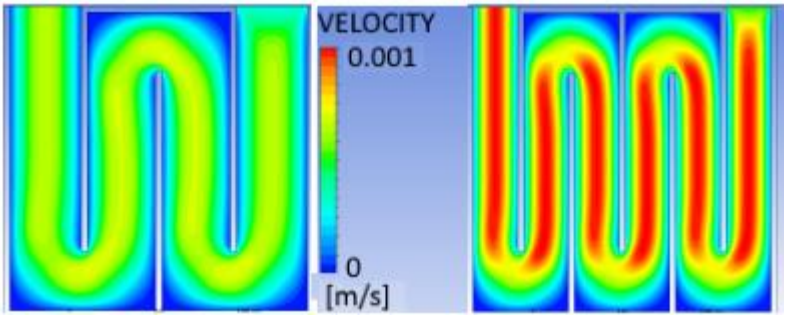

Figure 76: Flow cell velocity distribution for different baffle configurations.

From a heat loss point of view this is beneficial since it reduces the convective heat transfer co-efficient at the transparent surface by increasing the boundary layer thickness. In the experimental section it was observed that as the carbon black content is increased the thermal fluid tends to heat up very rapidly in the topmost portion. This can lead to nucleate boiling and bubble formation which leads to scattering, dropping the radiation absorption and causing undesirable two-phase flow. From the calculated Reynolds number the system is in reality operating in the turbulent flow region which leads to a flatter temperature profile or a more even temperature distribution across the cell depth. This profile is largely unaffected by further increases in velocity. At low flow rates the creation of large dead zones at low velocity can however be qualitatively seen from the simulation in Figure 77. As the number of baffles is reduced the corner areas where the flow velocity becomes zero increases, as indicated by the blue/light blue regions.

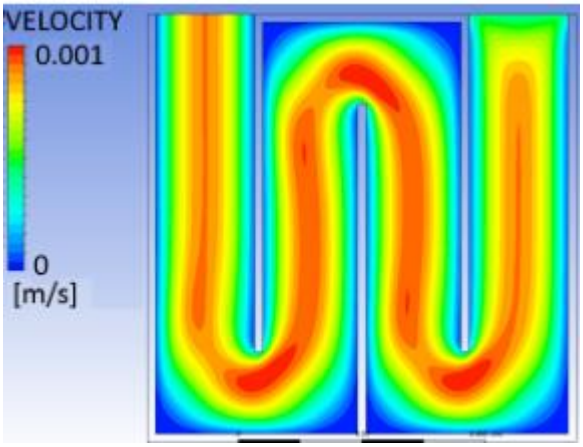

Figure 77: Flow cell channel velocity distribution for limited baffles.

It should be kept in mind that the real cell experiences turbulent flow which would reduce the size of said dead zones. With more baffles these areas decrease in size but increase in number, effectively offsetting this potential benefit. Thus, ideally, from a velocity point of view, the cell should contain a single flow zone which has no stagnant areas, but from a cost and manufacturing point of view however, this is difficult to achieve as a very gradual entrance is required that grows from the pipe diameter to the entire flow cell size. In addition, this may reduce the velocity so much that a relapse into laminar flow region occurs which is undesirable. For a 3 cm deep cell as used in the experimental section the Reynolds number would be close enough to 2000 to cause uncertainty. Therefore the number of baffles should not be reduced below three.

As mentioned, from the experimental work on the foams it was shown that from a cost perspective it is clear that higher concentration ratios, i.e. smaller cell sizes, are more economical. However the current design is quite different, in the foam case heating was done in a batch fashion onto a fixed target, in this case the medium to be heated is flowing and it is the target. Based on the modelling and experimental work it is clear that if the carbon black concentration is increased too far, preferential absorption occurs in the top layers of fluid which leads to a high temperature gradient in the cell. This is mainly detrimental due to the increased convective heat loss at the transparent boundary but also limits the absorption due to bubble formation and can lead to structural damage. The reason for this behaviour is the well-known Beer-Lambert law which states that intensity of light travelling through a medium varies logarithmically with depth. Thus as the absorbance increases, the distance across which the vast majority of absorption occurs will decreases exponentially. Conversely the depth required for complete absorption of the incoming radiation increases exponentially when the carbon black concentration is reduced. Thus a trade-off between the previously mentioned benefits for doing this and the increased manufacturing cost exists.

However, it was found that below carbon black concentrations of 0.001% the carbon black tends to settle out of the mixture over extended periods of time and the suspension becomes unstable. This would be detrimental to the operation of the system and thus places a limit on the minimum achievable carbon black concentration. As demonstrated experimentally the path length required for full absorption at this concentration is roughly 60 mm. Given the additional benefit of diffuse reflectance at the bottom of the channel a depth of 3 cm is enough to ensure full absorption. The experimental investigation also showed minimal thermal stratification for this depth and concentration combination without any bubble formation. Thus it may be concluded that this low concentration is still high enough to avoid excessive depth requirements while maintaining an even temperature distribution. An additional factor which may be adjusted is the light intensity; however since the carbon black concentration is fixed at a minimum due to practical considerations the light intensity is effectively fixed. If the intensity is decreased the cell depth is reduced but the cell area is increased, thus due to a quadratic proportionality costs would increase. If intensity, at fixed carbon black concentration, is increased the opposite happens. However, because the light intensity is now higher, a larger amount of energy is absorbed in the upper layers leading the higher surface temperatures and higher losses. Thus this is not a feasible option as

the carbon black concentration cannot be reduced. Based on the fact that the experiments were conducted at an intensity corresponding to a cell area of 10 cm by 10 cm, this is also the optimal area.

In summary, the modelling and experimental work have indicated that the lowest carbon black concentration is desirable to reduce cost, ease recovery and limit thermal stratification or the development of hot zones at the top surface of the flow cell. The latter would result in increased convective losses. In addition, the Reynolds number should be considered to check the minimum number of baffles is used, in order to further reduce thermal losses, but no less than is required to maintain flow in the turbulent region. Based on experimental results it was found that a carbon black concentration of 0.001 % is optimal for cost and taking into account settling considerations. Furthermore this fixes the cell design at a depth of 3 cm, an upper surface area of 10 cm by 10 cm and an implied concentration ratio of 100. Under these conditions it is estimated that the cell will have an overall capture efficiency of 75% based on an energy balance for the experimental measurements and accounting for the modelled heat losses.

6.3 OVERALL SYSTEM DESIGN

Of the two collector options considered only the DASC or carbon nanofluid delivered a significant improvement over existing collector options. For this reason only this alternative was selected for detailed modelling. A potential process flow diagram for the system is shown in Figure 78 below and a description of the plant operation is given.

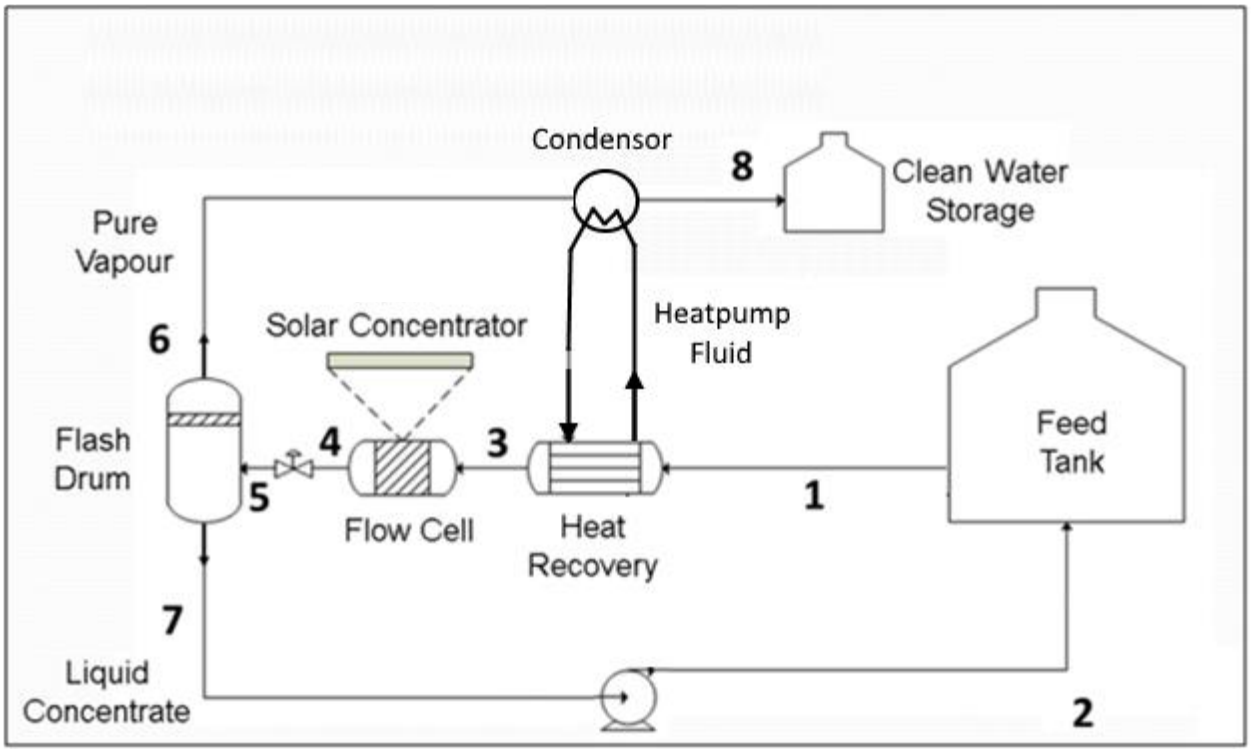

Figure 78: Basic plant design.

During the evening the clean water storage is emptied and the remaining concentrate in the feed tank is removed and replaced with a new batch of water to be purified. The concentrate can be stored in an evaporation pan to recover the salt in the case of seawater. During crystallization the salt crystals will separate from the carbon black which should settle into a separate phase. Given the low concentration of carbon black required this material can either be recycled to the feed tank or calcined to recover additional salt.

In the early morning as the sun rises, water begins circulation through the flow cell and is exposed to low intensity solar radiation. This will gradually heat up the circulating water, with the heating rate increasing as

the sun rises further. At some point during the morning the normal boiling point of the water is approached. To achieve flashing the control valve will be set to achieve a pressure of 2 ATM in the upstream section. This will allow the water to be heated beyond the normal boiling point of 100 ºC in this section to a maximum value of around 125 ºC. The pressure will then be released across the valve to atmospheric to induce flashing. As the temperature just starts to reach beyond 100 ºC a very small amount of vapour will be generated. However, this will increase throughout the day as progressively more energy is added to the system and the water temperature in the loop is increased.

A key aspect to the design is the recovery of the heat in the generated vapour stream. Once the water in the loop reaches the normal boiling point, the vapour generated by the flash at 1 ATM cannot exchange heat with the liquid stream already at 100 ºC. For this reason a heat pump is required to affect this energy transfer. A low boiling fluid will be vaporized using the 100 ºC steam, this gas will be compressed to a higher temperature and then allowed to condense through heat exchange with the liquid feed stream at 100 ºC in a closed cycle. This arrangement does require an additional energy input to drive the compressor which can be achieved using the same photovoltaic array that drives the slew motors for the mirror. Without this crucial element the only heating of the liquid feed will be in the flow cell during each pass. This will largely limit the temperature which can be achieved just before the flashing control valve. By increasing the temperature of the liquid feed to the flow cell through heat recovered from the vapour a much higher overall efficiency and yield can be achieved. Each stream in the process flow diagram is numbered with the stream initial and nominal operating condition is shown in Table 6.1.

Table 6.1. Stream properties.

Number	Pressure [atm]	Phase	Initial Temp [ºC]	Final Temp [ºC]
1	2.3	liquid	25	100
2	2.3	liquid	25	100
3	2.2	liquid	25	125
4	2.1	liquid	25	125
5	1	liquid	25	125
6	1	vapour	25	100
7	1	liquid	25	100
8	1	liquid	25	100

The final tank temperature is chosen to avoid two phase flow in the pump. To model the operation of this system a set of mass and energy balances are used, firstly the mass balance across the flash drum:

$$F_F = F_V + F_L \qquad (6.3.1)$$

Then the energy balances across heat pump, flow cell and flash drum:

$$Q_{hp} = F_F C_p (T_3 - T_2) = \eta_{hp}\left[F_V C_p (T_6 - T_8) + F_V \Delta H_{vap}\right] \qquad (6.3.2)$$

$$Q_{fc} = Q_{inc}\eta_{fc} = F_F C_p (T_4 - T_3) \qquad (6.3.3)$$

$$Q_{fd} = F_F C_p (T_5 - 100) = F_V \Delta H_{vap} \qquad (6.3.4)$$

The equations contain two efficiencies, namely that of the heat pump and that of the flow cell (i.t.o. incident solar radiation) as a starting point the values are set conservatively at 33% for the heat pump and 75% for the flow cell. Design sensitivity to these values will be investigated shortly. The solar irradiation profile for a typical summer's day is given in Figure 79.

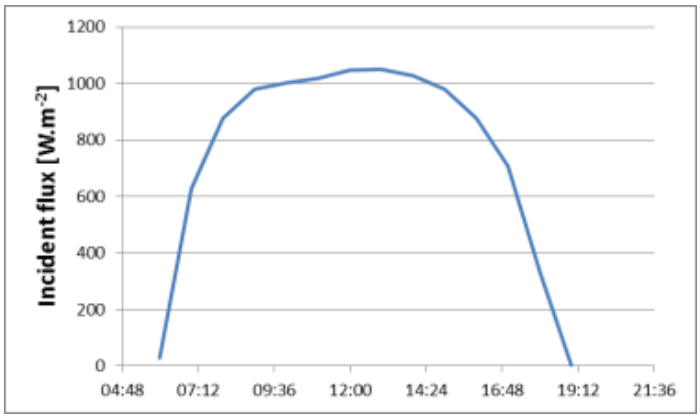

Figure 79: Summer solar irradiation curve.

The curve is not the typical bell shape observed during winter; instead the irradiation rapidly increases during the morning and achieves a roughly constant value from around 8 am through to 4 pm. As a first estimate of the operating condition it is assumed that the unit is exposed to 8 hours of constant irradiation at 1 kW. There are two possible operating modes for the system; the first would be to keep the initial feed flow rate low, in this way a large change in temperature can be affected across the flow cell. This will allow vapour generation to start almost immediately. Then gradually as the feed tank temperature increases, the feed flow rate can be increased and the vapour production will grow. In this design the feed temperature to the flash drum is effectively fixed, initially at 125 ºC. The feed rate, vapour production rate and feed tank temperature for this configuration (feed tank size = 14.5 kg) are shown in Figure 80.

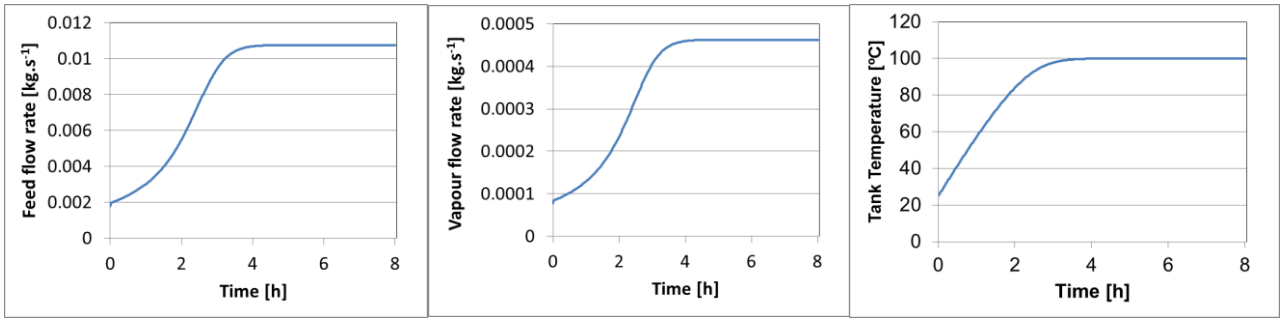

Figure 80: System performance for constant flash temperature.

As can be seen from these figures the system achieves steady state operation after roughly 3 hours after which the vapour flow is constant. The steady state vapour flow rate is 0.01076 kg/s[1] which results in a yield of 10.4 kg distilled water. An alternative configuration would be to maintain the feed flow rate at a constant value and allow the storage tank to heat up to operating temperature before flashing starts. For this setup the temperature before the flash valve, T_4, gradually increases and flashing starts once it exceeds 100 ºC. The performance of this arrangement is demonstrated in Figure 81.

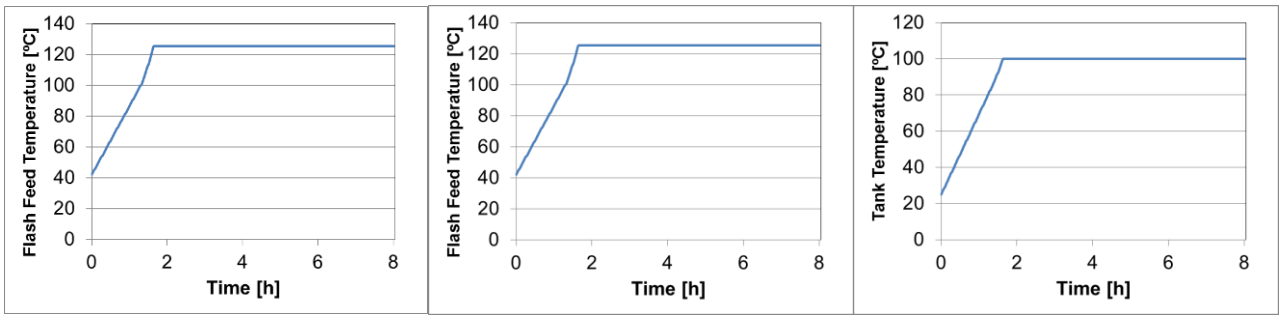

Figure 81: System performance for constant feed flow rate.

The simulation shown is for a feed rate of 0.0106 kg/s[1], which roughly corresponds to the steady state feed rate of the previous case. As a consequence the steady state flash feed temperature and vapour flow rate both correspond very closely with the previous case. In this case though steady state operation is achieved in slightly more than 1.5 hours. A slightly higher yield of 10.8 kg is achieved, this should also be weighed against the cost and complexity of a flow control system cascaded to control the flash feed temperature. For this reason the second arrangement is chosen as the basis for the system design. The circulating feed flow dependence should be considered in conjunction with the accompanying increase in the feed flash temperature, as shown in Figure 82.

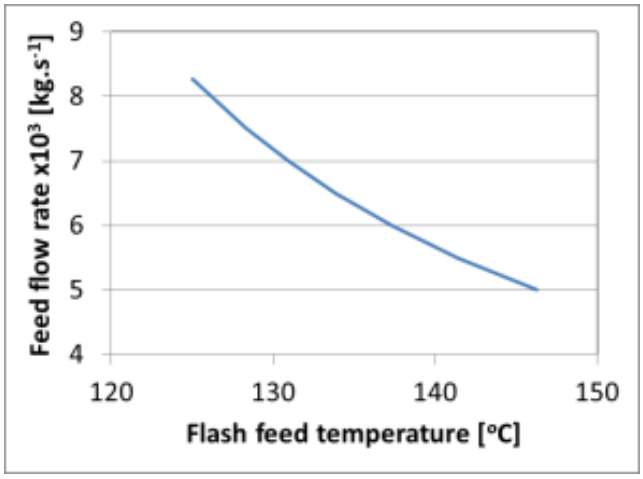

Figure 82: Feed flash temperature change with feed rate.

As the flow rate is decreased the flash feed temperature increases, this has strong implications for safety and the required pump. To maintain the feed to the flash drum in the liquid phase the pressure must be increased, from 2 bar for 125 ºC up to 4 bar for 150 ºC. This creates a safety hazard and requires a pump which can deliver twice the required head not to mention the increased costs of seals that operate at elevated temperatures. Thus it is imperative that the system is operated at a maximum of 125 ºC. This indirectly fixes the feed flow rate because at steady state the tank temperature is fixed. During the initial portion of daily operation the hot returning liquid from the flash drum heats up the storage tank. However, this cannot continue indefinitely as it would require increasingly higher pressures in the tank to stop the fluid from boiling. In this design the maximum tank temperature is limited to 100 ºC to avoid excessive material costs. This in turn means that at steady state the delta temperature across the flow cell and heat recovery unit is fixed at 25 ºC. At a given efficiency for these two units the feed rate is fixed.

In order to assess the system performance on a relative scale it is useful to consider the maximum yield achievable yield for a system where 0.75 kW of energy (1 kW at 75% efficiency) is used to purely evaporate water for 8 hours (no energy recovery) which is 11.85 kg. This represents the “ideal” scenario where every kJ of energy is used to evaporate water and the vapour is condensed by rejecting the heat to atmosphere. It is troubling to note that despite the fact that the system under consideration recovers 33% of the energy in the vapour stream, it does not achieve the yield of the “ideal” system. The reason for this is the limitation on the vapour generation rate. The amount of vapour that can be generated is fixed by the by the temperature difference between the flash feed temperature, set to a maximum of 125 ºC and the flash drum temperature, set by atmospheric pressure at 100 ºC. This delta temperature is the amount of sensible heat which can be converted to latent heat and generate vapour and fixes the vapour production rate, irrespective of how much energy recovery takes place. Since this delta T cannot be changed, the only way in which the yield can be improved is by decreasing the feed tank size or increasing the feed flow rate. In doing the former the time required for the system to achieve steady state is reduced and the yield over the same time period is increased. The variation in yield for a change in feed flow rate and feed tank size are displayed in Figure 83.

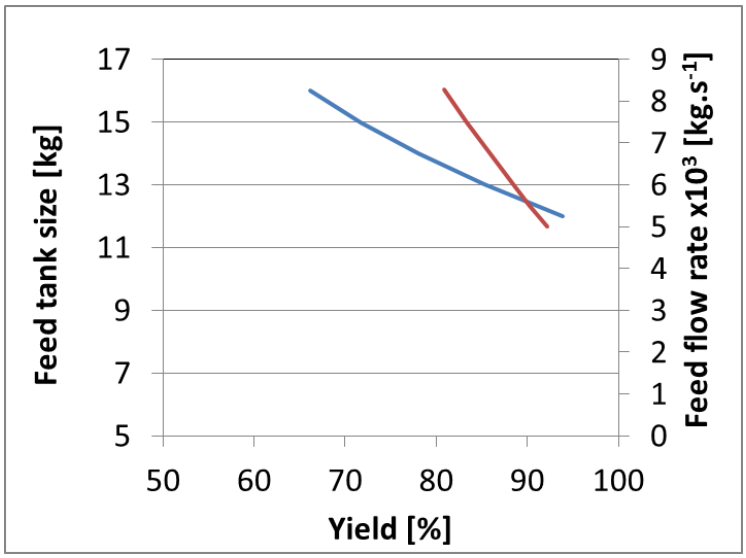

Figure 83: Yield dependence on feed flow and tank size.

The yield increases as this variable is reduced, thus the feed tank should be sized based on the required final concentration of the impurity in the feed. This will vary depending on the type of feed and scaling considerations of the brine, which at high yields or recovery this can become a big issue. A 75% recovery was chosen as a maximum limit, this is a safe margin to avoid excessive precipitation and as can be seen from Figure 83, the impact on yield is comparatively low.

The other major influences on the overall yield which must be considered are the two efficiencies for the heat pump and flow cell respectively. These are presented in Figure 84.

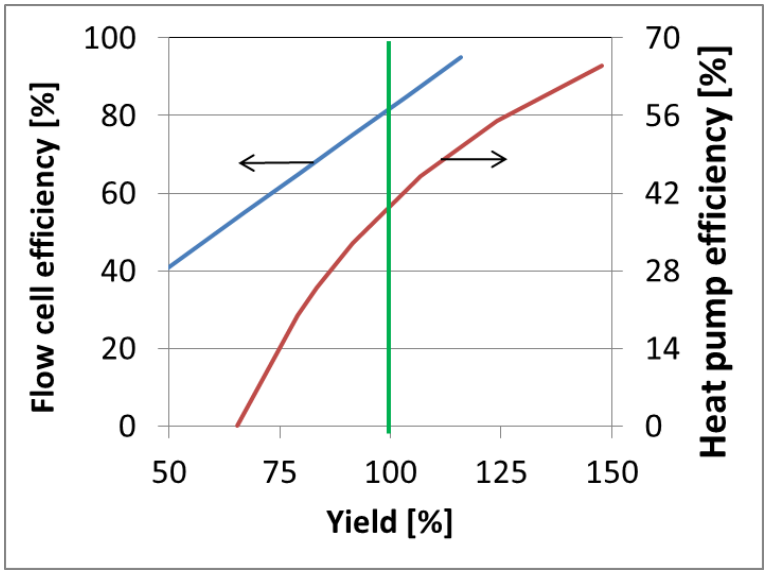

Figure 84: Yield dependence on efficiencies.

The dependency on flow cell efficiency is linear while the heat pump influence is closer to second order. Both have the same impact on the yield. This is because both have the same impact on the feed flow rate. As mentioned earlier the delta temperature rise from the feed tank to the flash drum inlet is fixed at 25 ºC. If either the flow cell or heat pump efficiency is increased, it means that a higher flow is possible at the same delta temperature. Thus increasing either has the same effect of higher steady state flow and hence vapour generation. It is interesting to note that only at efficiencies of around 80% and 40% for the flow cell and heat pump respectively, the yield starts to exceed what is possible using the “ideal” situation with zero energy recovery.

If it is found in the practical implementation that a heat pump is too expensive it can be removed from the design. As can be seen from Figure 84 this would have a maximum reduction of the yield to 65% of the ideal case, i.e. 7.76 kg/day. At efficiencies for the flow cell and heat recovery device of 75% and 33% respectively, the yield was found to be 10.8 litres per day which corresponds to the experimentally determined efficiency for the carbon black nanofluid flow cell. On the other hand for the graphitic foams as collector this value is around 40% which results in a daily yield of 5.8 litres per day.

6.4 CONDENSOR MODELLING

Despite the fact that the aims of this project did not include the development of the external condenser for the traditional still design, this portion of the system was still modelled. This generated useful insights for future projects and as such the results are presented here.

Based on the literature review it was decided to use a separate condenser section in an effort to enhance efficiencies. Furthermore, preliminary indications were that a multi-stage unit augmented by the addition of phase change materials (PCMs) would be the most effective design. It is intended that each section will be tested independently. As mentioned previously the lack of a descriptive model for many of the evaporator systems found in literature make it difficult to identify the origin of system inefficiencies. For this reason it was decided from the start to first develop a model to simulate the design and perform preliminary optimization of the configuration.

In general two approaches can be taken to simulate the conditions within a multi-stage solar still [97]: diffusion limited and convection driven. A survey of the available literature revealed that no studies have been conducted on designs employing forced convection. It is thought that forced convection would largely achieve heat transfer between the adjacent hot and cold stages instead of evaporation and condensation. For this reason designs operate under natural convection and the Grashof number, which indicates the relative influence of buoyant to viscous effects, is a critical design parameter.

For the diffusion limited case the system model is identical to that of the widely used pseudo-steady state approach to represent an Arnold diffusion cell [98]. This governs the evaporative mass transfer and the mass of liquid evaporated over a certain time, *t*, can be shown to be equal to:

$$m = \rho A \left[\left(h_0^2 + \frac{2cD_{AB}MMt}{\rho} ln\left\{ \frac{1 - y_{h2o}^{top}}{1 - y_{h2o}^{bott}} \right\} \right)^{0.5} - h_0 \right] \qquad (6.4.1)$$

On the condensation side it is expected that slow drop-wise condensation will occur. By utilising a sloped surface, droplets will coalesce and run downhill to be collected in the condensate channel. This mode of heat transfer is known to be one of the most efficient, capable of achieving heat transfer coefficients as high as 100 000 W/(m.K) [99]. For this reason it is not expected that the condensation side will pose any significant limitation to heat transfer. This is true for both the diffusion and convection controlled cases.

The diffusion model is applied to six case studies, starting with a single stage and increasing the number of stages to six. A small desktop still is modelled with a diameter of 5 cm, running for 12 hours during a single night. This is a base case which acts a baseline for discriminating between different preliminary designs. Based on literature a realistically achievable maximum temperature of 80 ºC was chosen and a night-time average temperature of 20 ºC. This spread of 60 ºC is evenly distributed between all stages for each of the cases. It is assumed that a PCM is available with a phase transition at this temperature. The PCM is melted during the day and freezes during the night; enough PCM is supplied to maintain the stage water temperature at the given value throughout the night. This is an ideal scenario as a cost-benefit analysis may indicate that less PCM is more economical.

For each of the stages the initial diffusion path is constant throughout at 2 cm. This should be as small as possible within fabrication limits to achieve the maximum mass transfer. It is assumed that each stage is loaded with the exact amount of water required to sustain evaporation throughout the night. Based on this model the yield results are shown in Figure 85 below.

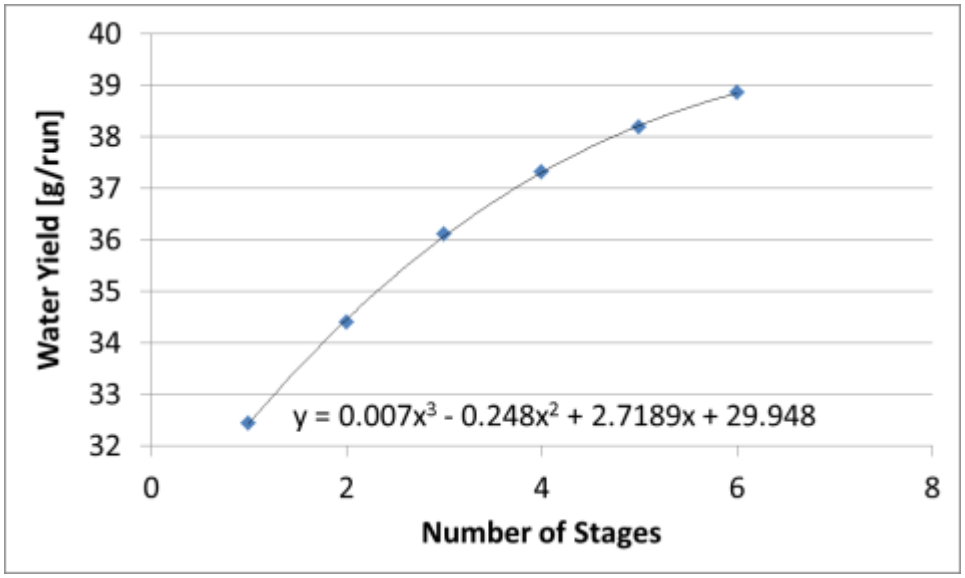

Figure 85: Diffusion limited PCM model yield

The behavior is as might be expected, the yield increases but with diminishing returns as the number of stages is increased. It should be noted however that the increase in yield is not substantial, starting at 6% with the first additional stage and decreasing to just under 2% for the sixth.

For the convection driven case it is neccesary to find a suitable correlation for the evaporative heat/mass transfer coefficient. Several past studies have focused on this problem [100,101] and the correlation found by Adhikari and co-workers [102] will be used as given below:

$$h_{evap} = 16.273 \times 10^{-3} h_{conv} \left[\frac{\mathcal{P}_{evap} - \mathcal{P}_{cond}}{T_{evap} - T_{cond}}\right] \quad (6.4.2)$$

and

$$h_{conv} = 0.884 \left[\left(T_{evap} - T_{cond}\right) + \frac{\left(\mathcal{P}_{evap} - \mathcal{P}_{cond}\right)\left(T_{evap} + 273.15\right)}{268.9 \times 10^{3} - \mathcal{P}_{evap}}\right]^{1/3} \quad (6.4.3)$$

The evaporation rate is then simply given by the conventional relationship:

$$m = \frac{h_{evap} A}{\Delta H}\left(T_{evap} - T_{cond}\right) \quad (6.4.4)$$

For the purposes of this preliminary investigation heat losses to ambient and due to distillate production are neglected. To validate the approach the model predictions are compared to the experimental results of Estahbanati and associates [103]. The model consistently over predicts the yield as the number of stages are increased by 30%, this is to be expected given the deficiency in accounting for heat losses. However, the trends accurately reflect the experimental results, as given below in Figure 86:

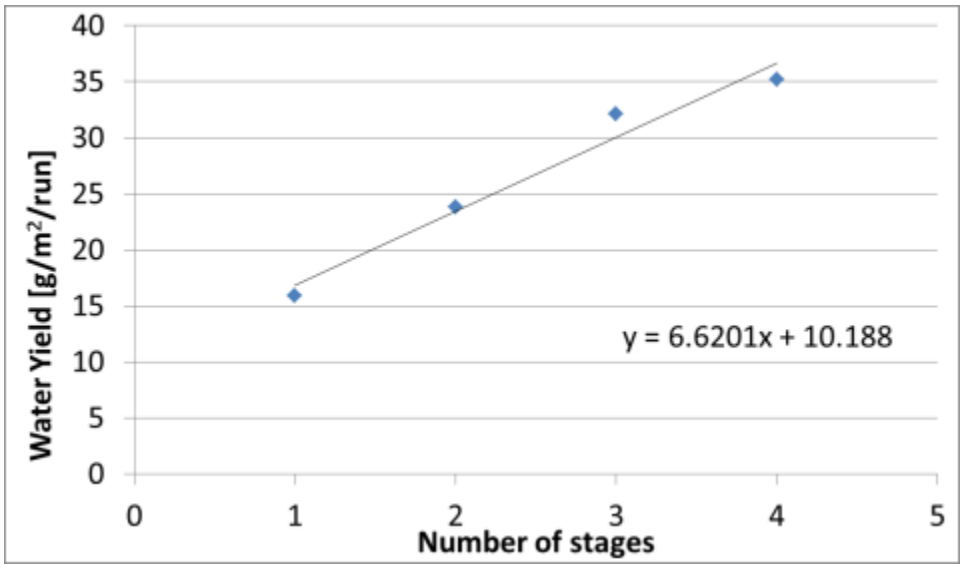

Figure 86: Convection driven experimentally modelled yield

The results are normalized for the still area in order to compare with the literature data. If this is multiplied by the still area, the daily yield for the desktop still would be 31 g, increasing to 69 g for four stages. The yield value for a single stage still is similar to that achieved with the diffusion limited model. However, for this system the yield rapidly increases as more stages are added. This is consistent with literature [97].

The data shown in Figure 86 are for the operating conditions indicated by the experimental measurements. If instead the approach using the PCM as for the diffusion model is applied, the results are shown in Figure 87.

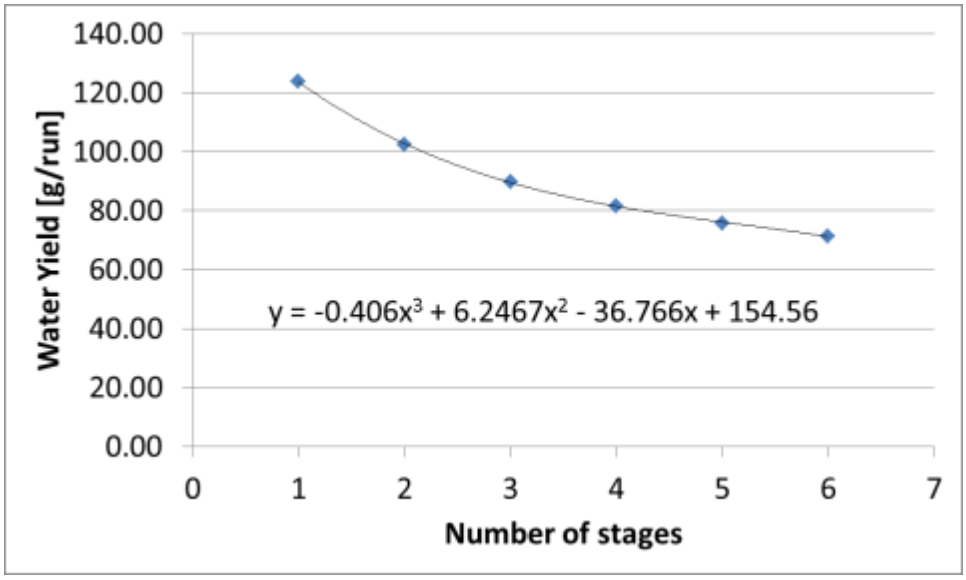

Figure 87: Convection driven PCM model yield

The result is quite counter-intuitive, indicating that the yield in fact decreases as the number of stages is increased. The reason for this is the completely different operating regimes of the two systems. For the experimental work, the first tray of the system is heated and the unit undergoes a transient cycle during which distillation occurs. The temperatures achieved in the still are intimately linked with the achievable yield. Examination of the experimental data shows the following:

- As additional stages are added, the average temperature of the same stage at the prior configuration increases. This is due to a slowing of heat transfer from each stage.

- As additional stages are added, the delta temperature between evaporation and condensation for the lower stages drops but the delta temperature at the top most stage remains more or less constant. Thus in this case the main evaporation “driver” is the top most stage and its performance remains more or less constant. The other stages run at a reduced efficiency but each is an incremental increase in the yield.
- As additional stages are added, the average temperature of the cooling water (the heat rejection reservoir at the top of the stack) decreases. This is due to the increased thermal capacity within the still due to additional stages.

All of these factors lead to an increase in the overall efficiency of the still. For the system proposed here conditions are quite different. With the designcurrently under consideration, the PCM keeps the temperature of a given stage constant throughout the night and it is assumed that the heat rejection reservoir, in this case a fanned heat sink will also remain at ambient temperature throughout. Thus the driving force for evaporation is constant. By adding additional stages the driving force is decreased since each stage causes a subdivision of the temperatures. This in turn leads to a reduced evaporative heat transfer coefficient for each stage and the system cannot achieve the yield of the single stage system despite having multiple evaporators.

An additional point to take note of is the yield for a single stage using the PCM: it is almost four times as much as either of the other cases. The reason for this is a) the low nature of diffusion limited transfer and b) the transient nature of the convective transfer in the experimental case. During the experiment a certain heat load is added to the bottom stage. This propogates upward, then as the load is removed the system returns to ambient temperature. This transient means that the delta temperature in each stage of the still is in flux and is limited by the thermal mass of each stage. For the PCM design the temperature driving force remains constant throughout the night, i.e. Grashof is at its maximum all the way through. This increases the yield by a factor of two compared to the experimental system with four stages. It is probable that the multi-stage system can approach that of the PCM system if the number of stages are increased further. However, the increased capital cost would make this an unattractive option. Preliminary indications are that theoretically a single stage PCM condensor will in fact provide the maximum yield of distilled water.

This touches on a critical issue that must be addressed in these systems which is that of energy recovery as compared to energy reuse. Energy recovery implies that streams enter and exit the system at roughly the same temperature they entered without any losses to ambient. Energy reuse on the other hand implies that the energy delivered to the process is used repeatedly to increase the yield of product per kW of energy. In the latter case the process efficiency increases but it is a well-known chemical engineering principle that for the same size unit this will invariably result in lower throughput [104]. This can easily be proven by considering any one of the multi-stage still investigations such as the one by Estahbanati [103]. If it is assumed that the material cost of a two stage still is roughly equivalent to two single stage stills, one can examine the yields for such systems. In the mentioned investigation a single stage still operating continuously generated 12.4 litre/day, whereas a two-stage system operating under the same conditions delivered 10.2 and 7.4 litre/day from the two stages respectively. Clearly at the same capital cost two single stage stills delivers more purified water per day than the total of the two-stage still. Such multi-stage, energy reuse designs only make sense in the context of very high energy costs, in such cases increasing efficiency increases capital cost (at a constant throughput) but decreases operating cost. This is not true for solar systems where the operating cost of the energy is virtually zero. It should be noted that this assumes the collector cost is minor compared to the still itself, i.e. the two single stage stills require double the energy input and hence collector size. Thus for solar stills it is usually not sensible to reuse energy but it is still important to achieve the highest possible energy recovery.

6.5 ECONOMIC AND OPERATIONAL EVALUATION

As stated in the introduction the industry standard for solar based desalination is reverse osmosis coupled with photovoltaic (RO-PV) [16]. One of the reasons for this is the striking process energy recovery, as mentioned in the prior section this relates to the enthalpy of streams entering and leaving the process. Since RO is not thermally based, all process streams enter and leave at virtually the same temperature. This means that energy recovery is very high and water can be practically produced at energy costs as low 8 kJ/kg [17]. To simply boil and vaporize 1 kg of water requires approximately 2430 kJ of energy, at such a low energy cost this would imply that 99,7 % of the energy must be recovered from the vapour stream (neglecting any sensible heat) for the system to achieve the same energy cost as RO. There are limitations however to this since RO cannot be applied to all water source of any salt content (level and composition) and at very high recoveries the energy costs increase sharply. Thus from an industrial perspective it is virtually impossible to beat RO on an energy recovery basis.

However two additional factors must be considered: energy cost and scale. The RO processes mentioned hinge heavily on economies of scale and as such are not used in systems operating at a throughput of less than 1 m^3/day. The objective of this investigation was to develop small scale options for delivering less than 0.1 m^3/day. Thus a direct comparison to RO systems is somewhat irrelevant since they cannot supply in this bracket. From an energy cost perspective it also only makes sense to compare apples with apples. The objective for the current project is to develop systems which operate purely off-grid, to circumvent the need to install costly infrastructure in unconnected regions. Very little cost information is available on systems which use PV in conjunction with RO. This would require the annualised cost of the PV installation to be considered. Furthermore these industrial systems are invariably built to operate continuously and as such are never truly off-grid. The reason being that at present the cost of battery storage systems are far too expensive to economically justify 24/7 operation, instead of simply using fossil fuel driven electricity that is readily and cost-effectively available when there is no sunshine. For these reasons it is more sensible to compare the three systems developed and tested in this project to units operating at similar throughputs.

As discussed in the prior section in the context of solar energy, energy efficiency in the sense of energy reuse is also somewhat overvalued. Energy efficiency improvements are only capable of offsetting the higher capital costs they require when the energy cost is very high. In the case of solar energy, the operating energy cost is virtually zero and as such the additional capital expense cannot be justified. Thus for this and future investigations, multi-stage condenser units should be disregarded. Taking all of these issues into consideration it is sensible to compare the throughputs and costs of the current systems to conventional, single stage, solar stills, operating off-grid on small scale. For such systems production costs are found to be around 5 US$ / m^3 or R 0.08 / litre [17]. These estimates consider the fully annualized capital cost of the system over a twenty year lifetime at an interest rate of 5% [105].

Throughputs for the two carbon based concentrated systems were estimated at 10.8 and 5.8 litres per day, respectively for the carbon black nanofluid and graphitic foam concepts. Both of these utilize the solar concentrator platform which was manufactured at a cost of R 180 000. It should however be borne in mind that this was a prototype design which did not benefit from large scale production cost reductions. In addition, as mentioned in the prior work section, the system can easily be increased to carry a four times larger mirror. This would effectively quadruple the solar aperture area from 1 m^2 to 4 m^2 with only a minor increase in cost for three additional Fresnel lenses. Thus it is possible to achieve four times the throughput at a conservative capital cost estimate of R 180 000. Using the previously mentioned amortization approach this brings the cost for purified water to R 0.92 and R 1.71 / litre using the carbon nanofluid and graphitic foams respectively. These costs are summarized in Table 6.1. For both options the costs are significantly above the market price for a comparable technology. It may be possible to reduce the capital cost of the system; however it is unlikely that this could be reduced by an order of magnitude. It should also be noted that this estimate is lower than the expected true cost since the material and production costs have been neglected. They may be considered

comparatively small for a single still but if the units are to be rolled out on a larger scale this would contribute significantly to the cost.

The third system tested in this investigation is an improved version of a traditional still design which delivered 0.544 litre of distilled water per day. However it should be noted that this was only for an aperture size of is 0.348 m^2. If it is assumed that cost scales linearly for this type of collector since it is essentially a flat plate, this would place the yield at 1.56 litres per day at a cost of R for the unit. From the experimental section it was however noted that after twenty minutes the still had not yet achieved steady state. Thus operating at steady state for the entire hour period the unit throughput could conceivably be raised to 2.4 litres per day. This is slower than expected for these types of solar stills which normally operate at a daily production rate of 3 to 4 litres per m^2 per day [17]. This would bring the annualized cost to R 0.11 / litre which is in line with the expected market price. The design could be improved through further experimentation to achieve more consistent operation over extended periods of time. In addition, indications are that throughput could be further enhanced by coupling the evaporator to an external condenser. However, this would come at an additional cost which must be taken into consideration. The costs are summarized in Table 6.1.

From an operational perspective the solar concentrator platform appears to have significant additional complexity. However, this system has been extensively automated and operates autonomously. The unit has been used for experimentation continuously over the two year duration of the project. The only minor maintenance required was the replacement of an SD memory card and the washing of the mirrors. The primary mirror has in the interim developed a crack due to thermal expansion, however this can be overcome in future designs by adding flexibility into the mirror mounting through rubber fasteners. In addition, it must be stressed that the unit has operated completely off-grid, with no electricity consumption from the grid whatsoever. Thus once the system has been setup it requires only minor operator intervention. However, this excludes the operation of the proposed flash distillation circuit. Although this only adds an additional pump and control valve to the unit it is anticipated that for the fully operational system, brine handling and equipment maintenance will require some skilled labour.

The traditional still unit has very little complexity but as pointed out in the experimental section, maintaining an even distribution of liquid over the evaporator's wick surface poses a significant challenge. This task cannot be conducted manually and must be automated. It is possible that a procedure could be developed to prepare the system for continuous operation by first soaking the wick and then having a continuous liquid flow over the surface. The problem with such an approach is that, depending on conditions such as cloud cover, etc. it would invariably result in liquid pooling at the bottom of the inclined box. This water could simply be recycled to the feed tank but a comprehensive experimental investigation would be required to determine the optimal flow rate which does not cool the wick excessively but maintains even flow and good wetting.

Table 6.1. Comparison of heating rates at different concentrations compared to that of salt water.

Method	Yield (litre/day)	Cost (R/litre)
Traditional Still [17]	3 - 4	0.08
Graphite Foam	10.8	1.71
Carbon Black Nanofluid	5.8	0.92
Modern Evaporator	2.4	0.11

CHAPTER 7: CONCLUSIONS AND RECCOMENDATIONS

7.1 CONCLUSIONS

The need for identifying an affordable, small-scale (<0.1 m^3/day), off-grid desalination process using solar energy in the South African context is clear. Not only from the perspective that the country faces a lack of fresh water but also from a sustainable energy supply point of view. By integrating solar energy and desalination two key problems can be solved simultaneously. A review of the available literature indicated that solar thermal based flash distillation can provide a competitive option to fulfil this niche. Traditional solar “stills” are in fact more accurately described as evaporators. These stills cannot achieve the high purity and efficiency of industrial scale, thermal desalination options. True phase change based desalination such as thermal flash can be used to treat a wide spectrum of brine sources and produces high purity, fully disinfected water. On small-scale operations in terms of flexibility and cost, reverse-osmosis is not considered economically viable, despite being the industry standard for renewable energy based desalination when coupled to photo-voltaic systems.

Nonetheless, traditional solar stills have however recently been subject to a great deal of research and many modern modifications have been proposed to improve system performance. Two of these are the use of thin-film or wick based, inclined still configurations, coupled to multi-stage condenser units. These can in addition be linked with thermal energy storage in the form phase change materials to extend operating hours into the night when driving forces for condensation are optimal. For this investigation, such a modern evaporative still was considered as the benchmark against which new thermal flash based designs should be measured. To achieve small-scale, thermal flash distillation two key aspects had to be developed and incorporated into a system design.

First, a method to cost-effectively achieve the high temperatures required for this type of operation had to be created and tested. This necessitated the use of concentrated solar energy. The solar concentrator platform developed at the University of Pretoria, demonstrated very high solar concentration levels using only cheap, off the shelf components. Secondly a suitable solar collector had to be discovered in order to utilize the solar radiation and efficiently transfer the energy to the water for flash distillation. Finally, the most suitable option had to be incorporated into an overall system design to estimate the total yield of desalinated water from such an arrangement for comparison to the chosen benchmark. Prior work indicated that two options existed, name a surface based absorber in the form of highly graphitic carbon foams and a volume based, or direct absorption solar collector namely carbon black nanofluids. This report described the detailed testing and evaluation of these three options.

The aim of the investigation were to extend the prior lab testing of the three methods (concentrated solar energy coupled to a graphitic foam target and a carbon black suspension respectively, as well as the thin-film solar evaporator concept), to field testing using real, concentrated in two cases, sunlight as input. Furthermore all three methods should be compared based on efficiency, cost, maintenance and operator input. This was to be done using simulated seawater only as the first step.

The graphite foam materials offered a cost-competitive option to more expensive, mesophase based foams available in the market. These high thermal conductivity foams demonstrated a low density and a high surface area, ideal for transferring captured solar radiation to a fluid such as water. The foams were extensively tested and their configuration optimised to ensure maximum heat transfer at the lowest cost. However, in the final experimental testing the foam materials did not manage to perform any better than traditional flat plate solar collectors with an overall efficiency of around 40%. Several potential causes for this exist:
1) The thermal conductivity of the foam is not high enough; this is caused by the use of low cost raw materials.

2) The porosity of the foam is not low enough to allow complete free flow of water through the structure. The porosity can however not be reduced further as this compromises the structural integrity of the foam.
3) The reflective nature of graphite may be reducing the ability of the foam to fully absorb the sunlight. This can potentially be overcome through the use of a carbon black additive.

A carbon black based, solar absorbing, nanofluid was successfully developed using the non-toxic, commercial surfactant, Tween 20. The photo-thermal, absorption and flow characteristics of the nanofluid were extensively characterized as a function of concentration. Ultimately it was found that at a concentration as low as 0.001 vol % of carbon black, the fluid could achieve 100% solar radiation absorption within a flow cell. A detailed model of the flow cell was developed to optimize its design and fully understand the operational behaviour. The experimental and simulation results enabled an optimized flow cell to be designed and the overall efficiency of the carbon black nanofluid in such a solar collector is estimated at 75%.

The experimentally determined solar radiation capture efficiencies of both the foam and carbon black nanofluid were incorporated into an overall system model to estimate the daily water yields using these materials. The overall system model assumes the collector is used in a continuously circulating system with 33% heat recovery from the vapour stream. It is envisioned that this can be achieved using a small heat pump. The solar platform is currently has a 1 m^2 aperture. Under these conditions, the two options deliver 10.8 and 5.8 litres per day at a cost of R 0.92 and R 1.71 / litre for the nanofluid and foam respectively. The yields are excellent in comparison with traditional solar evaporative stills which generally achieve around 3 to 4 litres per m^2 per day. However, when compared with reported market values for similar small-scale systems, at around R 0.08 / litre, the costs are an order of magnitude higher.

The modern still or thin-film evaporator on the other hand has proven to be market competitive at a price of R 0.11 / litre. Unfortunately however, the yield of this still is slightly below the expected value at around 2.4 litres per day. This yield could be greatly improved through the use of an external condenser. The modelling investigation has shown that this does not have to be a complex multi-stage design since the cost of solar energy is zero. Instead it is recommended that a single stage design should be tested using phase change material to extend operating time into the evening for optimal condensation conditions and maximum yield. It will be essential to identify a low cost PCM however to ensure that the cost per litre of produced water does not increase. A subsequent economic analysis will be required for a final conclusion.

From an operability and maintainability point of view the solar concentrator platform, despite its complexity has been operated autonomously for more than a year. The only maintenance requirements are a periodic cleaning of the mirror. The flow system design is also very straightforward since it only includes a single flow controller. Thus this system would require minimal operator input while the modern still also has very little complexity and no moving parts. The unit would also require periodic cleaning to ensure optimal operation. A more significant issue is that of maintaining an even distribution across the wick to ensure a thin-film of liquid is always present. In light of varying sunlight conditions this could prove a difficult problem to overcome. No easy solution is possible from a control perspective since complex meteorological measurements and process control would be required. Instead it is recommended that future designs explore the possibility of using capillary action to draw the fluid up the inclined still rather than have a distributor with liquid running in a downward direction. In this way as fluid is depleted the system will self-regulate irrespective of varying irradiation from the sun. This would require the consideration of additional wick materials and varying thicknesses.

The objective was to overcome the issues identified and develop practically implementable systems. Practical representations of both a concentrated solar absorber and the conventional evaporative type still were successfully built and tested, in accordance with the project aims. The overall conclusion which can be drawn from this investigation is that despite the improved yields and other benefits offered by flashing (distillation), compared to evaporation, cannot justify the additional capital cost on the small scale considered here.

7.2 RECCOMENDATIONS

Despite the high efficiency, low maintenance and easy operation of the solar concentrator platform coupled to the direct absorption solar collector, it is not recommended that this option be pursued further. The capital costs associated with concentrating the solar energy are simply too high. It is difficult to see where the design could be further improved to reduce costs. The setup already uses inexpensive, off the shelf components and cheap Fresnel lens technology and did not consider the material costs. The investigation indicates that unless the collector material is exceptionally expensive, for example multi-junction photo-voltaic cells, it is not possible to economically justify the costs of concentration.

A key consideration in yield improvement is the capture and re-use of the energy in the system, in the current case achieved by the heat pump. It is recommended that future investigations focus on the cost-benefit and practicality of achieving good heat recovery.

If a suitable technology can be found to compete with conventional evaporative stills, it is critical that these be assessed in the context of a specific application, i.e. a location where the solar irradiance is known and a representative water sample can be obtained. In this way clearer consideration can be given to issues such as scaling, brine concentration levels and brine disposal.

In future it is recommended that a tube based design is considered as the model system. As opposed to the square channel arrangement used in this study as the heat losses for the current system were difficult to fully quantify. More detailed modelling of the flow cell, nanofluid and the evaporative type still can yield additional insight for other potential projects. For the evaporative still a psychometric modelling approach should also be considered.

Based on the current work it has become clear that concentration infrastructure costs cannot be justified on a low price, commodity-type and public product. However, the detailed modelling and study of the flow cell unit has indicated that concentration is not required to achieve high temperatures. If the system can be suitably insulated it may be possible to achieve the temperatures required for flash distillation without the need for costly concentration infrastructure. This will be the topic of the project which will be the follow-on for the current effort. The aim of this investigation will be to determine if it is possible to achieve high temperatures using affordable and available components combined with only ambient sunlight. A key consideration will be the recovery of the captured energy to increase system yield.

REFERENCES

[1] South African Human Rights Commission, 2014. Report on the Right to Access Sufficient Water and Decent Sanitation in South Africa: 2014
[2] South African Department of Water Affairs, 2013. Annual national state of water report for the hydrological year 2012/2013.
[3] European Commission. Concentrating solar power - From research to implementation. Published in Luxembourg by Office for Official Publications of the European Communities; 2007. ISBN 978-92-79-05355-9. ec.europa.eu.
[4] Sargent & Lundy LLC Consulting Group. Assessment of parabolic trough and power tower solar technology cost and performance forecasts. Report NREL/SR-550-34440, NREL (National Renewable Energy Laboratory), Golden, CO,USA; 2003.
[5] Gevrek ZE, Uyduranoglu A. Public preferences for carbon tax attributes. Ecol Econ, 2015;118:187-97.
[6] Hertwich EG, Peters GP. Carbon Footprint of Nations: A Global, Trade-Linked Analysis. Environ Sci Technol, 2009; 43:6414–20.
[7] Tian Y, Zhao CY. A review of solar collectors and thermal energy storage in solar thermal applications. Appl Energy, 2013;104:538-53.
[8] Winkler H. Renewable energy policy in South Africa: policy options for renewable electricity. Energy Policy. 2005;33(1):27-38.
[9] Bugaje IM. Renewable energy for sustainable development in Africa: a review. Renewable and Sustainable Energy Reviews. 2006;10(6):603-12.
[10] Baharoon DA, Rahman HA, Omar WZW, Fadhl SO. Historical development of concentrating solar power technologies to generate clean electricity efficiently – A review. Ren Sust Energy Rev, 2015;41:996-1027.
[11] Heller L, Gauché P. Modeling of the rock bed thermal energy storage system of a combined cycle solar thermal power plant in South Africa. Solar Energy. 2013;93:345-56.
[12] Dekker J, Nthontho M, Chowdhury S, Chowdhury SP. Investigating the effects of solar modelling using different solar irradiation data sets and sources within South Africa. Solar Energy. 2012;86(9):2354-65.
[13] Fluri TP. The potential of concentrating solar power in South Africa. Energy Policy. 2009;37(12):5075-80.
[14] Hamadou OA, Abdellatif, K. Modeling an active solar still for sea water desalination process optimization. Desalination. 2014;354:1-8.
[15] Ali MT, Fath HE, Armstrong PR. A comprehensive techno-economical review of indirect solar desalination. Renewable and Sustainable Energy Reviews. 2011;15(8):4187–99.
[16] Hasnain SM, Alajlan SA. Coupling of PV-powered RO brackish water desalination plant with solar stills. Desalination 1998;116:57–64.
[17] Li C, Goswami Y, Stefanakos E. Solar assisted seawater desalination: A review. Ren Sust Energy Rev, 2013;19:136-163.
[18] Focke WW, Badenhorst H, Ramjee S, Kruger HJ, van Schalkwyk R, Rand B, Graphite foam from pitch and expandable graphite. Carbon. 2014;73:41-50.
[19] Han D, Meng Z, Wu D, Zhang C, Zhu H. Thermal properties of carbon black aqueous nanofluids for solar absorption. Nanoscale Res Lett. 2011;6:457-464.
[20] Molewa E. Minister of Water and Environmental Affairs, South African Governement Gazette No 34796 of 28 November 2011, last access 06/09/2013: http://www.sanews.gov.za/south-africa/waste-tyre-management-plan-gazetted
[21] Flanne MG, Lui X, Zhou C, Penner JE. Enhanced solar energy absorption by internally-mixed black carbon in snow grains. Atmos. Chem. Phys. Discuss. 2012;12:2057-2113.
[22] Neumann O, Urban A, Day J, Lal S, Nordlander P, Halas NJ. Solar Vapor Generation Enabled by Nanoparticles. ACS Nano. 2012;7:42-49.
[23] National Renewable Energy Laboratory, 2014. SolTrace Optical Modeling Software. <http://www.nrel.gov/csp/soltrace> (accessed on 01.12.15).

[24 Mukhopadhyay SM, Mahadev N, Joshi P, Roy AK, Kearns KM, Anderson DP. Structural investigation of graphitic foam. Journal of Applied Physics. 2002;91(5):3415.
[25] Yadav A, Kumar R, Bhatia G, Verma GL. Development of mesophase pitch derived high thermal conductivity graphite foam using a template method. Carbon. 2011;49(11):3622-30.
[26] Kuhn J, Ebert HP, Arduini-Schuster MC, Büttner D, Fricke J. Thermal transport in polystyrene and polyurethane foam insulations. International Journal of Heat and Mass Transfer. 1992;35(7):1795-801.
[27] L.J. Gibson MFA. Cellular solids: structures and properties. New York: Pergamon Press; 1988.
[28] Doermann D, Sacadura JF. Heat transfer in open cell foam insulation. Journal of Heat Transfer. 1996;118(1):88-93.
[29] Klett J, Hardy R, Romine E, Walls C, Burchell T. High-thermal-conductivity, mesophase-pitch-derived carbon foams: Effect of precursor on structure and properties. Carbon. 2000;38(7):953-73.
[30] Gallego NC, Klett JW. Carbon foams for thermal management. Carbon. 2003;41(7):1461-6.
[31] Klett JW, McMillan AD, Gallego NC, Walls CA. The role of structure on the thermal properties of graphitic foams. Journal of Materials Science. 2004;39(11):3659-76.
[32] Kearns, KM (1999) Process for preparing pitch foams, US Patent 5868974
[33] Klett JW, McMillan AD, Gallego NC, Burchell TD, Walls CA. Effects of heat treatment conditions on the thermal properties of mesophase pitch-derived graphitic foams. Carbon. 2004;42(8–9):1849-52.
[34] Gaies D, Faber KT. Thermal properties of pitch-derived graphite foam. Carbon. 2002;40(7):1137-40.
[35] Chen C, Kennel EB, Stiller AH, Stansberry PG, Zondlo JW. Carbon foam derived from various precursors. Carbon. 2006;44(8):1535-43.
[36] Moriyama, R Kumagai, H Hayashi, J. Yamaguchi, C Mondori, J Matsui, H ,Chiba, T (1999) Formation of mesophase spheres from a coal tar pitch upon heating and subsequent cooling observed by an in situ H-NMR Carbon, 38, 749-758.
[37] Matsumo, T (1985) “Meosphase pitch and its carbon fibres” Pure and applied chemistry, 57(11) , 1553-1562.
[38] Ragan, S and March, H (1983) “Science and technology of graphite” Journal of Material Science, 18, 3161-3176.
[39] Anderson HJ, Anderson DP, Kearns KM. Microcellular pitch-based carbon foams blown with helium gas. p. 756-62.
[40] Zhu J, Wang X, Guo L, Wang Y, Wang Y, Yu M, et al. A graphite foam reinforced by graphite particles. Carbon. 2007;45(13):2547-50.
[41] Celzard A, Marêché JF, Furdin G. Modelling of exfoliated graphite. Progress in Materials Science. 2005;50(1):93-179.
[42] Furdin G. Exfoliation process and elaboration of new carbonaceous materials. Fuel. 1998;77(6):479-85.
[43] Wissler M. Graphite and carbon powders for electrochemical applications. Journal of Power Sources. 2006;156(2):142-50.
[44] Chung DDL. Exfoliation of graphite. Journal of Materials Science. 1987;22(12):4190-8.
[45] Chung DDL. Review: Graphite. Journal of Materials Science. 2002;37(8):1475-89.
[46] Inagaki M. On the formation and decomposition of graphite-bisulfate. Carbon. 1966;4(1):137-41.
[47] Afanasov IM, Morozov VA, Kepman AV, Ionov SG, Seleznev AN, Tendeloo GV, et al. Preparation, electrical and thermal properties of new exfoliated graphite-based composites. Carbon. 2009;47(1):263-70.
[48] Lise W, van der Laan J. Investment needs for climate change adaptation measures of electricity power plants in the EU. Energy Sustain Dev, 2015;28:10-20.
[49] Zhoa X, Du D. Forecasting carbon dioxide emissions. J Environ Manage, 2015;160:39-44.
[50] European Commission. Concentrating solar power - From research to implementation. Published in Luxembourg by Office for Official Publications of the European Communities; 2007. ISBN 978-92-79-05355-9. ec.europa.eu.
[51] Sargent & Lundy LLC Consulting Group. Assessment of parabolic trough and power tower solar technology cost and performance forecasts. Report NREL/SR-550-34440, NREL (National Renewable Energy Laboratory), Golden, CO,USA; 2003.
[52] Gevrek ZE, Uyduranoglu A. Public preferences for carbon tax attributes. Ecol Econ, 2015;118:187-97.

[53] Hertwich EG, Peters GP. Carbon Footprint of Nations: A Global, Trade-Linked Analysis. Environ Sci Technol, 2009; 43:6414–20.
[54] Wu Z, Lui Z, Parvez K, Feng X, Müllen K. Ultrathin Printable Graphene Supercapacitors with AC Line-Filtering Performance. Adv Mater, 2015;27:3669-75.
[55] Konios D, Petridis C, Kakavelakis G, Sygletou M, Savva K, Stratakis E, Kymakis E. Reduced Graphene Oxide Micromesh Electrodes for Large Area, Flexible, Organic Photovoltaic Devices. Adv Func Mater, 2015;25:2213-21.
[56] Tian Y, Zhao CY. A review of solar collectors and thermal energy storage in solar thermal applications. Appl Energy, 2013;104:538-53.
[57] Baharoon DA, Rahman HA, Omar WZW, Fadhl SO. Historical development of concentrating solar power technologies to generate clean electricity efficiently – A review. Ren Sust Energy Rev, 2015;41:996-1027.
[58] Ho CK, Iverson BD. Review of high-temperature central receiver designs for concentrating solar power. Ren Sust Energy Rev, 2014;29:835-46.
[59] Behar O, Khellaf A, Mohammedi K. A review of studies on central receiver solar thermal power plants. Ren Sust Energy Rev, 2013;23:12-39.
[60] Alonso E, Romero M. Review of experimental investigation on directly irradiated particles solar reactors. Ren Sust Energy Rev, 2015;41:53-67.
[61] Krueger KR, Davidson JH, Lipinski W. Design of a New 45 kWe High-Flux Solar Simulator for High-Temperature Solar Thermal and Thermochemical Research. J Sol Energy Eng, 2011;133:0110131-8.
[62] Alxneit I, Schmit H. Spectral Characterization of PSI's High-Flux Solar Simulator. Research. J Sol Energy Eng, 2012;134:0110131-5.
[63] Petrasch J, Coray P, Meier A, Brack M, Haberling P, Wuillemin D, Steinfeld A. A Novel 50 kW11,000 Suns High-Flux Solar Simulator Based on an Array of Xenon Arc Lamps. ASME J Sol Energy, 2007;129:405-11.
[64] Xie WT, Dai YJ, Wang RZ, Sumathy K. Concentrated solar energy applications using Fresnel lenses: A review. Ren Sust Energy Rev, 2011;15:2588-606.
[65] Sani E, Mercatelli L, Francini F, Sans J-L, Sciti D. Ultra-refractory ceramics for high-temperature solar absorbers. Scr Mater, 2011;65:775-8.
[66] Pierson HO. Handbook of Carbon, Graphite, Diamond and Fullerenes. Properties, Processing and Applications. 1993; Noyes Publications, New Jersey, USA.
[67] Avila-Marin AL. Volumetric receivers in Solar Thermal Power Plants with Central Receiver System technology: A review. Sol Ener, 2011;85:891-910.
[68] Focke WW, Badenhorst H, Ramjee S, Kruger HJ, van Schalkwyk R, Rand B. Graphite foam from pitch and expandable graphite. Carbon, 2014;73:41-50.
[69] Becker M, Fend T, Hoffschmidt B, Pitz-Paal R, Reutter O, Stamatov V, Steven M, Trimis D. Theoretical and numerical investigation of flow stability in porous materials applied as volumetric solar receivers. Sol Energy, 2006;80:1241-8.
[70] Long, CM, Nascarella, MA and Valberg, PA (2013) "Carbon black vs. black carbon and other airborne materials containing elemental carbon: Physical and chemical distinctions" Environmental pollution, 181, 271-286.
[71] Maquin, B, Goyhénèche, J-M, Derré, A, Trinquecoste, M, Chadeyron, P and Delhaès, P (2000) "Thermal conductivity of submicrometre particles: carbon blacks and solid solutions containing C, B and N" Journal of Physics D: Applied Physics, 33, 8.
[72] Magasinski, A, Dixon, P, Hertzberg, B, Kvit, A, Ayala, J and Yushin, G (2010) "High-performance lithium-ion anodes using a hierarchical bottom-up approach" Nature materials, 9, 353-358.
[73] Pritchard, G (1998) Plastics additives : an A-Z reference, Chapman & Hall, London.
[74] Han et al. "Thermal properties of carbon black aqueous nanofluids for solar absorption" Nanoscale Research Letters 2011, 6:457
[75] Neumann, O. et al., 2012. Solar vapour generation enabled by nanoparticles. ACS Nano.
[76] Smith, YR, Bhattacharyya, D, Willhard, T and Misra, M (2016) "Adsorption of aqueous rare earth elements using carbon black derived from recycled tires" Chemical Engineering Journal, 296, 102-111.

[77] Hita, I, Arabiourrutia, M, Olazar, M, Bilbao, J, Arandes, JM and Sánchez, PC (2016) "Opportunities and barriers for producing high quality fuels from the pyrolysis of scrap tires" Renewable and Sustainable Energy Reviews, 56, 745-759.
[78] Martínez, J, Murillo, R and García, T (2013) "Production of carbon black from the waste tires pyrolysis".
[79] BSH Priya, V Sridevi, RS Kumari, MT Bai. Review on Water Desalination using Renewable Solar Energy International Journal for Innovative Research in Science & Technology 2015;2:7
[80] JP Davim. Modern Mechanical Engineering, Materials Forming, Machining and Tribology (2014) Springer - Verlag Berlin.
[81] DC Kantesh. Design of solar still using Phase changing material as a storage medium. International Journal of Scientific & Engineering Research 2012;3:1.
[82] E Deniz. Solar-Powered Desalination, Desalination Updates, ISBN: 978-953-51-2189-3 (2015) InTech
[83] Hanson A, Zachritz W, Stevens K, Mimbela L, Polka R, Cisneros L. Distillate water quality of a single-basin solar still: laboratory and field studies. Solar Energy. 2004;76(5):635–45.
[84] R Sathyamurthy, DGH Samuel, PK Nagarajan, SA El-Agouz. A Review of Different Solar Still for Augmenting Fresh Water Yield. Journal of Environmental Science and Technology 2015;8:244-265.
[85] KP Vishwanath, A Kumar, O Prakash, A Kaviti Solar stills system design: A review. Renewable and Sustainable Energy Reviews 2015;51:153-181.
[86] Deniz E. An investigation of some of the parameters involved in inclined solar distillation systems. Environmental Progress & Sustainable Energy. 2013;32(2):350–4.
[87] Kumar PV, Kumar K, Prakash P, Kaviti K. Solar stills system design: A review. Renewable and Sustainable Energy Reviews 2015;51:153-81.
[88] Hansen R, Narayanan C, Murugavel K, Performance analysis on inclined solar still with different new wick materials and wire mesh. Desalination 2015:358:1-8.
[89] Velmurugan V, Prakash P. Parameters influencing the productivity of solar stills – A review. Renewable and Sustainable Energy Reviews 2015;49:585-609.
[90] Somanchi NS, et al. Performance of Solar Still with Different Phase Change Materials. International Journal of Energy and Power Engineering 2015;4:33-37.
[91] Swetha K, Venugopal J. Experimental investigation of a single slope solar still using PCM. International Journal of Research in Environmental Science and Technology 2011;1:30-33.
[92] Gugulothu G, Somanchi S, Devi RSR, Vilasagarapu V. EXPERIMENTAL STUDY OF SOLAR STILL WITH ENERGY STORAGE MATERIAL. Journal of Sustainable Manufacturing and Renewable Energy 2014;3:121-28.
[93] Kalbasi R, Esfahani E, Multi-Effect Passive Desalination System, An Experimental Approach. World Applied Sciences Journal. 2012;10:1264-71.
[94] Mahkamov K, Akhatovb JS. Experimental Study of the Performance of Multieffect Solar Thermal Water Desalination System. Applied Solar Energy 2008;44:31-34.
[95] Reddy KS, Kumar KR, O'Donovan TS, Mallick TK. Performance analysis of an evacuated multi-stage solar water desalination. Desalination 2012;288:80-92.
[96] Patel P, Solanki AS, Soni UR, Patel AR “A Review to Increase the Performance of Solar Still: Make It Multi Layer Absorber” International Journal on Recent and Innovation Trends in Computing and Communication 2014;2:173-177.
[97] Adhikari RS, Kumar A, Sootha GD “Simulation studies on a multi-stage stacked tray solar still” Solar Energy 1995;54:317-25.
[98] Welty, JR, Wicks CE, Wilson RE, Rorrer GL “Fundamentals of momentum, heat and mass transfer” 5th Ed 2008; John Wiley and Sons, NJ, USA.
[99] Incropera FP, Dewitt DP, Bergman TL, Lavine AS “Fundamentalsof heat and mass transfer” 6th Ed 2007;John Wiley and Sons, NJ, USA.
[100] Schwarzer K, Vieira da Silva E, Hoffschmidt B, Schwarzer T “A new solar desalination system with heat recovery for decentralised drinking water production” Desalination 2009;248:201-11.
[101] Mahmoud I, Shatat M, Mahkamov K “ Determination of rational design parameters of a multi-stage solar water desalination still using transient mathematical modelling” Renewable Energy 2010;35:52-61.

[102] Adhikari RS, Kumar A, Kumar A “Estimation of mass-transfer rates in solar stills” International Journal of Energy Research 1990;14:737-44.
[103] Estahbanati MRK, Feilizadeh M, Jafarpur K, Feilizadeh M, Rahimpour MR “Experimental investigation of a multi-effect active solar still: the effect of the number of stages” Applied Energy 2015;137:46-55.
[104] Coulson JM, Richardson JF, Backhurst JR, Harker JH. Coulson and Richardson's Chemical Engineering Volume 1 - Fluid Flow, Heat Transfer and Mass Transfer (6th Edition), Elsevier 1999, USA.
[105] Banat F,J Waied N. Economic evaluation of desalination by small-scale autonomous solar-powered membrane distillation units. Desalination 2008;220:566–73.